CHARACTERIZING THE OPERATION OF A DUAL-FUEL DIESEL-HYDROGEN ENGINE NEAR THE KNOCK LIMIT

A Thesis
Submitted to the Graduate Faculty
of the
North Dakota State University
of Agriculture and Applied Science

By

Lee Allan Kersting

In Partial Fulfillment
for the Degree of
MASTER OF SCIENCE

Major Department:
Mechanical Engineering

May 2014

Fargo, North Dakota

North Dakota State University
Graduate School

Title

Characterizing the Operation of a Dual Fuel Diesel-Hydrogen Engine Near the Knock Limit

By

Lee Kersting

The Supervisory Committee certifies that this ***disquisition*** complies with North Dakota State University's regulations and meets the accepted standards for the degree of

MASTER OF SCIENCE

SUPERVISORY COMMITTEE:

Dr. Robert Pieri
Chair

Dr. Majura Selekwa

Dr. Yildirim Bora Suzen

Dr. Mariusz Ziejewski

Dr. Scott Pryor

Approved:

7/7/2014
Date

Dr. Alan R. Kallmeyer
Department Chair

ABSTRACT

A CAT C6.6 turbocharged diesel engine was operated in dual-fuel diesel-hydrogen mode. Hydrogen was inducted into the intake and replaced a portion of the diesel fuel. Hydrogen was added across multiple engine speeds and loads until reaching the knock limit, identified by a threshold on the rate of in-cylinder pressure rise. In-cylinder pressure and emissions data were recorded and compared to diesel-only operation. Up to 74% H_2 substitution for diesel fuel was achieved. Hydrogen addition increased thermal efficiency up to 32.4%, increased peak in-cylinder pressure up to 40.0%, increased the maximum rate of pressure rise up to 281%, advanced injection timing up to 13.6°, increased NO_x emissions up to 224%, and reduced CO_2 emissions up to 47.6%. CO and HC emissions were not significantly affected during dual-fuel operation. At 25% load an operating condition was observed with low NO_x and nearly 0 CO_2 emissions, which however exhibited unstable combustion.

TABLE OF CONTENTS

ABSTRACT iii

LIST OF TABLES vi

LIST OF FIGURES vii

LIST OF ABBREVIATIONS ix

LIST OF APPENDIX FIGURES xii

CHAPTER 1. RESEARCH IMPORTANCE 1

1.1. World Petroleum Overview 1

1.2. Global Warming 4

1.3. Emissions Regulations 6

CHAPTER 2. RESEARCH OBJECTIVES 8

CHAPTER 3. BACKGROUND 9

3.1. Hydrogen as a Fuel 9

3.2. CI Diesel Combustion 13

CHAPTER 4. LITERATURE REVIEW 19

4.1. NDSU Engine Research Lab 19

4.2. Dual-Fuel Combustion 20

4.3. Knock Mechanisms 23

4.4. Knock Detection 25

4.5. Engine Performance in Dual-Fuel Operation 26

4.6. Emissions in Dual-Fuel Operation 27

CHAPTER 5. RESEARCH APPROACH 31

5.1. Experimental Setup 31

5.2. Data Acquisition 34
5.3. Experiment Design 36
5.4. Experimental Procedure 37
CHAPTER 6. RESULTS AND DISCUSSION 39
6.1. Engine Performance 39
6.2. Combustion 42
6.3. Emissions 55
CHAPTER 7. CONCLUSIONS 61
REFERENCES 63
APPENDIX A. SAMPLE SPREADSHEETS 67
APPENDIX B. ADDITIONAL EMISSIONS RESULTS 71
APPENDIX C. INJECTION DELAY CIRCUIT 73

LIST OF TABLES

Table Page

1. Properties of diesel and hydrogen fuel [16] [23]..... 9

2. CAT C6.6 Engine Specifications. 31

LIST OF FIGURES

Figure Page

1. World Liquid Fuels Consumption by Sector, 2008-2035 (million barrels per day) [1]. 2

2. 2008 Fuel Shares of Total Final Consumption (million tons of oil equivalent) [2]. 2

3. Primary (U.S.) Energy Consumption by Source and Sector, 2011 (Quadrillion Btu) [3]. 3

4. EPA/EU non-road emissions regulations: 37-560 kW (50-750 hp) [11]. 7

5. Energy density of H_2 at various states compared to diesel. 12

6. Four stroke engine cycle operation [31]. 14

7. Idealized air-standard dual cycle pressure-specific volume diagram [31]. 16

8. Idealized fuel zones around an injection jet [31]. 17

9. Shift in air-standard cycle with increasing hydrogen percentage. 21

10. Schematic diagram of the hydrogen induction system. 32

11. CAT C6.6 engine setup in test cell. 33

12. LabVIEW front panel. 35

13. Operable and inoperable speed-load set points for the experiment. 37

14. Hydrogen percentage at the knock limit on an energy basis. 40

15. Thermal efficiency of both diesel-only and dual-fuel operation at different loads. 41

16. In-cylinder pressure curves at 1300 rpm. 43

17. In-cylinder pressure curves at 1500 rpm. 44

18. In-cylinder pressure curves at 1800 rpm. 45

19. In-cylinder pressure curves at 2100 rpm. 46

20. Comparison of variability in the shape of averaged pressure curves between 25% load and 77.5% load. 47

21. Comparison of the curves for individual combustion cycles between 25% load and 77.5% load. 47

22. Example of the rate of pressure rise in the absence of combustion in a reciprocating piston engine. 48

23. Rate of pressure rise curves for 1300 rpm. 49

24. Rate of pressure rise curves for 1500 rpm. 50

25. Rate of pressure rise curves for 1800 rpm. 51

26. Rate of pressure rise curves for 2100 rpm. 52
27. Main injection timing during diesel-only and dual-fuel operation. 53
28. Shift in injection timing between dual-fuel and diesel-only combustion. 54
29. Pilot injection timing during diesel-only and dual-fuel operation. 55
30. NO_x emissions for diesel-only and dual-fuel operation. 56
31. NO_2/NO_x ratio for diesel-only and dual-fuel operation. 57
32. CO_2 emissions for diesel-only and dual-fuel operation. 58
33. CO emissions for diesel-only and dual-fuel operation. 59
34. HC emissions for diesel-only and dual-fuel operation. 59

LIST OF ABBREVIATIONS

Φ.....Equivalence Ratio

ACERT .....Advanced Combustion Emission Reduction Technology

AF .....Air-Fuel

ATDC.....After Top Dead Center

BDC.....Bottom Dead Center

BTDC.....Before Top Dead Center

Btu .....British Thermal Unit

CA .....Crank Angle

CAD.....Crank Angle Degrees

CAFE.....Corporate Average Fuel Economy

CAT .....Caterpillar

CI.....Compression Ignition

CNG .....Compressed Natural Gas

CO .....Carbon Monoxide

CO_2.....Carbon Dioxide

DAQ.....Data Acquisition System

DEF .....Diesel Exhaust Fluid

DI.....Direct Injection

ECM .....Engine Control Module

EGR.....Exhaust Gas Recirculation

EPA .....Environmental Protection Agency

EU .....European Union

FA.....Fuel-to-Air

GHG .....Greenhouse Gas

H_2.....Hydrogen

H_2O.....Water

HC .....Hydrocarbon

HCCI.....Homogeneous Charge Compression Ignition

HCN.....Hydrogen Cyanide

HPCR .....High Pressure Common Rail

HRR.....Heat Release Rate

IC .....Internal Combustion

LFL .....Lower Flammability Limit

LHV .....Lower Heating Value

LPG .....Liquefied Petroleum Gas

MC .....Measurement Computing

mpg .....Miles per Gallon

MRPR.....Maximum Rate of Pressure Rise

Mtoe .....Million Tons of Oil Equivalent

N_2.....Nitrogen

N_2O.....Nitrous Oxide

NDSU .....North Dakota State University

NO .....Nitric Oxide

NO_2.....Nitrogen Dioxide

NO_x.....Nitrogen Oxides

O_2 .....Oxygen

OECD .....Organization for Economic Cooperation and Development

OEM .....Original Equipment Manufacturer

PCB .....Printed Circuit Board

PID .....Proportional-Integral-Derivative

PM .....Particulate Matter

ppm .....Parts per Million

psi.....Pounds per Square Inch

rpm .....Revolutions per Minute

RPR.....Rate of Pressure Rise

SCR.....Selective Catalyst Reduction

SOC.....Start of Combustion

TDC .....Top Dead Center

LIST OF APPENDIX FIGURES

Figure Page

A1. Partial sample of output file from LabVIEW with calculations. 67

A2. Partial sample of DYNOmite output data spreadsheet with calculations. 68

A3. Partial sample of pressure curve averaging spreadsheet. 69

A4. Sample of injection timing graph. 70

B1. O_2 emissions for diesel-only and dual-fuel operation. 71

B2. NO emissions for diesel-only and dual-fuel operation. 71

B3. NO_2 emissions for diesel-only and dual-fuel operation. 72

C1. Injector signal with injector delay circuit parameters and values. 74

C2. Nearly complete circuit on the left. A model of the injector delay circuit on the right. 74

CHAPTER 1. RESEARCH IMPORTANCE

1.1. World Petroleum Overview

Petroleum, herein used as synonymous with the term “crude oil,” is formed when organic materials, such as zooplankton and algae, are subject to intense heat and pressure far beneath the earth’s surface. This natural process, which is a form of anaerobic decomposition, takes millions of years to produce petroleum. The current rate of petroleum usage is far higher than the rate at which it can be produced by anaerobic decomposition. This unsustainability makes it imperative to investigate alternative sources of energy which can be responsibly sustained into the future.

According to the 2011 International Energy Outlook, a report by the US Energy Information Administration, world consumption of petroleum and other liquid fuels (including petroleum-derived fuels and non-petroleum-derived liquid fuels, natural gas liquids, crude oil consumed as a fuel, and liquid hydrogen) is projected to increase from 85.7 million barrels per day in 2008 to 112.2 million barrels per day in 2035, a 31% increase [1]. Figure 1 is a graph of projected world liquid fuels consumption by sector. Of the total liquid fuel consumed, the transportation sector is projected to increase in percentage from 54% in 2008 to 60% in 2035, accounting for 79% of the increased demand [1]. The transportation sector, which is defined as moving people or goods via road, air, water, rail, or pipeline [1], is a strategic target for reducing liquid fuel usage. Additionally, the largest increases in liquid fuel consumption are expected in non-member countries of the Organization for Economic Cooperation and Development (OECD), particularly China and India who are expected to increase their consumption of liquid fuels by 2.6% per year. This is in contrast to the 0.3% per year increase in liquid fuel consumption expected in OECD countries [1]. The increased consumption in non-OECD countries is due mainly to the increased ability of consumers to acquire vehicles and expansion of the transportation sector. The expected increase of liquid fuel consumption by the transportation sector highlights the importance of seeking alternative sustainable fuels as a means to replace petroleum-based fuels for the future.

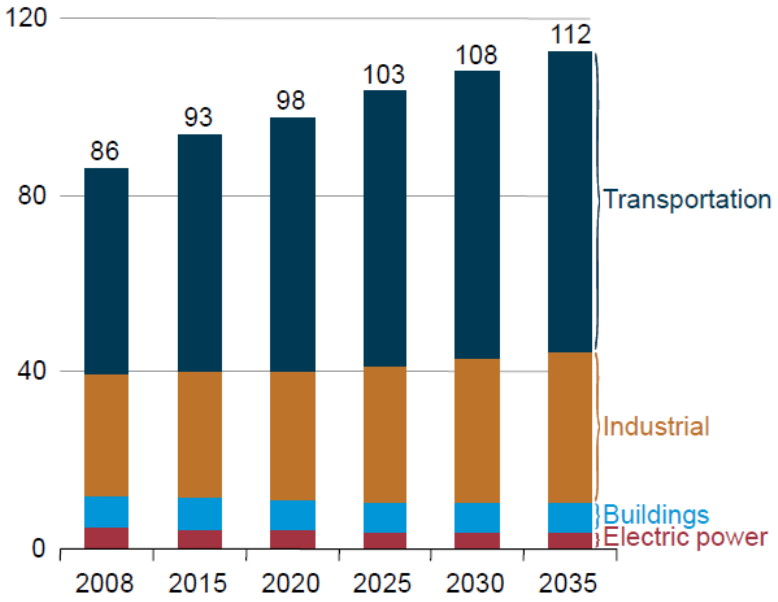

Figure 1. World Liquid Fuels Consumption by Sector, 2008-2035 (million barrels per day) [1].

As discussed above, transportation accounts for the majority of liquid fuel consumption. Liquid fuels, of which petroleum (oil) products are the chief component, represent a significant portion (41.6%) of the total world energy usage as seen in Figure 2 [2]. This again reinforces the impact reducing petroleum usage will have on energy security for the future.

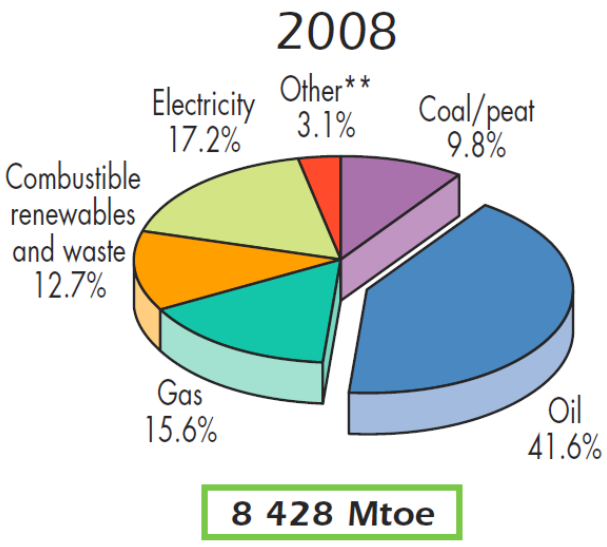

Figure 2. 2008 Fuel Shares of Total Final Consumption (million tons of oil equivalent) [2].

Figure 3 shows the primary energy usage in the U.S. in 2011, broken out into the source and sector. In the U.S, petroleum accounts for 36% of the total energy supplied and the transportation sector accounts for 28% of all energy consumed [3]. Of the total petroleum supply, 71% goes to the transportation sector; this accounts for 93% of the energy supplied to the transportation sector. This is the largest percentage any one energy source has for a sector. Reducing petroleum usage by the transportation sector would have the greatest impact on reducing total petroleum usage in the U.S., and since petroleum is the largest energy source in the U.S. it would also have the greatest impact on reducing total energy usage.

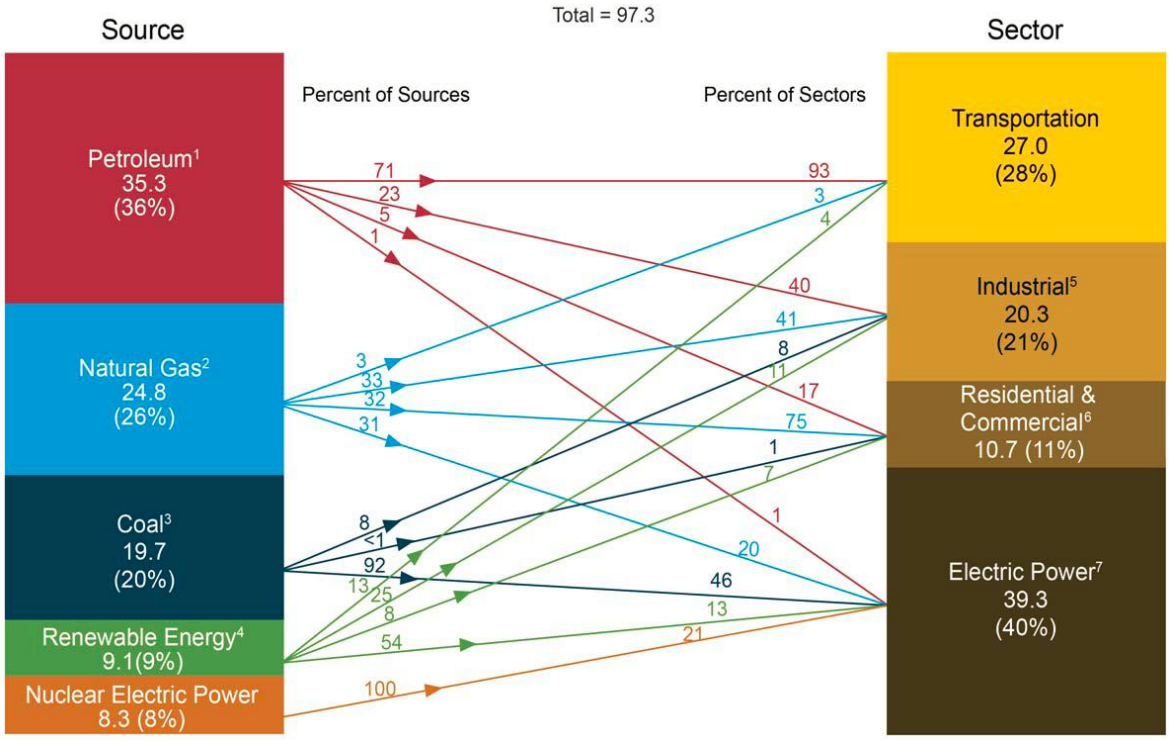

Figure 3. Primary (U.S.) Energy Consumption by Source and Sector, 2011 (Quadrillion Btu) [3].

A popular discussion in the world oil debate is about the timing of peak oil. Peak oil is defined as when the rate of oil production reaches a maximum. After peak oil occurs, the rate of oil production will begin to decrease, making oil increasingly scarce, though not necessarily meaning it is close to exhaustion [4]. Some experts maintain peak oil occurred in 2005, while others expect it to occur sometime after 2030 [4]. Regardless of when it happens, peak oil will occur at some point. When it occurs, oil prices will begin to rise due to a reduction in supply. This price increase will be

accelerated when coupled with the predicted increase in demand for oil. Eventually, oil will become an uneconomical energy solution. When this happens, alternative energy technologies must be ready.

One aim of this work is to provide technical information to advance the possibility of using hydrogen as a large portion of the fuel in a diesel engine. Diesel engines are already popular in heavy-duty on-highway, off-highway, and agricultural applications; these three account for 74.6% of distillate fuel oil (diesel) consumption in the US [3]. Increasingly, passenger and light-duty vehicles are adopting diesel engine solutions as well. In Europe, approximately 50% of new passenger vehicles are diesel powered [5]. The widespread use of diesel engine technology makes the potential impact of reducing diesel fuel usage significant. Distillate fuel oil (which includes No. 1, No. 2, and No. 4 diesel fuels and No. 1, No. 2, and No. 4 fuel oils) in the U.S. was consumed at a rate of 3.85 million barrels per day in 2011 while motor gasoline was consumed at a rate of 8.47 million barrels per day, which together account for 67% of petroleum use in the U.S. in 2011 [3]. Motor gasoline has more than double the use of distillate fuel oils in the U.S. and so represents a greater potential for reducing petroleum usage. Distillate fuel oil, which includes diesel fuel, still represents over 20% of petroleum usage in the U.S. In markets such as Europe that have more readily adopted diesel technology in light-duty vehicles, the impact of reducing diesel consumption would be even greater. Additionally, on-highway applications, which accounted for 65% of distillate fuel oil usage in the U.S. in 2011 [3], use much more fuel per vehicle than light-duty applications. Heavy-duty trucks used 4,174 gallons per vehicle in the U.S. in 2011 versus 894 and 453 gallons per vehicle for light-duty long and short wheelbase vehicles, respectively. Such high fuel usage per vehicle means that implementing changes on a smaller number of vehicles can have a greater impact on reducing total fuel usage.

1.2. Global Warming

Global climate change is a scientifically verifiable phenomenon: the earth goes through natural cycles of warming and cooling. In recent decades the earth's temperature has been rising,

giving way to a debate over global warming, its potential impacts, and what role burning carbon-based fuels has had on the earth's current climate trends.

Greenhouse gases such as water vapor, carbon dioxide, methane, nitrous oxide, and ozone help maintain a moderate climate on earth. These gases help regulate the temperature of the planet by absorbing and emitting infrared thermal radiation. At night these gases absorb heat radiated from the earth's surface and re-radiate it in all directions. Some of the re-radiated heat is directed back towards the earth keeping it much warmer than without the gases. This phenomenon is often called the greenhouse effect. The two gases that contribute most to the greenhouse effect are water vapor and CO_2, in that order [6]. Though water is a greater contributor to the greenhouse effect, its residence time in the atmosphere is on the order of 10 days -- very short compared to the residence time of CO_2 which is on the order of decades to centuries [6]. This indicates that perturbations of CO_2 in the atmosphere will have long lasting effects. It is also important to note that water vapor reacts to rather than drives climate change. Water vapor in the atmosphere is a direct function of temperature: it will remain stable at any given temperature. This means that any increase in CO_2 also brings with it an increase in water vapor, amplifying the greenhouse effect.

It is widely believed that human activity has been the leading cause of the increase in atmospheric CO_2 levels, mainly through the burning of fossil fuels. Burning large quantities of carbon-based fuels starting in the industrial revolution has increased the atmospheric CO_2 level. A 1987 study measured historical CO_2 level fluctuations over the last 400,000 years from as low as 180 ppm up to 280 ppm from cores cut from central Antarctica [7]. The current atmospheric CO_2 level is about 400 ppm and has been steadily rising since the 1950s [8]. Since 1750, roughly just before the industrial revolution, global average temperature has risen by 1.4 degrees F [8].

Regardless of the cause of global warming, it is a phenomenon that needs to be given attention. The appropriate response depends on the effects global warming will have on the planet and its inhabitants, which is still the topic of much debate. Among the proposed effects are: extreme polar climate change, melting of glaciers and ice sheets, increased extreme weather events, a rise in the sea level, and shifts in plant and animal territory. There are those who raise much alarm about the potential impacts of global warming as well as those who think global

warming may even be a positive change. As time continues, the effects of global climate change will manifest themselves and at that time it will be too late to avoid any negative impacts. Given the potential for drastic negative impacts and the unprecedented levels of CO_2, it would seem prudent to undertake efforts to reduce the amount of CO_2 emissions.

1.3. Emissions Regulations

Emissions regulations have been implemented to limit the amount of harmful pollutants produced by internal combustion (IC) engines in most places where they are used. The U.S. EPA has placed regulations on light-duty cars and trucks, heavy-duty on-highway vehicles, agricultural and construction equipment, locomotives, marine vessels, recreational vehicles, and aircraft [10]. European emissions regulations, which are controlled by the European Union (EU), are very similar to the U.S. regulations. Some developing world economies, most notably India and China, are starting to adopt similar regulations to those in Europe and the U.S. The exhaust constituents regulated by the EPA in the U.S. include: Nitrogen Oxides (NO_x), Hydrocarbons (HC), Particulate Matter (PM), and Carbon Monoxide (CO). Regulations are implemented incrementally, giving original equipment manufacturers (OEMs) time to develop technology and comply with the regulations. The EPA first started regulating on-highway vehicle emissions and later off-highway emissions. The aforementioned pollutants have been targeted for regulation because of their short-term, negative health effects, especially in heavily populated urban environments. Also, due to acid rain, sulfur content in fuels has been heavily regulated, being reduced from 300 ppm down to 30 ppm for gasoline and from 500 ppm down to 15 ppm for diesel [10].

U.S. EPA off-highway emissions regulations for compression ignition (CI) engines started in 1996 with Tier 1 and are set to be fully implemented by 2015 with Final Tier 4. Figure 4 shows the progression of the regulation of PM and NO_x by power range of the EPA's (and EU's) non-road emissions regulations [11]. Both species are given an allowance in g/kWhr with lower power engines getting a larger allowance.

Carbon dioxide as a pollutant does not pose any immediate, direct risk to human health. Rather, the negative effects of CO_2 emissions are experienced by way of climate change, which

may have adverse, long-lasting effects on the planet as a whole. Currently there are no direct regulations on CO_2 as an exhaust emission for any type of vehicle in the U.S. Via the corporate average fuel economy (CAFE) standards, CO_2 emissions are indirectly regulated by mandating automakers meet certain fleet fuel economy targets. Current regulations, which run through 2016, require auto manufacturers to have an average fleet fuel economy of 35.5 mpg. The next set of regulations, which runs through 2025, will require an average of 54.5 mpg for automakers [12]. Although no CO_2 regulations have been announced for non-road applications, as fuel prices continue to increase, OEMs will likely look for ways to improve fuel efficiency to foster environmental responsibility and gain a competitive advantage.

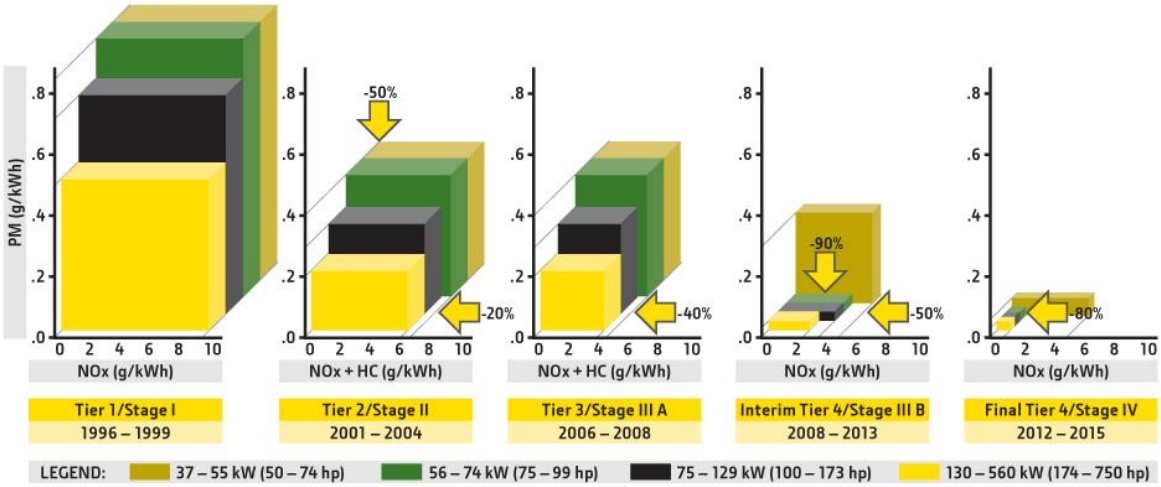

Figure 4. EPA/EU non-road emissions regulations: 37-560 kW (50-750 hp) [11].

Burning hydrogen as a fuel would reduce CO_2, CO, and HC emissions by directly displacing petroleum fuels. It has also been shown that H_2 addition greatly reduces smoke (PM) emissions from IC engines [13] [14] [15] [16] [17] [18] [19]. Engines in dual-fuel operation with hydrogen typically have higher NO_x emissions than diesel-only operation [14] [15] [16] [17] [18] [20] [21]. This presents a challenge to meeting emissions regulations. There are a number of technologies that can mitigate NO_x including exhaust gas recirculation (EGR), charge dilution, and selective catalyst reduction (SCR). Additionally, with a reduction in each of the other regulated exhaust gas constituents, vehicle manufacturers could place additional focus on reducing NO_x emissions.

CHAPTER 2. RESEARCH OBJECTIVES

The primary objective of the current work is to investigate the combustion process of a dual-fuel diesel-hydrogen engine operating near the knock limit. This technical knowledge is important for finding means to increase H_2 substitution. By increasing H_2 substitution in a diesel engine, a greater amount of carbon-based fuel can be displaced, extending the availability of fossil fuels further into the future.

The combustion process will be analyzed on the basis of the size and shape of the in-cylinder pressure trace, from which peak pressure, rate of pressure rise, and start of combustion can be determined. Another important parameter that will be considered is injection timing. These main combustion parameters along with engine speed, engine load, diesel energy, hydrogen energy, and NO, NO_2, CO, CO_2, and HC emissions will be used to characterize engine performance and suggest how increased H_2 substitution may be achieved.

CHAPTER 3. BACKGROUND

3.1. Hydrogen as a Fuel

Many different alternative fuels have been proposed for use in transportation including: ethanol, methane (CH_4), liquefied petroleum gas (LPG), compressed natural gas (CNG), and hydrogen (H_2) [22]. Of these fuels, H_2 is the only carbon-free option. For this reason H_2 has the greatest potential to reduce CO_2 emissions. Being a non-carbon fuel, H_2 would also eliminate CO, HC, and smoke (PM) emissions. Assuming no impurities in the H_2, there would also be no sulfur oxides, lead, sulfuric acid, ozone, benzene, or formaldehydes produced during combustion [17]. If H_2 can be produced from renewable sources it also has the potential to be a sustainable source of fuel and produce near-zero "well-to-wheel" CO_2 emissions.

Many properties of H_2 make it an attractive choice as a fuel for combustion. The first of these is its lower heating value (LHV). Hydrogen has a LHV of 51,500 Btu/lb compared to 18,250 Btu/lb for diesel. This means that on a per mass basis H_2 contains over 2.5 times the amount of energy as diesel. Other notable H_2 properties are its high diffusivity, large range of flammability (4-75% in air), high autoignition temperature (1085 F), low ignition energy (.1.9e-8 Btu), low quench gap (.025 in) and high flame speed (8.7-10.7 ft/s) [23]. A comparison of the properties of H_2 and diesel can be seen in Table 1.

Table 1. Properties of diesel and hydrogen fuel [16] [23].

Property	Diesel	Hydrogen
LHV (Btu/lb)	18,250	51,500
Flamability Range @ 80°F (vol. % in air)	0.6-5.5	4-75
Energy Density (Btu/ft3)	843,700	48,900 (3000 psi, 60°F)
Autoignition Temperature (°F)	494	1085
Ignition Energy (Btu)	-	1.90E-08
Quench Gap (in.)	-	0.025
Flame Speed (ft/s)	0.98	8.7-10.7
Stoichiometric Air-Fuel Ratio	14.5	34.3
Cetane Number	40-55	-
Octane Number	30	130

The wide flammability range of H_2 allows flexibility in the fuel-to-air (FA) equivalence ratio (φ) during engine operation, where the FA equivalence ratio is the actual FA ratio divided by the stoichiometric FA ratio. The range of equivalence ratios for H_2 is $0.1<\varphi<7.1$ [24]. This wide range allows a H_2

engine to be run lean where high thermal and combustion efficiencies and lower NO_x emissions can be obtained.

Hydrogen's high autoignition temperature presents challenges when used as the sole fuel source in a CI engine. Szwaja and Grab-Rogalinski [25] propose a minimum compression ratio of 16:1 based on numerical analysis for the autoignition of H_2 in a CI engine. This is in the range of a typical diesel engine; however, in practice, H_2 compression ignition does not appear to be sustainable under such conditions. Szwaja and Grab-Rogalinski [25] conducted experiments with H_2-only operation on a diesel engine with a 17:1 compression ratio. The results showed a highly stochastic combustion process. It was concluded that H_2 was not being auto-ignited by compression but ignited by hot spots in the combustion chamber. Stable operation was not achieved during testing. Antunes et al. [26] were able to achieve stable compression ignition of H_2 over a limited operating range via an inlet air heating system. The incoming fuel-air charge was heated to 80 °C to ensure adequate temperature for auto-ignition. Although it presents challenges when used as the sole fuel in CI combustion, when used in dual-fuel applications, hydrogen's high autoignition temperature can be a benefit. It allows higher compression ratios, which yield higher theoretical thermal efficiencies, to be used before the onset of knock. It also means that at the same compression ratio, H_2 is more resistant to knock than diesel. This is confirmed by hydrogen's much higher Octane Number, which is a measure of the knock-resistance of a fuel.

The low ignition energy of H_2 means that initiating combustion of H_2 requires little energy. This allows a wide variety of ignition sources to be used. In the case of dual-fuel operation, ignition is typically initiated by the autoignition of diesel fuel. It has also been suggested that a glow plug could be used to initiate combustion in a H_2-only CI engine [27] [28]. The low-ignition energy also requires care to be taken to avoid unintended ignition due to in-cylinder hot spots which can cause pre-ignition or backfire, which will produce unstable operation.

The high flame speed, small quench gap, and high diffusivity of H_2 all promote complete combustion and therefore contribute to excellent combustion efficiency. The low quench gap leaves less unburned fuel along the cylinder walls and piston face at the end of combustion. The high flame speed promotes rapid, turbulent combustion which promotes better mixing of the fuel-air

mixture which produces better combustion. Hydrogen's high flame speed also leads to higher thermal efficiencies; with a quicker burn, combustion approaches a constant-volume process which is thermodynamically more efficient that the typical constant-pressure combustion process of pure diesel. The high diffusivity of H_2 helps form a uniform mixture for combustion.

Hydrogen is often dismissed as dangerous due to the infamous Hindenburg accident. This, however, is a misconception. Hydrogen is no more dangerous than petroleum-based fuels; it simply has different safety considerations than either diesel or gasoline. Hydrogen is in fact safer than diesel/gasoline in many respects. Hydrogen is non-toxic and will not cause contamination in the event of a spill. Any H_2 leaks or spills will quickly rise and diffuse into the surrounding air. Hydrogen is dangerous primarily when used in enclosed spaces where it can collect to flammable concentrations. For this reason, H_2 should always be used in a ventilated area. If H_2 is being used in a test cell, the design should be such that the air in the test cell is refreshed 1-2 times every minute and appropriate H_2 sensors should be used [24]. Typically a warning will sound when the H_2 concentration reaches 1%, and an alarm and emergency ventilation will be initiated at the detection of 2% H_2 concentration. Although it burns hotter than diesel, H_2 has less time to transfer heat due to its high flame speed. In the case of a punctured H_2 tank that ignites, the flame will be predominantly vertical due to the high buoyancy of H_2 which can help prevent the flame from spreading [23]. Additionally, the gases produced in a H_2 fire are non-toxic, the only by-product being water vapor. Though the combustion products are non-toxic, the combustion process may consume enough oxygen in enclosed environments to be a risk for asphyxiation. Hydrogen flames burn very pale blue and are almost impossible to see. In darker lighting conditions, the visibility of the flame improves, but caution should be used whenever working with a H_2 flame. With small leaks, H_2 diffuses quickly enough to avoid the lower flammability limit except very near the leak source. Large leaks pose a much higher safety risk. Hydrogen also has poor electrical conductivity, which requires all H_2 conveying equipment to be grounded to avoid electrical discharge.

Although H_2 has many desirable characteristics that make in an attractive alternative fuel, it also poses a number of challenges. Among these are: storage, production, transportation, and acceptance of H_2 as a fuel.

As previously mentioned, H_2 has a high LHV, meaning it contains a large amount of energy per mass. When looked at in terms of energy density (energy per volume), H_2 is far behind conventional liquid petroleum fuels. As a gas under atmospheric conditions, H_2 has an energy density of 270 Btu/ft^3 compared to 843,700 Btu/ft^3 for diesel. This large disparity can be reduced by storing H_2 either as a liquid or under pressure. For instance, liquid H_2 has an energy density of 227,850 Btu/ft^3 and H_2 compressed to 10,000 psi at room temperature has an energy density of 121,000 Btu/ft^3. As can be seen in Figure 5, even in compressed or liquid form, H_2 fails to approach diesel fuel for energy density. This poses a problem since the fuel tanks would need to be much larger to obtain the same driving range as diesel fuel. Apart from the issue of driving range, the fuel tanks would be much more costly to store H_2 as either a liquid or under pressure. Additionally, compressing H_2 or cooling it to the liquid state both requires a significant amount of energy. In one estimate it takes 40-80% of the energy of the fuel to generate, compress, transport, and store H_2 at distributed filling stations, compared to 12% for gasoline, or 5% for natural gas [29].

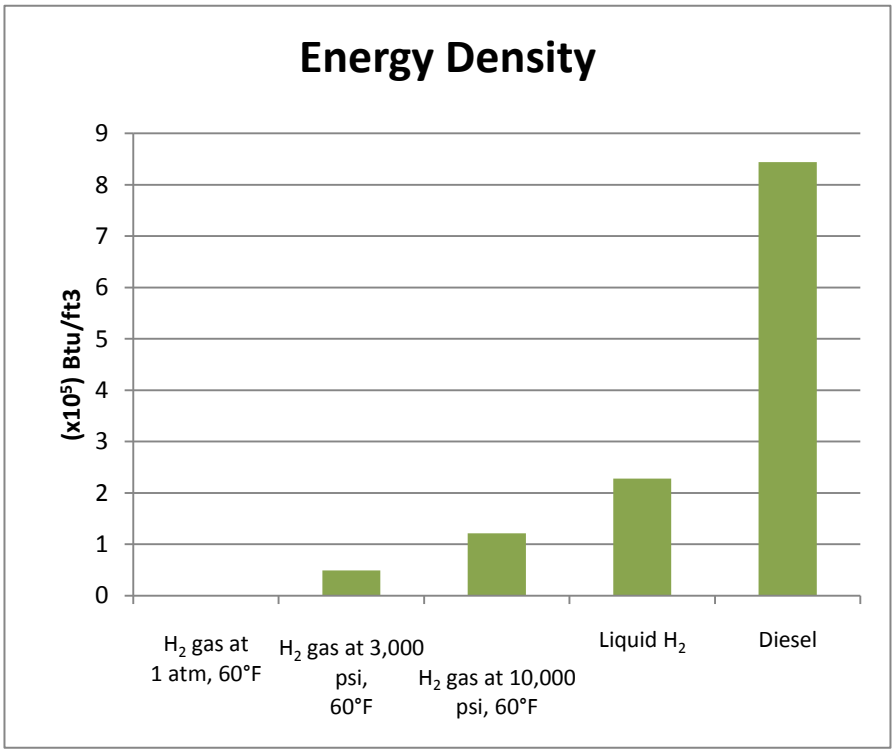

Figure 5. Energy density of H_2 at various states compared to diesel.

This last statistic brings up another of the difficulties with H_2 as a fuel: a lack of infrastructure. The production, distribution, and storage of H_2 remain a large challenge to its widespread use as a fuel. Currently 95% of US H_2 is produced by steam-methane reforming, a process that produces 10-tons of CO_2 for every ton of H_2 [29]. This quickly eliminates the advantage H_2 brings to reducing GHG emissions. Electrolysis from renewable sources is the only sustainable means of producing H_2. Electrolysis is 3-4 times more expensive than steam-methane reforming, however, and is expensive compared to directly using the electricity [29]. One situation that may favor H_2 production is if it can be used as a medium to store excess electrical production.

Another barrier to widespread H_2 adoption is public acceptance. Diesel and gasoline are widely accepted and familiar to the public. As with any new technology, there must be clear public and private (personal) benefits [30]. Although the benefits exist in theory, they have yet to be made feasible. It addition, push from the automotive industry would be necessary to foster a wider acceptance of the new technology. This is no trivial matter as can be seen with the slow acceptance of electric vehicle technology in spite of a push from automakers.

Were H_2 to gain prominence as an alternative fuel in IC engines, it could act as a bridge to H_2 fuel cell technology in the future. Internal combustions engines currently can be made to run on a large portion, if not entirely on H_2, and provide the benefit of zero CO_2 emissions. This can provide an impetus for building H_2 infrastructure: production, storage, and distribution facilities. With H_2 infrastructure in place, fuel cell technology, which promises efficiency increases over H_2 combustion in IC engines, can be more easily introduced.

3.2. CI Diesel Combustion

A diesel engine runs on a four-stroke cycle. The operation of a four-stroke engine is outlined in Figure 6. During the intake stroke (a) the intake valve is open and air is drawn into the cylinder while the piston travels from top-dead-center (TDC), or the highest point in the cylinder, to bottom-dead-center (BDC), or the lowest point in cylinder. In a naturally aspirated engine, air is drawn into the cylinder by the downward motion of the piston, while in a turbocharged or supercharged engine, the intake air is compressed above atmospheric pressure and is forced into

the cylinder when the intake valve opens. Only air is drawn into the cylinder of a diesel engine during the intake stroke.

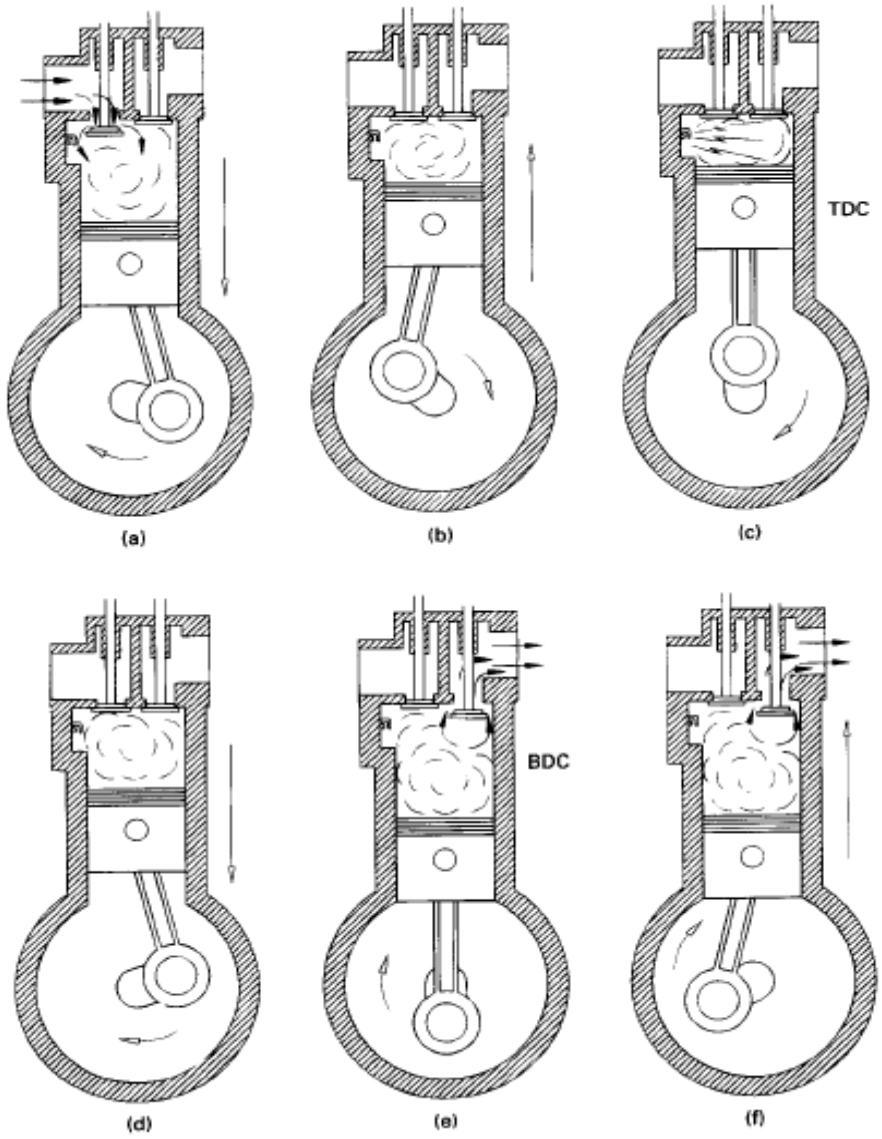

Figure 6. Four stroke engine cycle operation [31].

After the intake stroke, the compression stroke (b) occurs. During the compression stroke, both the intake and exhaust valves are closed, making the combustion chamber a closed thermodynamic system. As the piston travels from BDC to TDC, it does work on the air in the combustion chamber, raising the temperature and pressure of the enclosed mass of air. Near the end of the compression stroke, fuel is injected into the combustion chamber in a diesel engine.

Fuel is injected at high pressure to produce a fine mist of fuel droplets. These droplets must then go through additional processes before they can be ignited, which will be explained later in this section.

After fuel preparation has taken place, ignition (c) will occur due to the elevated temperature and pressure in the cylinder of a CI engine. This will typically occur 5-10 degrees before TDC (BTDC). The temperature and pressure required for auto-ignition of the fuel is largely dependent on the fuel properties.

Once ignition has taken place, the engine will go through the power stroke (d). In a diesel engine, combustion occurs well into the power stroke, over a range of 40-50 crank angle degrees (CAD). The gases in the combustion chamber are at a very high temperature after combustion and rapidly expand. During this time both the intake and exhaust valves are closed, allowing the expanding gases to do work on the piston, which forces it back down toward BDC.

When the piston is nearing BDC during the power stroke, the exhaust valve will open and blowdown (e) will occur. The exhaust valve opens prior to BDC, when temperature and pressure in the cylinder are still relatively high compared to the atmosphere. This causes the majority of the exhaust gases to rush out of the combustion chamber the moment the exhaust valve is opened.

After reaching BDC, with the exhaust valve open, the exhaust stroke (f) occurs. During the exhaust stroke, the piston travels from BDC to TDC, forcing out any remaining exhaust gas from the cylinder. As the piston nears TDC, the exhaust valve will close and the intake valve will open, starting the cycle again.

An idealized P-V cycle diagram of a modern CI engine can be seen in Figure 7. Piston motion from 1-2 represents the compression stroke. At 2, ignition occurs and premixed combustion takes place from 2-x. From x-3 diffusion-controlled combustion occurs. The power stroke takes place as the piston moves from x-3-4. From 4-5 is blowdown, from 5-6 is the exhaust stroke, and from 6-1 is the intake stroke.

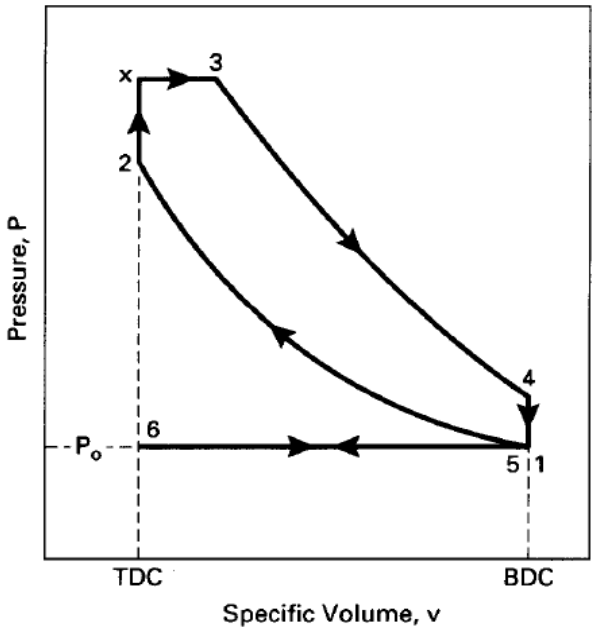

Figure 7. Idealized air-standard dual cycle pressure-specific volume diagram [31].

The steps fuel must go through before combustion play an important role in CI engines. Since the fuel is not injected until late in the compression stroke, the fuel must quickly form a combustible fuel-air mixture. The steps the fuel undergoes to prepare for combustion are: injection, atomization, vaporization, and mixing [31]. Fuel is first injected into the cylinder at high pressure, over 20,000 psi in many modern high-pressure common rail (HPCR) fuel injection systems. The high injection pressure causes the fuel to enter the combustion chamber at high velocity. The higher the injection pressure, the smaller the initial fuel drops will be. Turbulence of the air in the cylinder helps to break up the fuel drops. After injection the fuel undergoes atomization, where the fuel drops split up into smaller droplets. The droplets then vaporize very quickly due to the high combustion chamber temperatures. Once vaporized, the fuel needs to mix with air in the cylinder to form a combustible fuel-air mixture. The fuel-air mixture is heterogeneous, existing in various zones at different concentrations, as shown by the idealized representation in Figure 8. Immediately surrounding the fuel jet in zone A is a fuel-air mixture that is too rich (deficient oxygen) to burn. Zone B is rich-combustible, zone C is near stoichiometric, zone D is lean combustible, and zone E is too-lean to burn (excessive oxygen). Turbulence and swirl in the combustion chamber help the fuel to mix with the surrounding air.

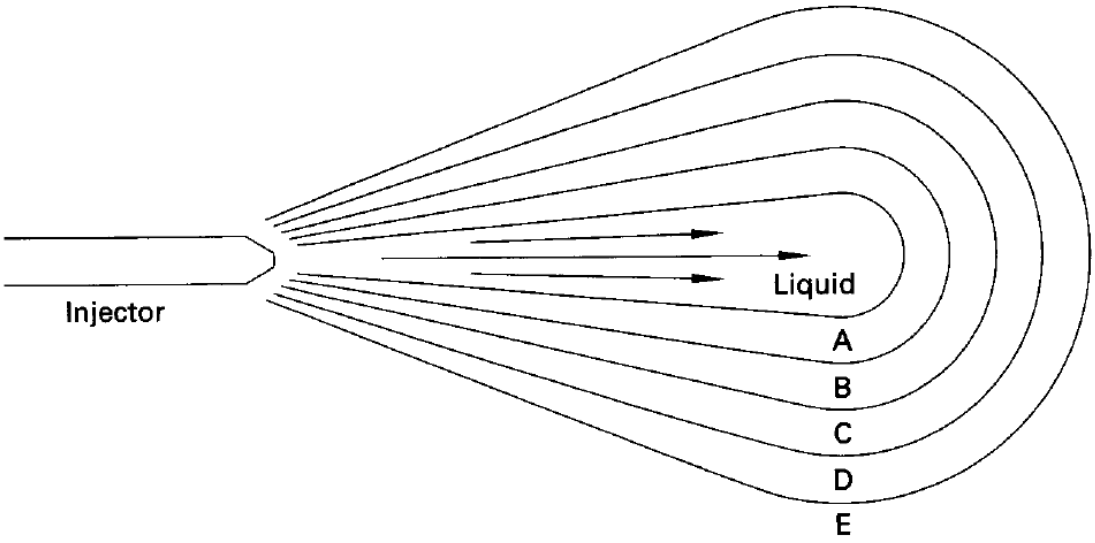

Figure 8. Idealized fuel zones around an injection jet [31].

Combustion in a CI engine is initiated when the combustible regions of the air-fuel (AF) mixture in the combustion chamber reach their auto-ignition temperature. Ignition is therefore caused solely by the increase in temperature related with compression by the ideal gas law. Diesel engines generally burn at a lean overall mixture with local combustion taking place in rich zones [31]. Once ignition starts, two modes of combustion occur: premixed and diffusive [32]. Pre-mixed combustion is the burning of the portions of the AF mixture which are at a combustible equivalence ratio at the start of combustion. In premixed combustion the rate of reaction is a function of temperature, equivalence ratio, and activation energy, but it is independent of location [32]. Diffusive combustion occurs as a mixture outside the combustible equivalence ratio becomes combustible due to diffusion of O_2 into the too-rich-to-burn zones. Gradients of both equivalence ratio and temperature are present. The rate of reaction during diffusive combustion is determined by the rate of diffusion [32].

Combustion in a CI engine is a complex process that can be broken up into a few basic steps: ignition delay, premixed burning, main diffusion burning, and end burning [32]. Ignition delay is the period between the start of injection and the start of combustion. The length of the ignition delay period depends on physical processes such as droplet size and combustion chamber temperature, as well as chemical processes such as the temperature at injection and the Cetane

number of the fuel. In practice, the injection delay can be measured as the time from when the injector fires to when there is a noticeable increase in pressure due to combustion. During the premixed burning period, the premixed fuel is burned and a sharp pressure rise occurs. A longer ignition delay will lead to more premixed fuel available at the start of the premixed burning period and lead to a sharper rise in pressure. This period is where engine knock associated with high rates of pressure rise is expected to occur. During the main diffusion burning period, fuel continues to be injected into an already present flame. The fuel burns as it reaches an ignitable mixture through diffusion. During the main diffusion burning period, the rate of reaction is lower than during the premixed burning period. The end burning period is defined as from the end of fuel injection to flame termination. The rate of reaction during end burning is lower yet due to decreased temperature in the expanding combustion chamber [32].

CHAPTER 4. LITERATURE REVIEW

4.1. NDSU Engine Research Lab

Dual-fuel diesel-hydrogen research has been ongoing at the North Dakota State University (NDSU) engine research lab since 2005. Stousland, in a work in progress, investigated the feasibility of operating a 4-cylinder CAT engine with a fixed-timing, mechanical injection system in dual-fuel mode with minimal modifications. The engine adapted easily to the introduction of H_2 and ran on 50% H_2 by energy-input before reaching the knock limit. The effect of H_2 substitution on emissions, engine efficiency and combustion were also investigated.

Next, Bottelberghe conducted testing with a 6-cylinder CAT C6.6 engine equipped with an Advanced Combustion Emission Reduction Technology (ACERT) engine control module (ECM), designed to meet the U.S. EPA Tier 3 emissions standards [33]. The ECM controls the engine electronically and was able to adapt to engine operation changes due to increased amounts of H_2 by shifting injection timing, boost pressure, and other operating parameters. Bottelberghe observed a knock limit at roughly 60% H_2 by energy. The effects of H_2 substitution on exhaust emissions, operating efficiency, and combustion were investigated.

Stousland and Bottelberghe were both able to achieve significant H_2 substitution before the knock limit was reached. Both found that as operation approached the knock limit, the peak cylinder pressure increased and occurred earlier in the cycle. Bottelberghe additionally found that the ACERT ECM compensated for H_2 addition by advancing the injection timing and adjusting boost pressure. Stousland observed a slight increase in operating efficiency up to a point at each speed tested, after which the efficiency began to drop. Bottelberghe observed a decrease in engine efficiency with the addition of H_2 up to a point, after which the efficiency began to increase. The difference in these observations may be due to the different fuel delivery systems on the two engines. The engine Stousland used for testing was a mechanically injected, mechanically governed engine, while the engine Bottelberghe used was ECM controlled with a HPCR fuel system and unit injectors. The presence of H_2 may have initially increased the combustion efficiency of the mechanically injected engine by promoting better fuel preparation.

In both prior research projects at the NDSU engine research lab, the engine was run only at 50% load, initially due to engine limitations with a mechanical fuel injection system, and later to compare directly with previous research. The research presented in this paper is aimed at expanding understanding of the H_2 substitution limit over a broader range of operating conditions. In the future, being able to control injection timing (and other operating parameters) via an aftermarket ECM would allow for a more systematic investigation of dual-fuel combustion.

4.2. Dual-Fuel Combustion

There are three main H_2 injection strategies for dual-fuel diesel-hydrogen engines: manifold injection, port injection, and direct injection. Manifold and port injection can be either continuous or intermittent. Direct injection is always intermittent.

In manifold injection, H_2 is introduced into the intake manifold. Introducing the H_2 a distance upstream from the intake valve ensures adequate time to form a homogeneous mixture of H_2 and air. Manifold injection is often done in a continuous manner by passing H_2 from a high pressure storage tank through a pressure regulator and needle valve to control the flow rate. One of the main advantages of continuous manifold injection is a low implementation cost in terms of both price and complexity. The main disadvantage is that a portion of the incoming air is displaced by H_2, lowering the volumetric efficiency of the engine. This is termed the displacement effect, and is particularly distinct with H_2 due to its low density.

In port injection, H_2 is introduced near the intake valve. For consistent mixture formation, a H_2 injector capable of injecting H_2 timed to intake valve opening is necessary. Increased complexity and the high cost of gas injectors coupled with failure to resolve the undesirable displacement effect give port injection a poor cost/benefit ratio compared to manifold injection. In addition, Saravanan and Nagarajan [16] report negligible differences between manifold and port injection operation.

In direct injection, H_2 is introduced directly in the combustion chamber after intake valve closure. This type of injection strategy requires expensive double injectors for dual-fuel operation. The main advantage of direct injection is the elimination of the displacement effect. For the reasons indicated, this method will not be considered here.

Dual-fuel combustion differs from diesel-only combustion. Using either of the first two H_2 injection methods, the mixture of air and H_2 can be considered homogeneous when it enters the combustion chamber. This increases the fuel available during the premixed burning period of combustion (assuming the H_2 concentration is at least at the LFL). As H_2 is added in dual-fuel combustion, the constant volume combustion portion of the air-standard dual cycle is increased and the constant pressure portion is decreased. This is because of the increase in premixed fuel which burns rapidly following start of combustion (SOC). As H_2 percentage increases, the combustion cycle approaches the ideal Otto cycle. The shift in the combustion cycle can be seen in Figure 9. Cycle 1-2-xa-3a-4 represents a typical diesel-only combustion cycle. Similarly, cycle 1-2-xb-3b-4 represents operation of dual-fuel diesel-H_2 combustion, where a higher percentage of the total fuel is burned in the premixed burning phase (2-xb). Finally, cycle 1-2-3-4 represents the Otto cycle. As engine operation shifts towards the Otto cycle there is a theoretical increase in engine efficiency, as indicated by the increasing area enclosed within the curves. As will be discussed later, a real increase in engine efficiency is often observed during dual-fuel operation.

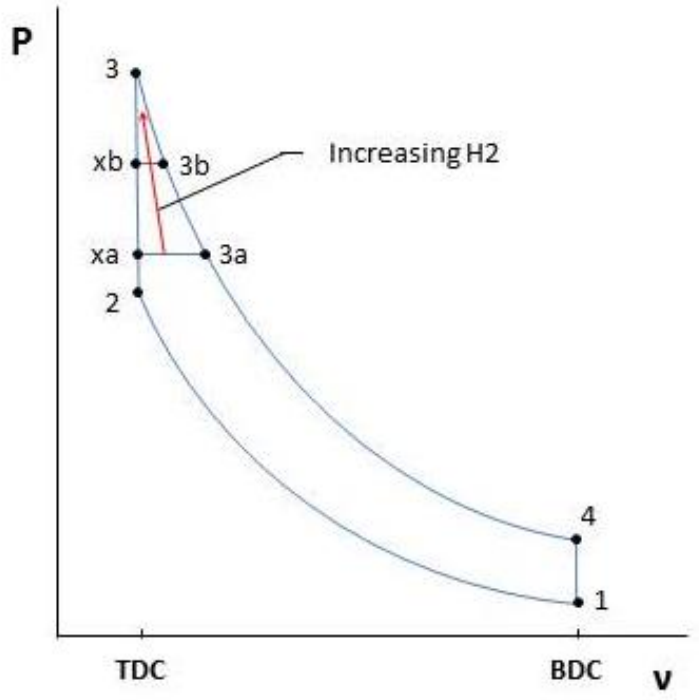

Figure 9. Shift in air-standard cycle with increasing hydrogen percentage.

More fuel burned during the premixed burning period leads to an increase in the heat release rate (HRR) at the beginning of combustion and a faster rate of pressure rise: these results are verified in the literature [16] [25] [15]. A higher peak pressure occurring earlier in the cycle would result from the increased HRR. This is consistent with work performed at NDSU [33] and elsewhere [25] [20] where peak pressure increased and occurred earlier in the cycle with increasing H_2 percentage.

The effect that H_2 addition has on ignition delay has been investigated by several authors. Factors that affect the ignition delay in dual-fuel diesel-H_2 engines are: temperature, pressure, and charge concentration. Changes in the physicochemical properties and pre-ignition reactions make dual-fuel ignition delays different from diesel-only [34]. In an investigation by Lata and Misra, ignition delay decreased as load increased across all H_2 fuel substitutions up to 50%. Ignition delay increased at each load until 20-30% H_2 substitution, then decreased up to 50% H_2 substitution [34]. Similar results were obtained with LPG substitution. It has been shown that the ignition delay has an Arrhenius temperature dependence, with increased ambient temperature reducing ignition delay [35] [26]. At higher load conditions, residual cylinder temperature increased. This explains the decrease in ignition delay with increasing load. It is suggested that the initial increase in ignition delay was caused by a reduction in the partial pressure of oxygen due to gaseous fuel aspiration or by unknown pre-ignition reactions [34] [36] [37]. Contrary to rest of the literature reviewed, Szwaja and Grab-Rogalinski report a decrease in ignition delay with the addition of 5% H_2 [25].

Tomita et al. [18] report an increase in ignition delay of a dual-fuel engine with advanced diesel injection timing. Fuel injected at advanced timing would be injected at a lower cylinder temperature, causing increased ignition delays, and likewise, fuel injected later in the compression process would be injected at a higher cylinder temperature, resulting in reduced ignition delays.

Naber and Siebers [35] investigated the ignition delay of H_2 using a constant volume combustion chamber. They reported a decrease in ignition delay with increasing fuel temperature. However, fuel temperature had less of an effect on ignition delay than ambient air temperature. They also identified ambient pressure and, H_2O, CO_2, and O_2 concentration as having a small effect

on ignition delay. This suggests pre-ignition reactions, rather than reduced O_2 as being the dominant mechanism in the initial increase in ignition delay in dual-fuel engines.

Many times it is assumed that H_2 burns completely when supplied to a diesel engine. Research has shown this is not true. Gatts et al. [38] investigated the H_2 emissions and combustion efficiency of a dual-fuel diesel-hydrogen engine. A modern, 6-cylinder heavy-duty engine with a Variable Geometry Turbocharger (VGT) and cooled EGR was used for testing. It was found that at low loads (10%), combustion efficiency of H_2 was low, in the range of 75-80%. As load was increased up to 70%, H_2 combustion efficiency came into the range of 95-98%. Only a slight increase in H_2 combustion efficiency was observed with increasing H_2 percentage.

The limiting factor on the amount of H_2 that can be substituted in dual-fuel combustion is knock. Understanding and mitigating knock is vital to achieving higher H_2 substitution percentages to reduce oil consumption. The increased burn rate of H_2 leads to higher in-cylinder temperatures and pressures during combustion. This can lead to excessive rates of energy release, causing a high rate of pressure rise. One method to mitigate knock is exhaust gas recirculation (EGR). The presence of exhaust gases in the combustion chamber lowers the temperature and slows the combustion process. Another similar method is intake charge dilution. An inert gas such as N_2 or He is added along with H_2 during intake. The gas does not take part in the combustion reaction, but serves as a heat sink, lowering the combustion temperature. It has also been proposed that DI of H_2 can help to mitigate knock [27]. By being able to control the timing and amount of H_2 added, pre-ignition could be eliminated and knock could be better controlled. This method would be benefited by the development of a double injector for both diesel and H_2 injection [27]. Knock could also be controlled by varying diesel injection timing to control the timing of peak pressure relative to TDC. Changing the injection timing would also change the ignition delay period, affecting the amount of premixed fuel, and thus the rate of pressure rise, during the premixed burning period.

4.3. Knock Mechanisms

Engine knock is the main limiting factor in the amount of H_2 that can be substituted in a diesel engine. Engine knock can be defined as a combustion event producing abnormally high

pressures and temperatures after the normal initiation of combustion. This phenomenon can manifest itself in two different ways: the first will be referred to as end gas knock, the second as diesel knock [38]. One or both types of knock may be present during dual-fuel operation.

End gas knock can be defined as the autoignition of the end gas region toward the end of combustion. This type of knock is typically associated with gasoline engines. As the flame front propagates through the premixed air-fuel charge, the gases behind the flame front, which are already burned, are at much higher temperature and thus expand. This expansion compresses the gases ahead of the flame front which are called end gases. If the end gases are compressed enough, autoignition may occur in the end gas region. This results in a high energy release rate which produces abnormally high temperatures and pressures and sends a pressure wave though the combustion chamber [31].

Diesel knock can be defined as an excessive rate of pressure rise [39]. This can occur when the pre-mixed charge at the start of combustion is large and burns rapidly. This causes excessive loads and is accompanied by increased operating noise. In an engine burning only diesel, this occurs when a large quantity of the fuel reaches a combustible mixture during the fuel preparation phase, such as with a low-Cetane fuel. In dual-fuel operation, a larger quantity of pre-mixed fuel is available at the start of combustion from the gaseous fuel content. When H_2 is used as the gaseous fuel, diesel knock is especially significant due to the fast burn rate of H_2. Liu and Karim [40], in a study on the knock characteristics of dual-fuel engines, concluded that the range of operating conditions that will produce knock is wider with H_2 than with other gaseous fuels.

Injection timing plays an important role in the heat release process and consequently in controlling knock. In a study by Miyamoto et al. [13], the maximum rate of pressure rise decreased as diesel injection was retarded from TDC to 6° ATDC in a naturally aspirated engine with 10.3% by volume H_2. This can be explained by combustion occurring at lower cylinder pressures as injection moves away from TDC and into the expansion stroke. Roy et al. [41] also reported a decrease in the maximum rate of pressure rise with retarded injection timing at different equivalence ratios in a supercharged engine operating on around 90% H_2 by energy. Injection timings tested were in the range of 4°-18° BTDC. A comprehensive study of the effect of diesel injection timing on the rate of

pressure rise in a dual-fuel diesel-hydrogen engine could help solve the problem of diesel knock. Tomita et al. [18] reported on the effect of diesel injection timing on the heat release rate of a dual-fuel engine. The heat release rate is related to rate of pressure rise except it is independent from the component of cylinder pressure from compression/expansion of the piston. Similarly, they found that retarding the diesel injection timing reduces the rate of heat release in the approximate range of 30° BTDC-5° ATDC. At significantly advanced injection timings, in the range of 30°-60° BTDC, the rate of heat release was found to increase when injection was retarded.

Other factors also affect the knock in dual fuel engines. Selim [22] reports that lowering the compression ratio retards the onset of knock in dual-fuel engines operating on LPG, methane, and natural gas. This is intuitively consistent with an understanding of diesel combustion since cylinder pressures in general are lower at lower compression ratios. Selim also reports a decrease in the rate of pressure rise as engine speed increases. This could be because, assuming a similar combustion event with respect to time, the engine travels through a greater CAD, lowering the pressure rise per CAD.

4.4. Knock Detection

Knock should be avoided for its negative effects on engine durability and performance. In order to avoid knock, it is necessary to identify when knock is occurring. End gas and diesel knock can both be detected audibly. End gas knock produces a characteristic “pinging” noise from the pressure wave created by the rapid combustion of the end gases. The tone of an engine with diesel knock is harsher than during normal operation. These methods of audible detection are unquantifiable and rely on an experienced ear, and therefore, are not well applied in scientific studies.

Other forms of knock detection can be classified as either indirect or direct methods. Indirect methods rely on the measurement of parameters outside the combustion chamber such as engine block vibration. The advantage of indirect methods is that they are cheaper to implement - from both a price and computational standpoint – than direct methods. This comes at the cost of decreased accuracy and effectiveness over direct methods. Direct methods measure in-cylinder

parameters directly: in-cylinder pressure being the most often used parameter. The sensors are costly since they are subject to the harsh in-cylinder conditions during combustion [42].

Burgdorf and Denbratt [43] compared a number of in-cylinder pressure based methods for end gas knock detection. The following methods were compared: maximum amplitude of bandpass filtered pressure, integral of bandpass filtered pressure, KI20 (a variant of the integral of bandpass filtered pressure), peak cylinder pressure, peak rate of pressure rise, third time derivative of cylinder pressure, and power spectral density. Of these, the maximum amplitude of cylinder pressure was least sensitive to the frequency window selected for analysis. By this method, a band pass filter is used to select the frequency range of interest, typically in the range of 5-25 kHz. End gas knock is then defined as when the maximum amplitude of the filtered pressure is greater than an experimentally determined threshold value.

Diesel knock can also be detected from the in-cylinder pressure signal. The rate of pressure rise can be found by taking the first derivative of the pressure signal with respect to crank angle. In order to avoid erroneous peaks due to high frequency pressure oscillations, the signal should first be filtered to obtain a smooth pressure curve. The maximum value of the rate of pressure rise can then be compared to a threshold value to identify diesel knock. A value of 6 atm/CAD is suggested in the literature [39].

While knock detection methods are well established, it also needs to be shown that these same methods can be applied to dual-fuel operation. In a study by Swaja, Bahandary, and Naber, it has been confirmed that this is the case [44]. The main difference is a shift to higher frequencies due to a change in the speed of sound in the cylinder with the presence of H_2.

4.5. Engine Performance in Dual-Fuel Operation

Hydrogen addition is generally reported as having a positive effect on the thermal efficiency, though the results vary somewhat. There are a number or sources that report an increase in thermal efficiency across all loads [14] [16] [17] [45] [46]. These researchers all used small, single-cylinder, naturally aspirated engines. It is difficult to tell from these papers what amount of H_2 is being added. Others report a drop in thermal efficiency with the addition of H_2 at

low loads, but an increase at high loads [19] [37]. In these papers, 50% or more H_2 substitution is being used. In an investigation by Lambe and Watson [19], water injection was used at high engine loads to avoid engine knock. Shirk et al. reported changes in efficiency for 5% and 10% H_2 substitution on a 1.3L engine at 8 steady-state points. The points at high engine speeds showed a consistent increase in thermal efficiency with H_2 substitution, while the results at low speeds did not show a consistent trend. Finally, there are those that report little or no change in thermal efficiency with H_2 substitution such as Tomita et al. [18].

Manifold injection of H_2 for dual-fuel operation is simple and low-cost, making it a widely used solution. Because a portion of the incoming air is displaced by gaseous H_2, power density is limited. The solution is to directly inject the H_2 into the combustion chamber. By switching from manifold H_2 injection to direct H_2 injection, a theoretical power density increase of 38% is possible under 100% H_2 operation [24].

Injection timing plays an important role in engine performance. In the case of dual-fuel diesel-hydrogen operation, the diesel fuel initiates combustion. Advanced injection timings generally lead to higher peak pressure and combustion temperatures. This is beneficial for power, but also increases NO_x emissions. Retarded injection timings generally reduce NO_x emissions and the occurrence of knock, but limit the engine power.

Roy et al. [40] investigated the effect of diesel injection timing in a dual-fuel engine with various gaseous fuels containing H_2. In their experiments with H_2 as the sole gaseous fuel, H_2 accounted for approximately 90% of the energy supplied for combustion. Compared to the other gaseous fuels tested, H_2 was limited to lower power and equivalence ratios to avoid knock. At a constant φ, retarding timing led to a drop in thermal efficiency and peak cylinder pressure.

4.6. Emissions in Dual-Fuel Operation

One large benefit of dual-fuel diesel-H_2 engines is their potential to greatly reduce the amount of CO_2 emissions by reducing the overall carbon content of the fuel. Hydrogen addition also tends to lower smoke emissions in diesel engines. These two benefits are typically countered by an increase in NO_x emissions.

There are three main mechanisms for NO_x formation: thermal formation, prompt formation, and N_2O intermediate mechanism. Thermal formation is due to the Zeldovich mechanism which is when O_2 molecules split into two oxygen atoms and attack N_2 molecules to form NO. This reaction starts around 1000 C and increases drastically beyond 1300 C [32]. This form of NO_x formation is the most prevalent in dual-fuel diesel-H_2 combustion. The prompt mechanism is observed in rich fuel zones and is due to the formation and subsequent oxidation of HCN. This mechanism is of little importance in diesel engine NO_x formation [32]. The N_2O intermediate mechanism is of importance only at low engine loads [47].

In the literature, it is typically reported that H_2 addition to a diesel engine has the effect of increasing NO_x and reducing particulate matter (PM or smoke) emissions. [14] [15] [17] [18]. These two emissions are of primary importance since they are subject to governmental regulations. The tradeoff where NO_x increases when PM decreases and PM increases when NO_x decreases is inherent in any diesel engine, whether dual-fuel or not. High combustion temperatures favor the formation of NO_x as well as the oxidation of PM, whereas low combustion temperatures tend to subdue NO_x formation but decrease PM oxidation. Given the higher flame temperature of H_2 than diesel it follows that H_2 combustion would increase NO_x while reducing PM. Since PM is composed of carbon-containing compounds, reducing the available carbon in the combustion chamber by replacing diesel with H_2 would also have the effect of decreasing PM emissions.

Hydrogen addition to a diesel engine reduces CO_2 emissions, and typically, CO and HC emissions as well. These carbon-containing emissions are expected to decrease from replacing a portion of the diesel fuel by H_2. In many cases CO and HC emissions of a diesel engine are already low enough to be of little interest.

H_2 addition, then, leaves the problem of high NO_x emissions to solve. Researchers have sought the solution to this problem in varied ways: changing injection timing, using EGR, using charge dilution, or using a Selective Catalytic Reduction (SCR) system. Many of these methods are already established as means to reducing NO_x during diesel-only operation.

By retarding injection timing so that ignition and combustion occur later in the cycle, especially after TDC, the in-cylinder temperatures and pressures will be lower, leading to lower

combustion temperatures. This is why retarding injection timing has the effect of reducing NO_x during dual-fuel combustion. This explanation is supported by the results of Roy et. al [21] [41], Tomita et al. [18], Miyamoto et. al [13], and Lilik et al. [20].

EGR is well established as a means to reducing NO_x. The recirculated exhaust gas acts as an inert heat sink, reducing combustion temperatures. Since H_2 has the effect of greatly reducing PM emissions, EGR can be used, even in relatively high quantities, to reduce NO_x emissions. Both Saravanan et Al. [14] and Bose and Maji [17] achieved a reduction of both NO_x and PM over diesel-only by using a combination of H_2 and EGR.

Charge dilution is another method for reducing NO_x which works on the same principle as EGR: an inert heat sink will reduce combustion temperatures, thereby reducing NO_x. Instead of using recirculated exhaust gas though, an inert substance from an external source is added. Roy et al. was able to achieve zero NO_x emissions by using 40-60% dilution with N_2. This method greatly limits the power density possible since a large portion of the incoming air is being displaced by an inert diluent.

In order to meet the stringent Final Tier 4 EPA regulations, many major diesel engine OEMs employ the use of an SCR system to reduce NO_x. An SCR system consists of a Diesel Exhaust Fluid (DEF) injector, a mixer, and a catalyst. DEF, which is a urea solution, is mixed with the exhaust gases and passed through a catalyzed substrate where the NO_x compounds are reduced to N_2 and H_2O. Saravanan and Nagarajan [16] have demonstrated the use of an SCR system with a dual-fuel engine. The NO_x emissions from a diesel engine are typically composed of mostly NO. In order for a SCR system to be effective, it is desirable to have the NO_x emissions divided evenly between NO and NO_2. The effect of H_2 addition on NO_2/NO_x ratio has been investigated by several authors. Chong et al. [47] report an increase in both NO_2 and NO_x when using H_2 and reformate gas in a diesel engine. Liu et al. [46] found that adding small amounts of H_2 increases NO_x very slightly, however greatly increases the NO_2/NO_x ratio. The ideal NO_2/NO_x ratio was only observed at low loads. They also reported that unburned H_2 is an important factor in NO_2 formation: more unburned H_2 leading to higher levels of NO_2. Lilik et al. [20] reported a decrease in NO and an

increase in NO_2 with increasing H_2 up to 15% by energy. These studies indicate dual-fuel combustion with H_2 as being favorable for NO_x conversion by an SCR system.

CHAPTER 5. RESEARCH APPROACH

5.1. Experimental Setup

A CAT C6.6, 6.6L, 6-cylinder diesel engine equipped with ACERT technology was used for testing. ACERT is a combination of technologies including a solenoid-actuated wastegate turbocharger, high-pressure common rail fuel delivery, direct injection, and electronic control designed to meet U.S. EPA Tier 3 emissions standards. Additional engine details can be seen in Table 2.

Table 2. CAT C6.6 Engine Specifications.

CAT C6.6 Engine Specifications	
Cylinders	6
Displacement	6.6L
Bore	4.13 in.
Stoke	5.0 in.
Compression Ratio	16.2:1
Rated power	183 hp @ 2100 rpm
Peak torque	582 ft-lb @ 1400 rpm
Valves/cylinder	4

Load was applied to the engine with a Land & Sea DYNOmite 13" single-rotor water brake dynamometer. The engine and dynamometer were controlled using DYNO-MAX software and operator console. The water supplied to the dynamometer for load control also served to cool the dynamometer and was discharged to a floor drain.

An Optrand D322B1-Q-WJ optical pressure transducer was used to measure in-cylinder pressure. The transducer was mounted in place of the glow plug in cylinder 6 with the tip flush with the inside of the cylinder head.

Exhaust emissions were analyzed with a Nova 7466K exhaust gas analyzer which reads O_2, CO, and CO_2 in percent and HC, NO and NO_2 in PPM. Exhaust gas was continuously drawn through a probe, probe-mounted filter, and two internal filters before being analyzed for constituent composition. The probe was mounted in the exhaust elbow while the analyzer sat outside the test cell. Emissions constituent readings were displayed on digital readouts and recorded manually.

Hydrogen was continuously inducted into the engine intake between the turbocharger and aftercooler. The position was chosen to allow the H_2 to mix well with the incoming air before entering the cylinder. Hydrogen was supplied from high pressure bottles then passed through a regulator to reduce the pressure. After the regulator, the H_2 passed through a heat exchanger to bring it up to room temperature before passing through a mass flow meter.

A Fox Thermal Instruments model 10A thermal mass flow meter was used to measure H_2 flow rate. After the flow meter, a needle valve was used to control the flow rate of H_2 entering the intake. The needle valve was equipped with a motor and pulley system so it could be operated remotely during testing. The addition of the motorized needle valve for H_2 flow rate adjustment was an innovation of the author to increase test cell safety. A schematic of the H_2 induction system can be seen in Figure 10.

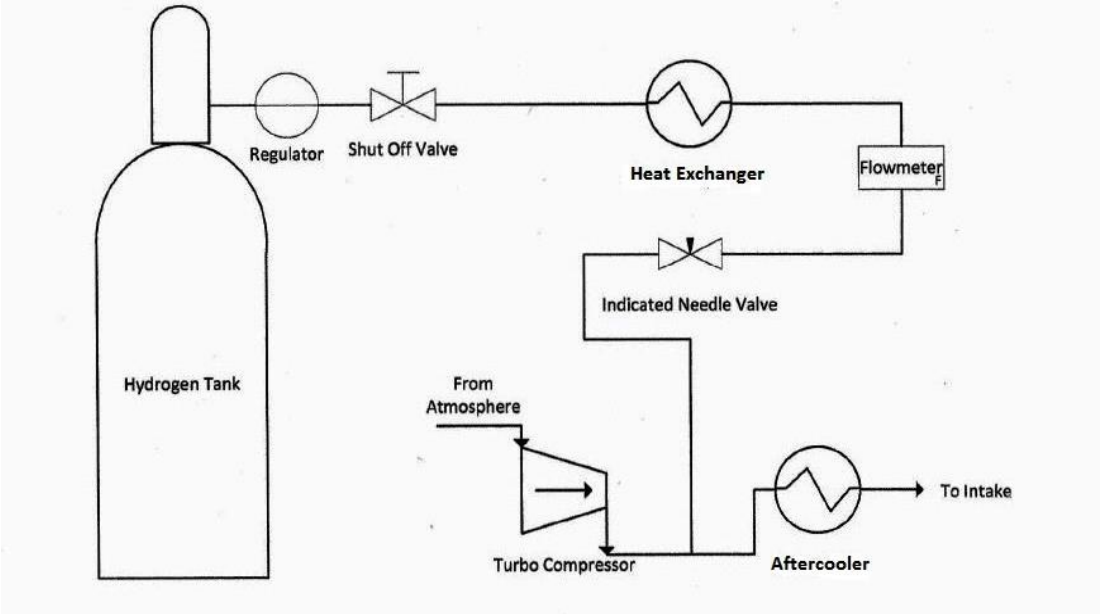

Figure 10. Schematic diagram of the hydrogen induction system.

Diesel fuel was delivered to the engine from a remote fuel tank. A fuel pump at the tank outlet ensured consistent delivery of fuel to the engine. The flow rate of diesel fuel was measured using a FloScan 236C flow meter.

An Omega JLD-612 PID temperature controller was used to control temperature of the engine coolant exiting the engine and the temperature of the air exiting the aftercooler. The flow rate of cooling water through the two heat exchangers was controlled by a circuit which included

two valves that ran on a 2 second cycle. During each cycle the valves would start closed, open, and close again. The length of time the valve was open depended upon the level of cooling required.

Pressure variations from the PID controlled valves opening and closing were detected in the water supply system. The variations were large enough to affecting the ability of the dynamometer to hold the engine at a steady load. In order to remedy this problem, a Well-X-Trol WX-202 water pressure damper was installed between the valves and the water supply.

Air to the engine was drawn from the test cell through a volumetric flow meter and air filter. A weather station recorded temperature, pressure, and humidity in order to calculate correction factors. Figure 11 shows a picture of the engine setup in the test cell.

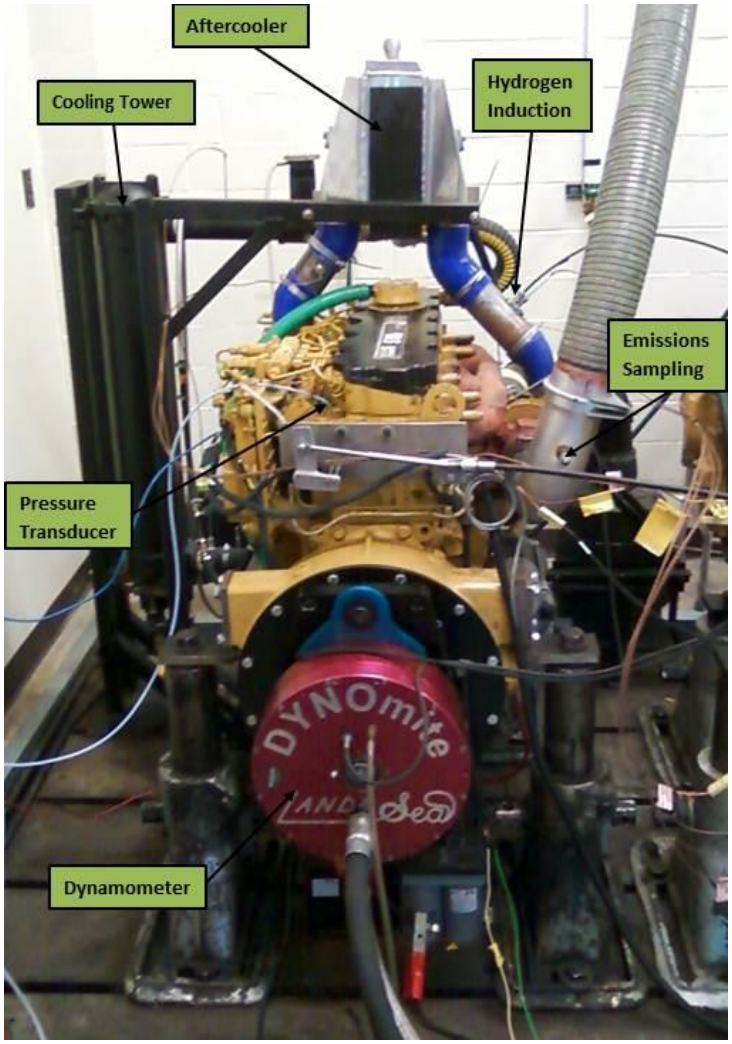

Figure 11. CAT C6.6 engine setup in test cell.

The engine was instrumented with thermocouples to record temperatures at compressor inlet, compressor outlet, coolant inlet, turbine inlet, and turbine outlet. Additionally there were thermocouples at coolant outlet and aftercooler outlet as inputs to the PID temperature controllers.

An inductive sensor mounted on the back of the engine was positioned to read at TDC. This signal was used to time in-cylinder events to crankshaft position.

5.2. Data Acquisition

Three types of data acquisition were employed during testing: high sample-rate, low sample-rate, and hand recorded.

A Measurement Computing (MC) USB-1208FS data acquisition system (DAQ) was used to capture high sample rate data. The MC DAQ had a total sample rate of 50 kHz with 4 differential analog inputs. Three signals were recorded using differential inputs yielding a sample rate of 16.6 kHz per channel. The resolution of the data at the highest engine speed (2100 rpm) was one sample every 0.76 degrees of crankshaft rotation.

The three signals recorded with the MC DAQ were: the pressure transducer signal, the inductive timing signal, and the injector pulse signal. The pressure transducer signal was read directly from the pressure transducer, which gave a 0.5-5 V output. A voltage dividing circuit was incorporated into the leads of the inductive sensor to bring the signal into the 0-5 V range. The signal sent from the ECM to the injectors was a 0-90 V signal. Since the maximum voltage range of the DAQ was ±20 V, an indirect means of recording the signal was used. Only the timing, not the magnitude, of the injector signal was of importance. Thus the injector signal was read by wrapping a length of wire around the insulated injector wire. The current traveling through the injector wire induced a signal in the wrapped wire by electromagnetic induction.

The MC DAQ was used in conjunction with a National Instruments LabVIEW program developed by the author to perform signal operations and write data to comma separated variable (CSV) files. Board time and the three signals from the DAQ were recorded directly. Board time starts at zero when recording is initiated and records in “real-time” along with the data. Additional signals that were recorded were: in-cylinder pressure calculated from the pressure transducer

signal, in-cylinder pressure after passing through a high-pass filter with a cutoff frequency of 4 kHz, in-cylinder pressure after passing through a low-pass filter with a cut off frequency of 2 kHz, and the derivative of the in-cylinder pressure after passing through the low-pass filter. Additionally, the LabVIEW program was used give a visual indicator of diesel knock. The derivative of the in-cylinder pressure was taken with respect to crank angle. The amplitude of this signal was monitored and a binary indicator would light up when it exceeded 90 psi/deg. Important elements of the LabVIEW front panel, which can be seen in Figure 12, include: waveform graphs of the various signals, the knock indicator, and the button to record data.

Low sample-rate data was also recorded. This was done at 2 Hz using the DYNOmite data computer included with the dynamometer software. Channels recorded with the DYNOmite DAQ were: board time, engine speed, engine torque, diesel flow rate, barometer, percent humidity, air temperature, and thermocouple readings (described in the previous section). Since the engine was run at steady state conditions, the low sample-rate data was averaged over 30 seconds.

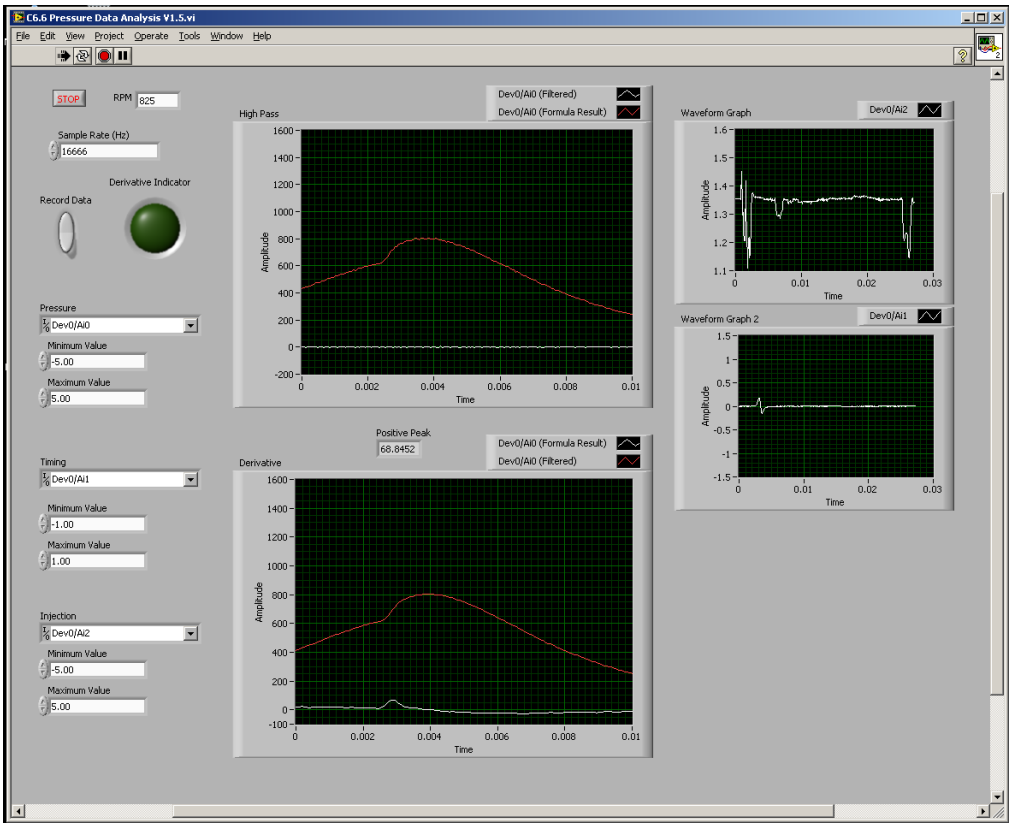

Figure 12. LabVIEW front panel.

Data from the exhaust gas analyzer was recorded by hand once per set-point during testing. Each exhaust gas constituent was displayed in an individual digital display. The H_2 flow rate was also recorded by hand at each set point.

5.3. Experiment Design

Testing was done in a steady state manner at a range of speed and load combinations. Four engine speeds were chosen for testing: 1300 rpm, 1500 rpm, 1800 rpm, and 2100 rpm. Around 1350 rpm, the ECM-controlled injection strategy switched from a single main injection to both a pilot and primary main injection. The 1300 rpm speed was selected to perform experimentation during single main injection operation. The 2100 rpm point was chosen since it is the rated speed of the engine. The 1500 rpm and 1800 rpm points were chosen as intermediate speeds to fill in the speed-load test matrix. Five different engine loads were chosen for testing: 25%, 50%, 65%, 77.5%, and 90%. The 50% load was chosen for comparison with past research at NDSU. The remaining load points were chosen to fill in the speed-load test matrix, with more points concentrated at higher loads, where there was more interest. Not all points in the test matrix could be reached; at 1300 rpm the dyno could not load the engine to 77.5% or 90% load and at 1500 rpm the dyno could not load the engine to 90% load. A chart of the operable and inoperable set points can be seen in Figure 13. An engine is typically not run at these low speed, high load points so their exclusion is acceptable.

Diesel-only runs were made at each of the matrix set points in order to characterize the change from diesel-only to dual-fuel diesel-hydrogen operation. In dual-fuel mode, H_2 was added at each set point until the LabVIEW program indicated the presence of diesel knock. This is the maximum amount of H_2 that can be safely added at each speed-load point.

Each speed-load set point was run at least three times to obtain statistical confidence in the results. The in-cylinder pressure data was analyzed by first averaging eight consecutive firing events to produce one pressure vs. CA curve for each separate run. The three (or more) pressure vs. CA curves were then averaged together to obtain a single curve for each set point.

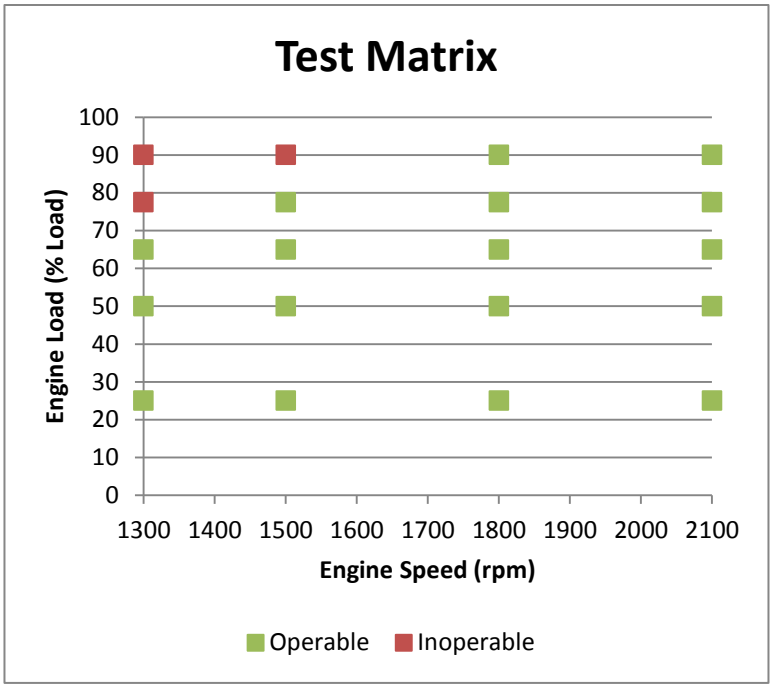

Figure 13. Operable and inoperable speed-load set points for the experiment.

5.4. Experimental Procedure

Before performing any testing, the engine was warmed up. Warm up was done by idling the engine for 5 minutes with light load (10-20 ft-lb). After idling, the engine was brought to 1200 rpm and additional load was applied until the engine-out coolant temperature reached 150 °F. Next, the engine was brought to the desired set point and allowed to reach equilibrium. Equilibrium conditions were identified as when the thermocouples read a constant temperature. For dual-fuel runs, H_2 was then added and manually adjusted until engine knock was indicated. As H_2 was added, diesel fuel was automatically reduced by the ECM to keep the engine speed approximately constant. A speed increase of around 30 rpm was seen with H_2 addition. This was corrected by adjusting the throttle and load to reach the original set point. For dual-fuel runs, H_2 flow was reduced to zero after each run. When testing was finished the engine was cooled down at idle for 5 minutes before being shut down.

A consistent data acquisition sequence was followed once equilibrium was reached at each set point. First, the LabVIEW program was started to read data from the MC DAQ. Next, the H_2

flow rate in standard cubic feet per minute (SCFM) was recorded for H_2 runs. Then, recording was started with the DYNO-max software and the board time was recorded for later reference. Next, approximately 2 seconds of data was recorded from the MC DAQ using the LabVIEW program. The file name was then recorded next to the DYNO-max board time for that run. After that, the emissions readings were recorded by hand from the exhaust gas analyzer. Finally, data recording from DYNO-max DAQ was stopped. Testing then proceeded to the next set point and the process was repeated.

Diesel-only testing and dual-fuel diesel-hydrogen testing were done separately. During diesel-only testing, testing was first done at 25% load. The order of the runs was to first make a single run at the lowest speed then move up to the next speed until the highest speed was reached. The sequence was then repeated two more times. For example, at 25% load the testing sequence was as follows: 1300 rpm – 25% load, 1500 rpm – 25% load, 1800 rpm - 25% load, 2100 rpm – 25% load, repeated two more times. Then the engine was brought to 50% load, 65% load, 77.5% load, and 90% load respectively. By testing in this sequence, the 3 runs at each set-point were spread out.

The dual-fuel testing sequence was done differently from the diesel-only sequence. First, all three runs at the lowest speed and load were run then all three runs at the next speed until the highest speed was reached. For example, all three runs were first done at 1300 rpm – 25% load, followed by all three runs at 1500 rpm – 25% load, 1800 rpm – 25% load, and 2100 rpm – 25% load. Since the speed and load needed to be adjusted at each set-point when H_2 was added, H_2 was being consumed during the adjustment. Once the adjustment was made, the H_2 could be shut off and reintroduced at that set-point without the need to readjust the speed or load. The reason all three dual-fuel runs at each set point were recorded in succession was to conserve H_2 usage. During dual-fuel testing, the H_2 was turned off between each of the runs at each set point and the engine was allowed to reach equilibrium before reintroducing H_2 for the next run.

CHAPTER 6. RESULTS AND DISCUSSION

The results and discussion chapter is split up into 3 sections: engine performance, combustion, and emissions. The first section will discuss the effects on percent H_2 substitution and thermal efficiency with H_2 addition up to the knock limit. The section on combustion will discuss the effects of H_2 addition on various combustion parameters such as the peak cylinder pressure, the shape of the in-cylinder pressure curve, the rate of pressure rise, and the injection timing. Finally, the effect on the emissions of NO_x, CO_2, CO, and HC from H_2 addition will be discussed.

6.1. Engine Performance

Engine power was held constant as H_2 was added up to the knock limit. The engine adapted to the induction of H_2 by reducing the amount of diesel fuel injected. Only slight adjustments were necessary to keep the engine at the same operating point during H_2 addition. Past research at NDSU [33] investigated H_2 addition up to the knock limit at only 50% load and 1300, 1800, and 2100 rpm. The current research expands the knock limit to a wider range of speeds and loads across the entire operating range of the engine. The maximum H_2 addition at each operating point can be seen in Figure 14, given in percent energy supplied to the engine. This was calculated by dividing the energy content of the H_2 by the total energy content of both H_2 and diesel. Hydrogen percentage at 25% load is not reported because the diesel flow rate for those cases was below the range of the diesel flow meter.

A maximum H_2 substitution of 74% was achieved at 2100 rpm and 50% load. At each rpm the maximum H_2 substitution decreased as load increased. This can be explained by observing the maximum rate of pressure rise (MRPR) at each rpm (as seen later in this chapter). As load increased at each rpm, the MRPR without H_2 also increased. Hydrogen has the effect of increasing the MRPR due to its rapid combustion and high flame speed. Since the H_2 substitution was limited by setting a threshold on MRPR, the lower loads, which had a lower MRPR to begin with, could be run with a higher percentage of H_2 before hitting the MRPR threshold for knock.

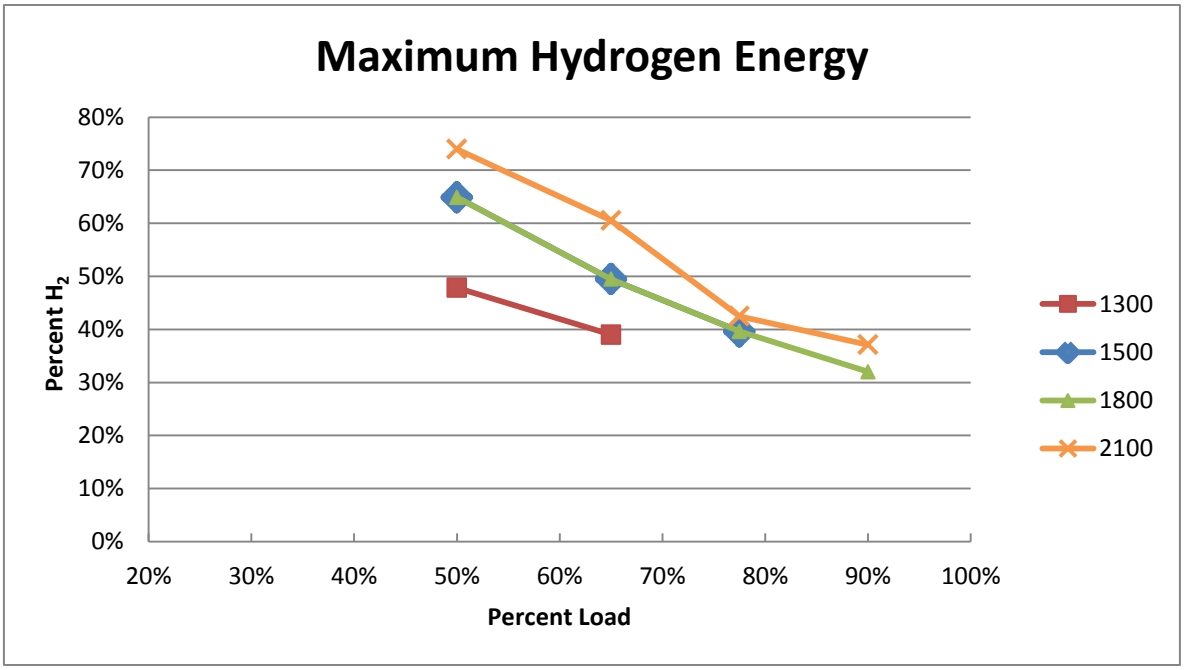

Figure 14. Hydrogen percentage at the knock limit on an energy basis.

It was also observed that at each load, maximum H_2 substitution increased with increasing engine rpm. Maximum H_2 percentages at 1500 and 1800 rpm were almost identical, with the max H_2 percent being lower at 1300 rpm at each load, and the max H_2 percent being higher at 2100 rpm at each load. Increasing H_2 substitution with increasing speed can be attributed to the reaction of the ECM to H_2 substitution.

Also of interest to engine performance is thermal efficiency. Thermal efficiency was calculated by dividing the measured engine power by the total rate of energy supplied to the engine. In dual-fuel operation, the total energy rate included energy from both diesel and H_2. Again, since the diesel flow rate was out of the range of the diesel flow meter during dual-fuel operation at 25% load, no thermal efficiency is reported at these points. The results of thermal efficiency for both diesel-only and dual-fuel operation are shown in Figure 15. The results show that thermal efficiency decreased with increasing load at constant engine speed. This is contrary to what is reported in most of the literature, where thermal efficiency increased with increasing load, peaking around 80% load [14] [15] [19] [37] [46]. The difference may be that injection timing was intentionally fixed in the literature, while in the current research injection timing was shifted by the ECM. As load was

increased injection timing was retarded, which releases the energy later in the cycle, leading to lower thermal efficiencies due to less work done per cycle.

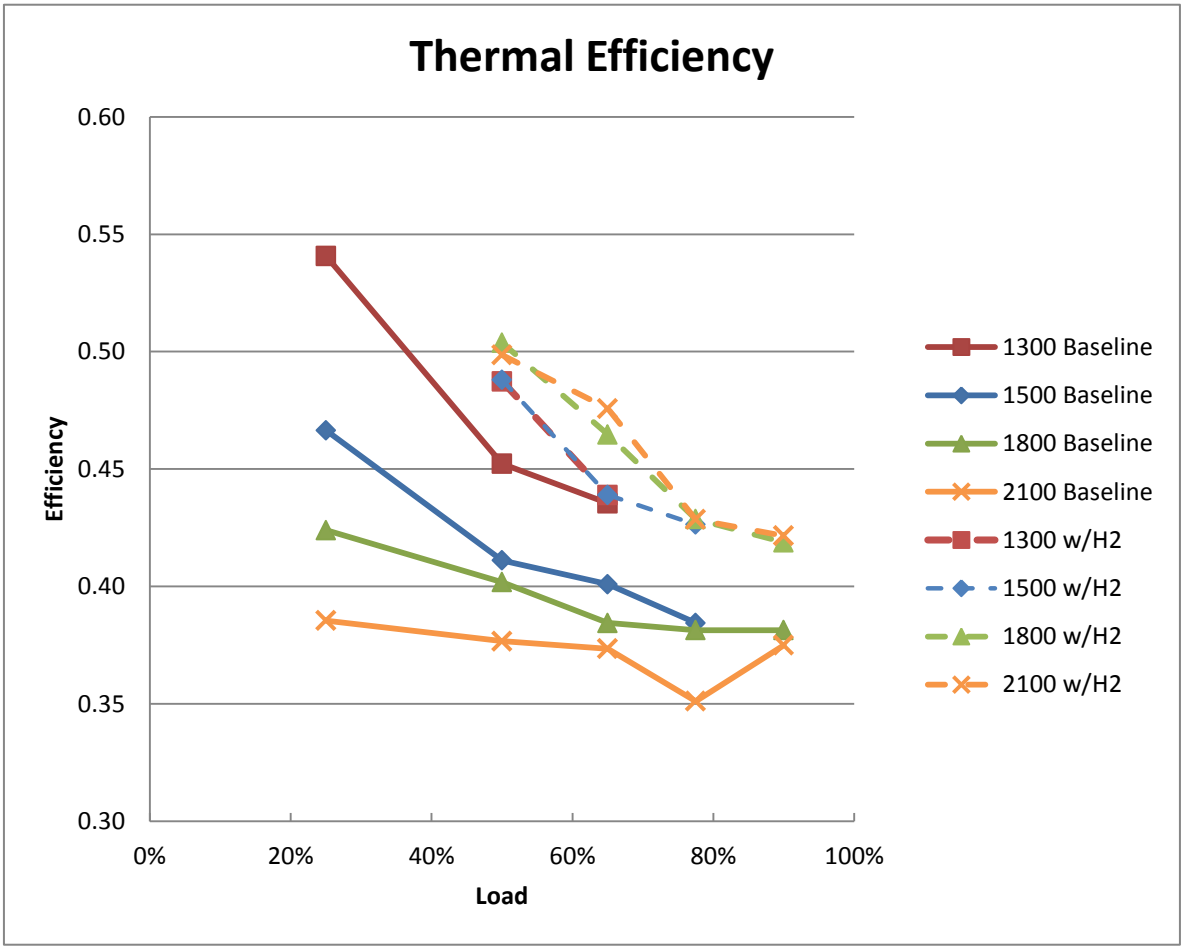

Figure 15. Thermal efficiency of both diesel-only and dual-fuel operation at different loads.

It was also observed that the thermal efficiency at each load decreased with increasing engine speed for diesel-only operation. There was not a clear trend in dual-fuel operation, except at 65% load, where the trend was reversed: the thermal efficiency increased with increasing engine speed. There are no results in the literature to compare this trend with since most research was conducted at a single engine speed.

Finally, the addition of H_2 increased the thermal efficiency of the engine between 32.4% and 0.8% at all speeds and loads, with all points increasing by at least 7.7% except for the 1300 rpm-65% load point. These results are in agreement with the literature, which widely reports increased thermal efficiency with H_2 addition. This increase makes sense based on the in-cylinder

pressure curves (shown later): with H_2 addition, there is a large energy release in the cycle between 1° and 12° after TDC, which produced a large amount of work. In the diesel-only combustion, the energy is released later in the cycle in a much more gradual manner, resulting in a "flatter" cylinder pressure trace. In addition, quicker combustion leaves less time for heat to transfer to the cylinder walls, which would increase thermal efficiency.

6.2. Combustion

Three different components of combustion will be discussed in the current section: the in-cylinder pressure curves, the in-cylinder rate of pressure rise, and the injection timing. In this section, data series labels beginning with a "B" indicate baseline or diesel-only operation, while those beginning with an "H" indicate operation with H_2 or dual-fuel operation. The number following the "B" or "H" is the percent load.

The in-cylinder pressure curves are important for understanding combustion. The changes to both the size and shape of the curves between diesel-only and dual-fuel operation will be discussed. At 1300 rpm both the size and shape of the in-cylinder pressure curves, which can be seen in Figure 16, changed significantly during dual-fuel operation. The pressure curve prior to the start of combustion shifted up with increasing load. This happens because boost pressure increases as engine power increases. At 50% and 65% load, the peak pressure increased by 40.0% and 27.8%, respectively, during dual-fuel operation. This is because of the rapid energy release of H_2 due to its high burn velocity. Peak pressure also occurred earlier in the cycle: 8° earlier at 50% load and 4.8° earlier at 65% load. In the 25% load case the peak pressure decreased under dual-fuel operation.

Dual-fuel combustion at 25% load at each engine rpm appears to have proceeded by a different means than the runs at 50% load and above. The combustion at 25% load will be discussed separately at the end of the pressure curve discussion and will not be included in the discussion of each engine speed.

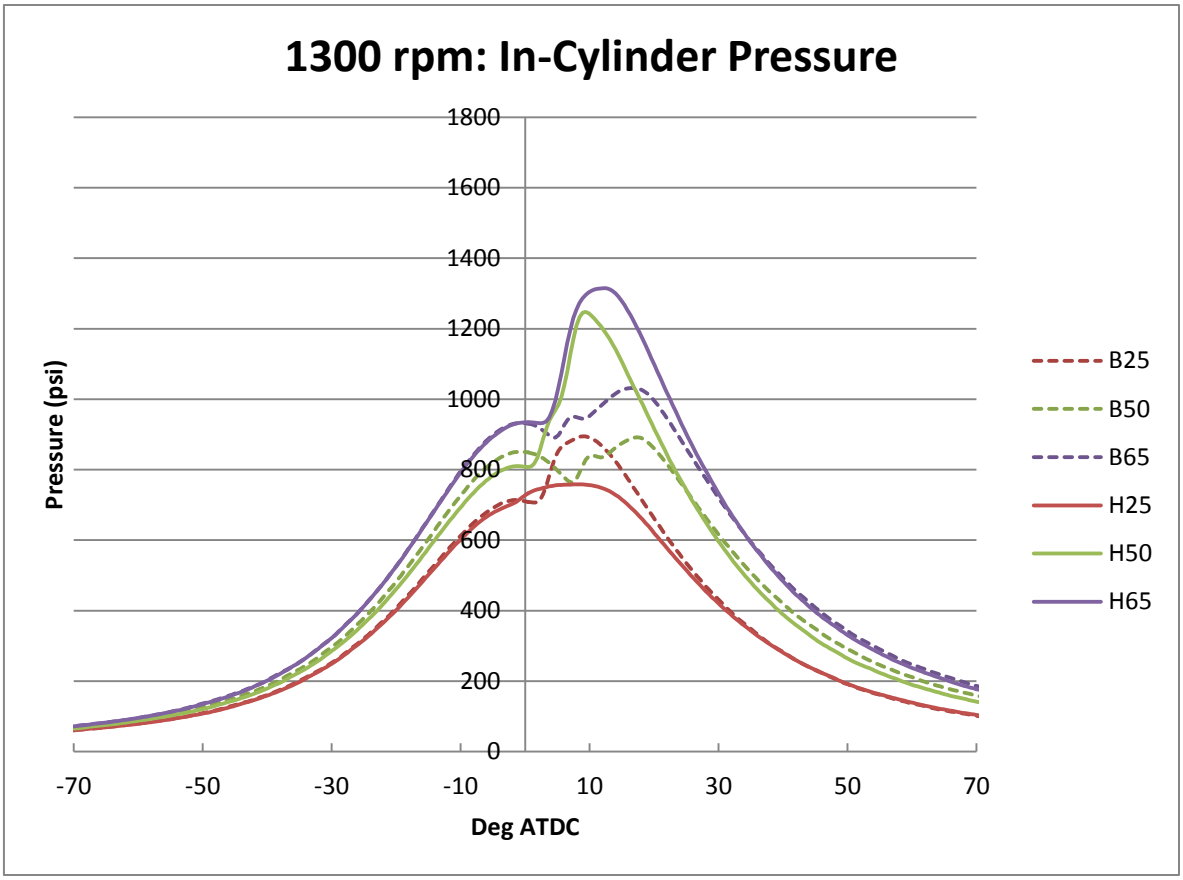

Figure 16. In-cylinder pressure curves at 1300 rpm.

At 1500 rpm the peak in-cylinder pressure increased at each load level during dual-fuel operation as can be seen in Figure 17. At 50%, 65%, and 77.5% load, the peak pressure increased by 30.7%, 20.8%, and 11.9%, respectively. Peak pressure occurred later in the cycle during dual-fuel operation at 1500 rpm. Peak pressure occurred 8.4°, 8.9°, and 9.1° later at 50%, 65%, and 77.5% loads, respectively. Under diesel-only operation, peak pressure occurred around TDC. With H_2 substitution, peak pressure was higher and shifted to later in the cycle at all loads. This can be explained by the fast burn rate of H_2 pushing peak pressure above the value at TDC during combustion. From the pressure curves, it is again observed that boost pressure increased as load increased. This is true for both diesel-only and dual-fuel operation. At each load level, the engine decreased boost pressure during dual-fuel operation relative to diesel-only. The drop in boost pressure with H_2 substitution may be due to a change in manifold air pressure from a reduction in the air flow through the compressor since a portion of the air was replaced by H_2.

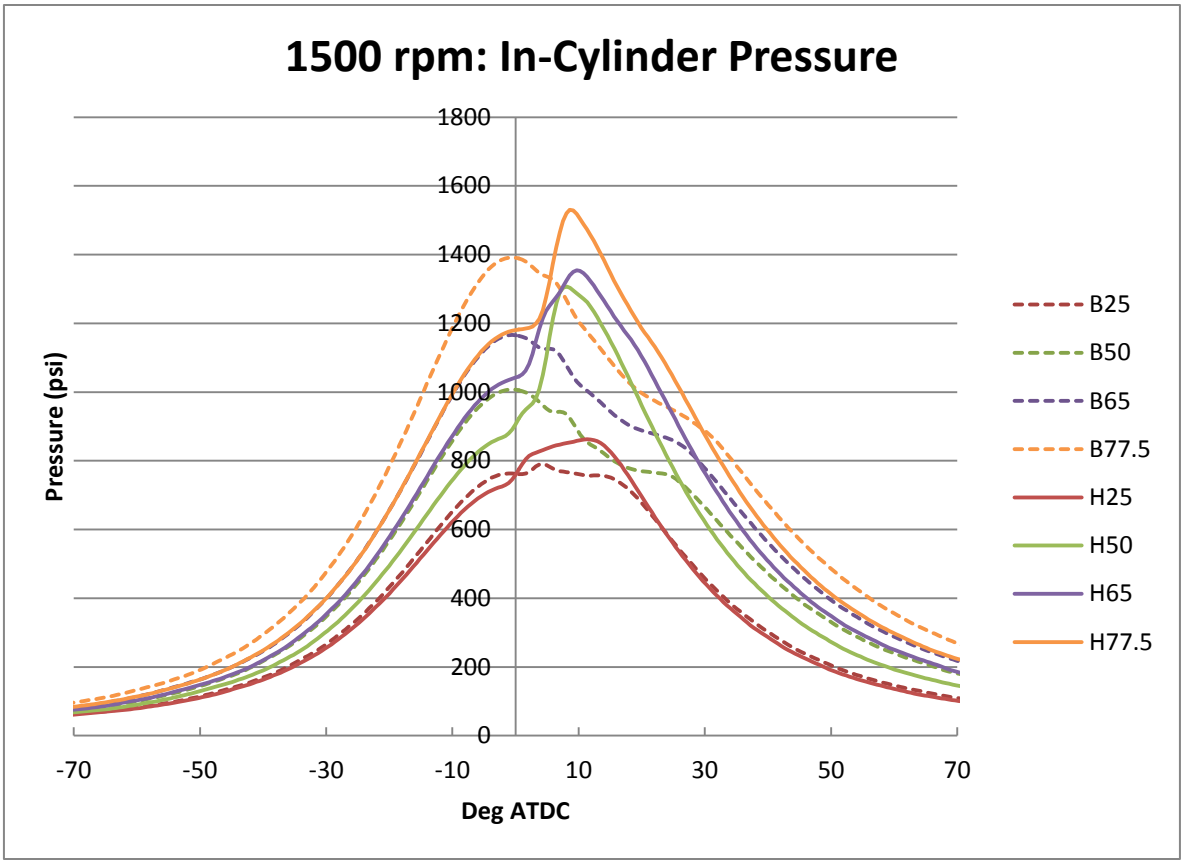

Figure 17. In-cylinder pressure curves at 1500 rpm.

The in-cylinder pressure curves at 1800 rpm can be seen in Figure 18. At 50%, 65%, 77.5%, and 90% load, peak pressure increased by 33.3%, 13.8%, 8.4%, and 9.4%, respectively, during dual-fuel combustion. Again, as H_2 was added, the engine reduced the boost pressure. Boost pressure was reduced by less at low loads compared to high loads, which led to larger increases in peak pressure at lower loads than at higher loads. The timing of peak pressure at 1800 rpm was similar to that at 1500 rpm: peak pressure occurred near TDC for diesel-only runs, and in the range of 10° ATDC for dual-fuel runs. For diesel-only runs, start of combustion occurred after TDC and the pressure rise was low enough that the cylinder pressure never exceeded the value at TDC. For dual-fuel combustion, pressure rise increased due to the high burn rate of H_2 and the peak pressure surpassed the value at TDC. At 50%, 65%, 77.5%, and 90% load, the timing of peak pressure occurred 2.6°, 8.9°, 6.3°, and 7.2° later, respectively, during dual-fuel combustion. At 1800 rpm, peak pressure increased more in dual-fuel operation at 90% load than at 77.5% load. The pressure curves indicate that the engine reduced boost to a greater extent during dual-fuel

operation at 77.5% load than at 90% load. This can be observed by looking at the difference in cylinder pressures at TDC between baseline and dual-fuel operation.

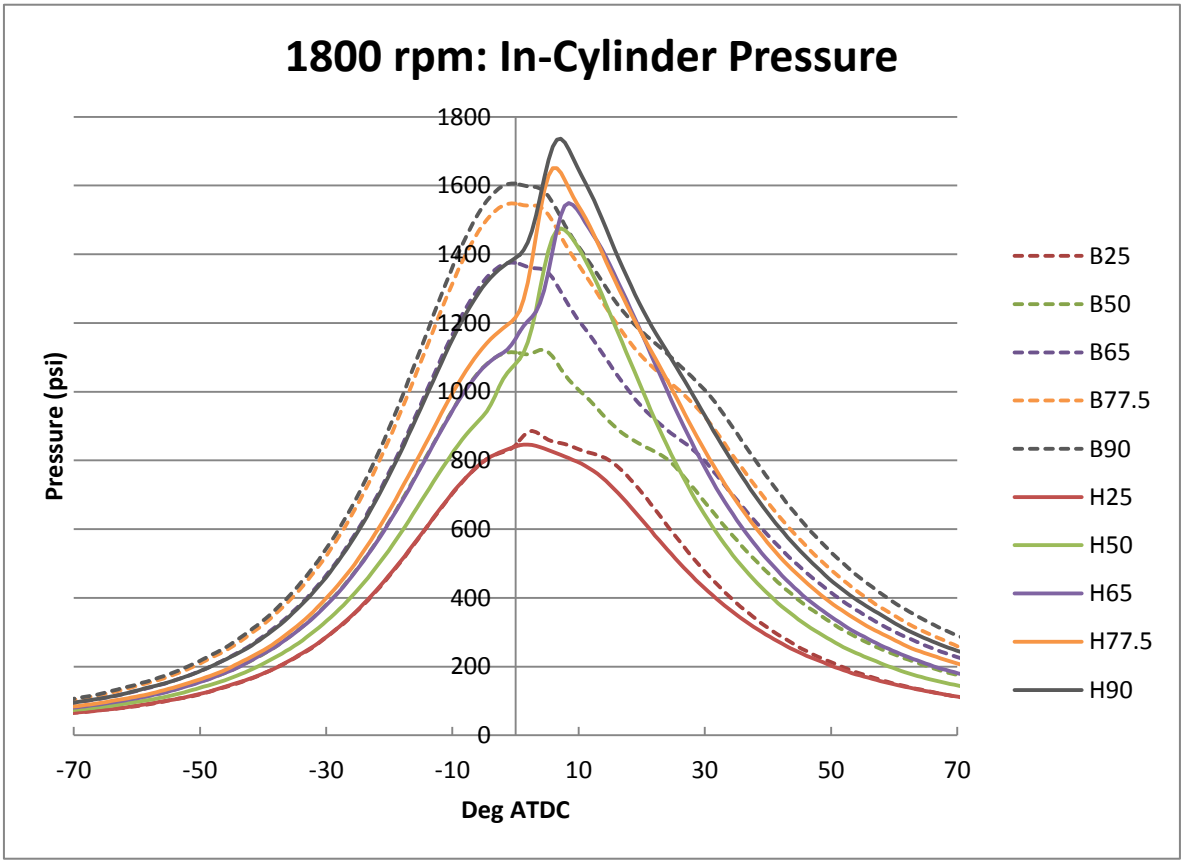

Figure 18. In-cylinder pressure curves at 1800 rpm.

The in-cylinder pressure curves at 2100 rpm, which can be seen in Figure 19, exhibited different behavior from 1500 rpm and 1800 rpm. At 50%, 65%, 77.5%, and 90% load, peak pressure increased by 22.7%, 11.8%, -3.1%, and 0.12%, respectively, during dual-fuel combustion. The percent increase in peak pressure between diesel-only and dual-fuel operation decreased as engine load increased, except for at 90% load where it increased from 77.5% load. At 2100 rpm, however, peak pressure actually decreased at 77.5% load during dual-fuel operation. The pressure curves reveal a significant reduction in boost pressure at 77.5% load. During dual-fuel combustion at 50%, 65%, 77.5%, and 90% load, the timing of peak pressure occurred 7.7°, 9.0°, 8.0°, and 5.9° later, respectively. The analysis of the change in peak pressure timing is similar to 1500 rpm and 1800 rpm: start of combustion ATDC combined with a low rate of pressure rise for diesel-only

combustion and a high rate of pressure rise for dual-fuel combustion lead to a peak pressure above the value at TDC during dual-fuel combustion, but not diesel-only combustion.

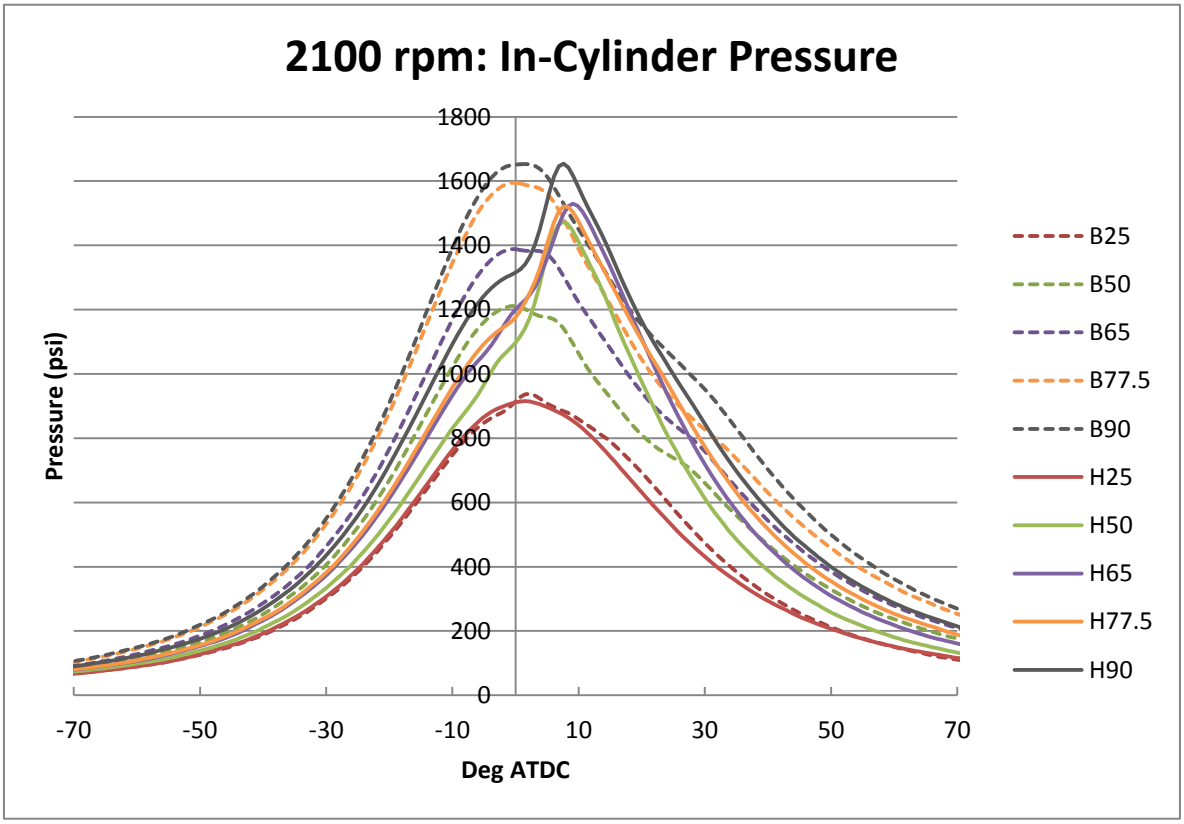

Figure 19. In-cylinder pressure curves at 2100 rpm.

As stated earlier, dual-fuel combustion at 25% load was different than dual-fuel combustion at all other loads. At 25% load, the rate of pressure rise never reached a value that tripped the knock detection trigger. Hydrogen was added until the engine started to "surge," then backed off until steady operation was achieved. A large variation in the shape of the pressure curves was observed, even at the same speed, load, and H_2 flow rate. Figure 20 shows a comparison of the average pressure curves from individual runs at 25% load-1300 rpm and 77.5% load-1800 rpm. Although the four runs at 77.5% load differ in magnitude, the basic profile shape remains the same. The runs at 25% load differ in shape in the rage of 0-25° ATDC. The reason for the variability in the shape of the run-averaged curves is inconsistency in the shape of the pressure curves for individual combustion events. The variability between combustion events for run 2 at 1300 rpm-25% load and run 1 at 1800 rpm-77.5% load can be seen in Figure 21. The individual cycle pressure curves at

77.5% load overlay each other, indicating stable combustion. The individual cycle pressure curves at 25% load are inconsistent from one cycle to the next, indicating unstable combustion. It is unclear simply from looking at the in-cylinder pressure data what caused unstable combustion during the 25% load cases. An analysis will be done at the end of the emissions section, which will provide additional data to assess.

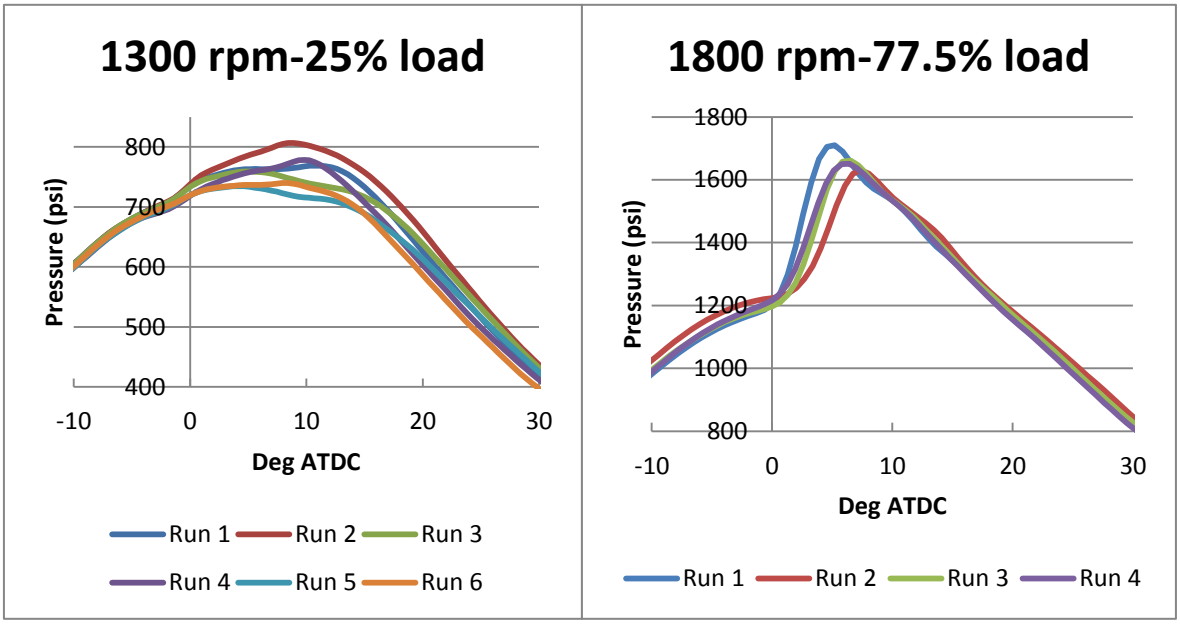

Figure 20. Comparison of variability in the shape of averaged pressure curves between 25% load and 77.5% load.

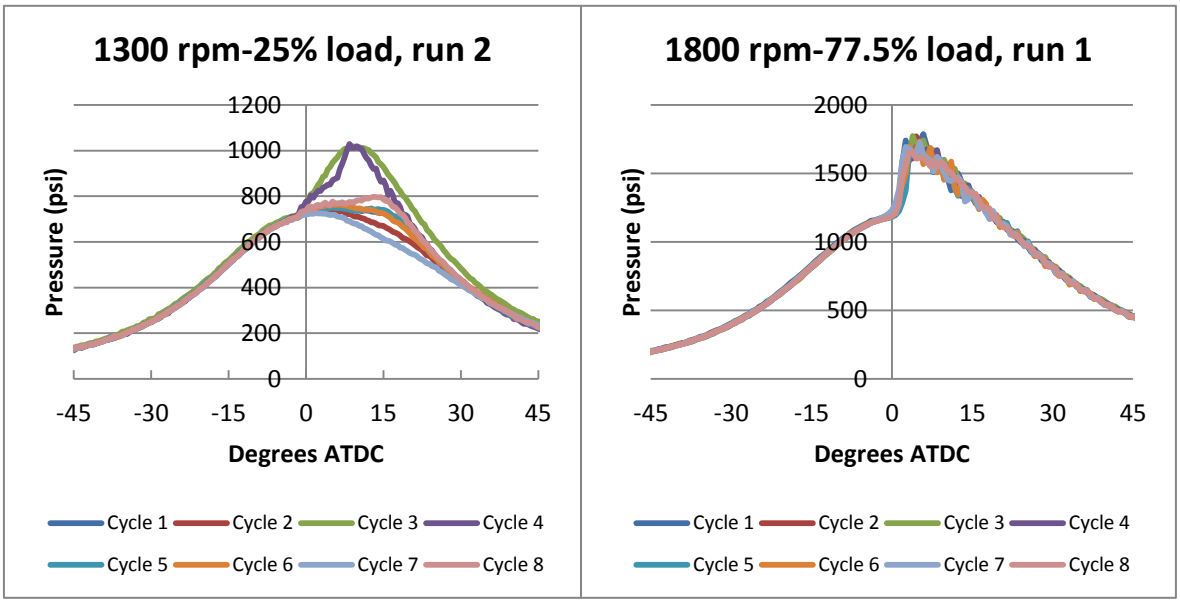

Figure 21. Comparison of the curves for individual combustion cycles between 25% load and 77.5% load.

The next parameter that is important to combustion analysis is the rate of pressure rise (RPR), which is calculated by taking the first derivative of the in-cylinder pressure curve. The maximum rate of pressure rise (MRPR) was used in this study to detect the occurrence of diesel knock at a threshold of 90 psi/deg. It can also be used to give an indication of the start of combustion (SOC) and the rate of heat release. Without a combustion event, the shape of the graph for the RPR would be symmetric about TDC as the example in Figure 22 shows. The point at which the measured rate of pressure rise deviates from the no-combustion curve would indicate SOC. The higher the peak above the no-combustion curve, the larger the heat release rate. Multiple peaks in the rate of pressure rise indicate multi-phase combustion [37]. An increased number of peaks can be thought of as indicating a more complex combustion process.

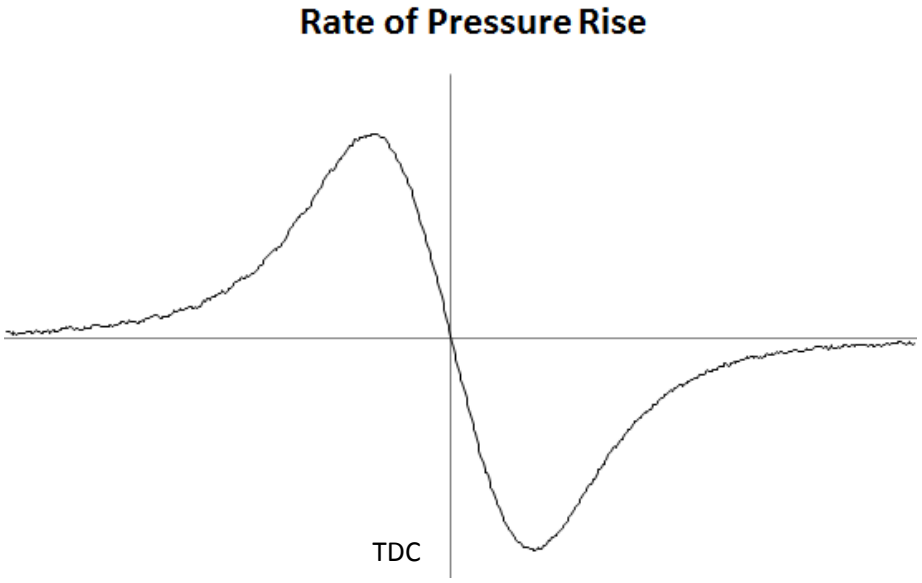

Figure 22. Example of the rate of pressure rise in the absence of combustion in a reciprocating piston engine.

The RPR curves for 1300 rpm can be seen in Figure 23. At 50% load and 65% load during dual-fuel combustion, the MRPR increased by 156% and 204%, respectively, compared to diesel-only combustion. Higher rates of pressure rise indicated an increase in the rate of combustion. The SOC also occurred earlier in dual-fuel combustion. Again, dual-fuel combustion at 25% load at all speeds was different, so the results for RPR differ from other load levels. At 1300 rpm MRPR decreased by 61% from diesel-only to dual-fuel combustion at 25% load.

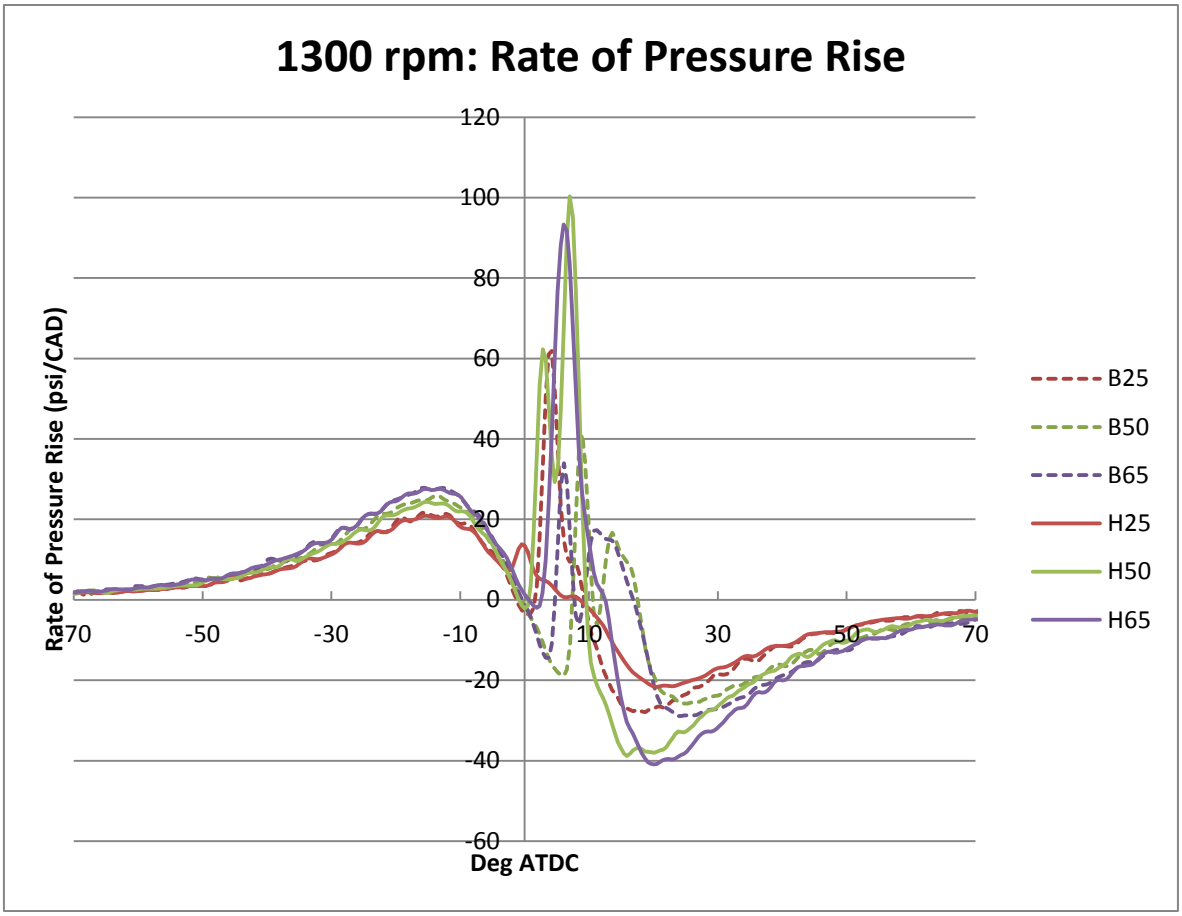

Figure 23. Rate of pressure rise curves for 1300 rpm.

The RPR curves for 1500 rpm can be seen in Figure 24. At 25%, 50%, 65%, and 77.5% load during dual-fuel combustion the MRPR increased by 39%, 281%, 215% and 190%, respectively, compared to diesel-only combustion. The curves also indicate an advanced SOC under dual-fuel combustion compared with diesel-only combustion. At 1500 rpm the MRPR at 25% increases during dual-duel operation, but to a much smaller degree than at other loads. The 50% dual-fuel case shows a small peak before the main peak. The double peak in the 65% load curve is a product of how the average rate of pressure rise curves for each run averaged together. In each case of diesel-only combustion, the MRPR occurs during compression, before TDC, and not during combustion. This is because of the relatively retarded SOC combined with the slower diffusion combustion mode. During dual-fuel combustion, the fast premixed burning phase dominates and the MRPR occurs during this phase of combustion rather than during compression.

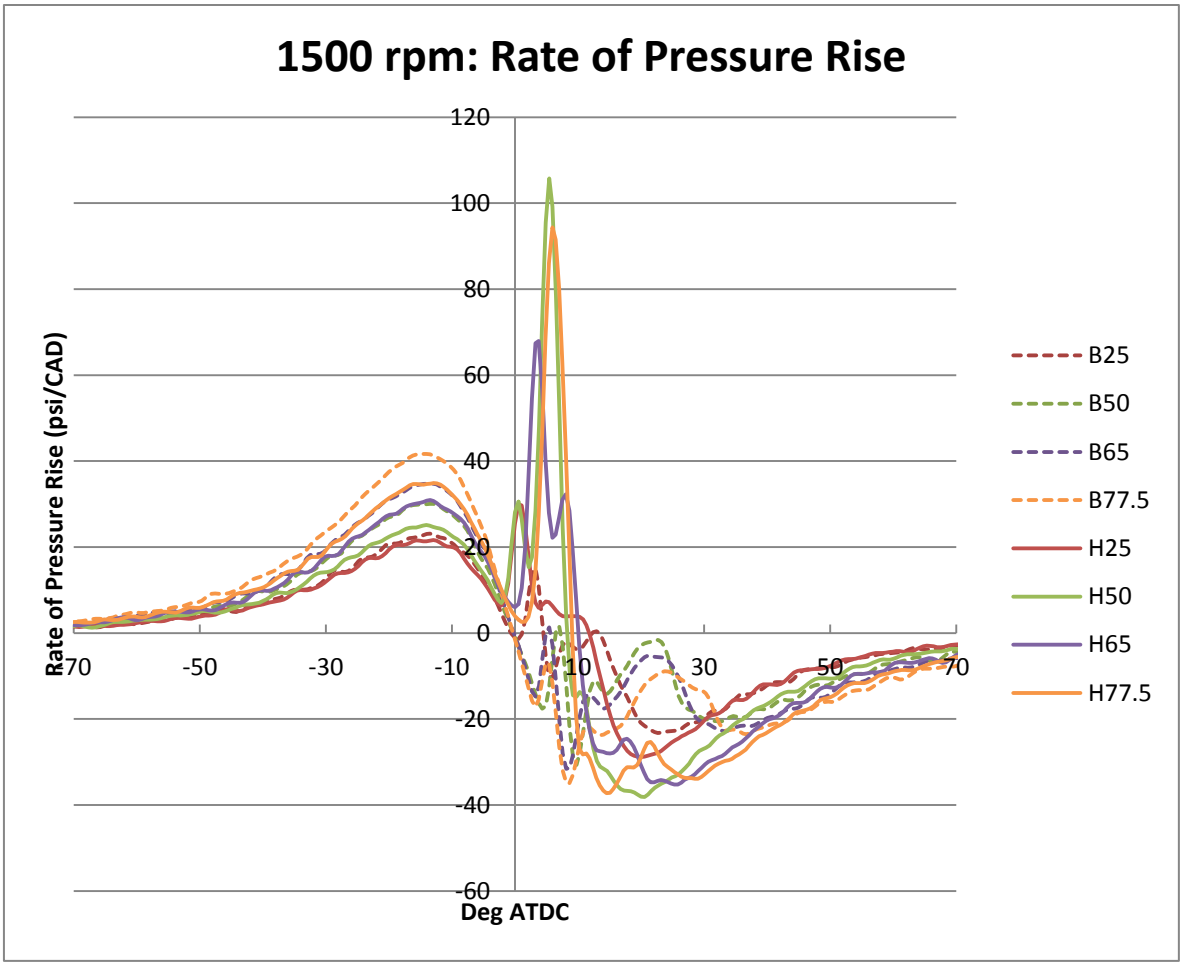

Figure 24. Rate of pressure rise curves for 1500 rpm.

The RPR curves for 1800 rpm are shown in Figure 25. At 25%, 50%, 65%, 77.5%, and 90% load, during dual-fuel combustion, the MRPR increased by 7%, 242%, 179%, 198% and 107%, respectively, compared to diesel-only combustion. In each of the diesel-only runs, the MRPR occurs during compression rather than during combustion, and the RPR curves indicate distinct premixed and diffusive combustion phases. In contrast, the MRPR during dual-fuel combustion occurs during combustion. Additionally, at 50% and 65% load during dual-fuel operation, a small heat release is observed prior to the main heat release. It seems unlikely a pilot quantity of diesel could combust without causing combustion of the H_2 in the cylinder to occur. One possible explanation could be a pre-ignition reaction between the H_2 and pilot diesel injection which released some heat without producing a flame. SOC occurs earlier during dual-fuel combustion than diesel-only combustion.

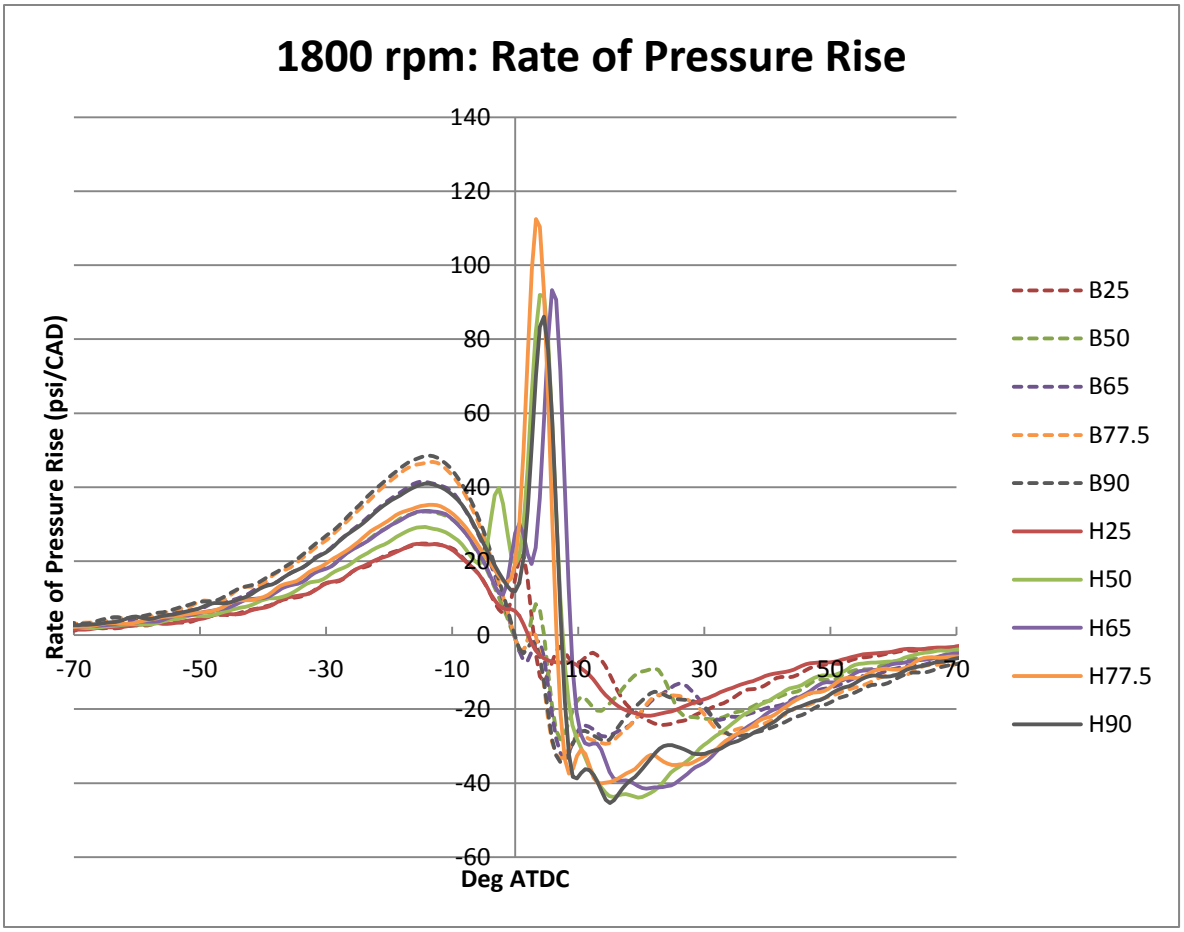

Figure 25. Rate of pressure rise curves for 1800 rpm.

The RPR curves for 2100 rpm can be seen in Figure 26. At 25%, 50%, 65%, 77.5%, and 90% load, during dual-fuel combustion, the MRPR increased by 8%, 155%, 96%, 85% and 60%, respectively, compared to diesel-only combustion. The 2100 rpm cases produced very similar results to the 1800 rpm cases. For diesel-only combustion, MRPR occurred during compression, while for dual fuel combustion, MRPR occurred during combustion. Again, as with the 1800 rpm case, the diesel-only cases showed a distinctive two phase combustion while the dual-fuel combustion showed a small heat release prior to the main combustion event for the 50% and 65% load cases. The SOC was advanced for dual-fuel combustion compared to diesel-only combustion. The percent increase in the MRPR during dual-fuel combustion was less for the 2100 rpm cases than the 1800 rpm cases. This was due to lower MRPR during dual-fuel combustion at 2100 rpm compared to 1800 rpm.

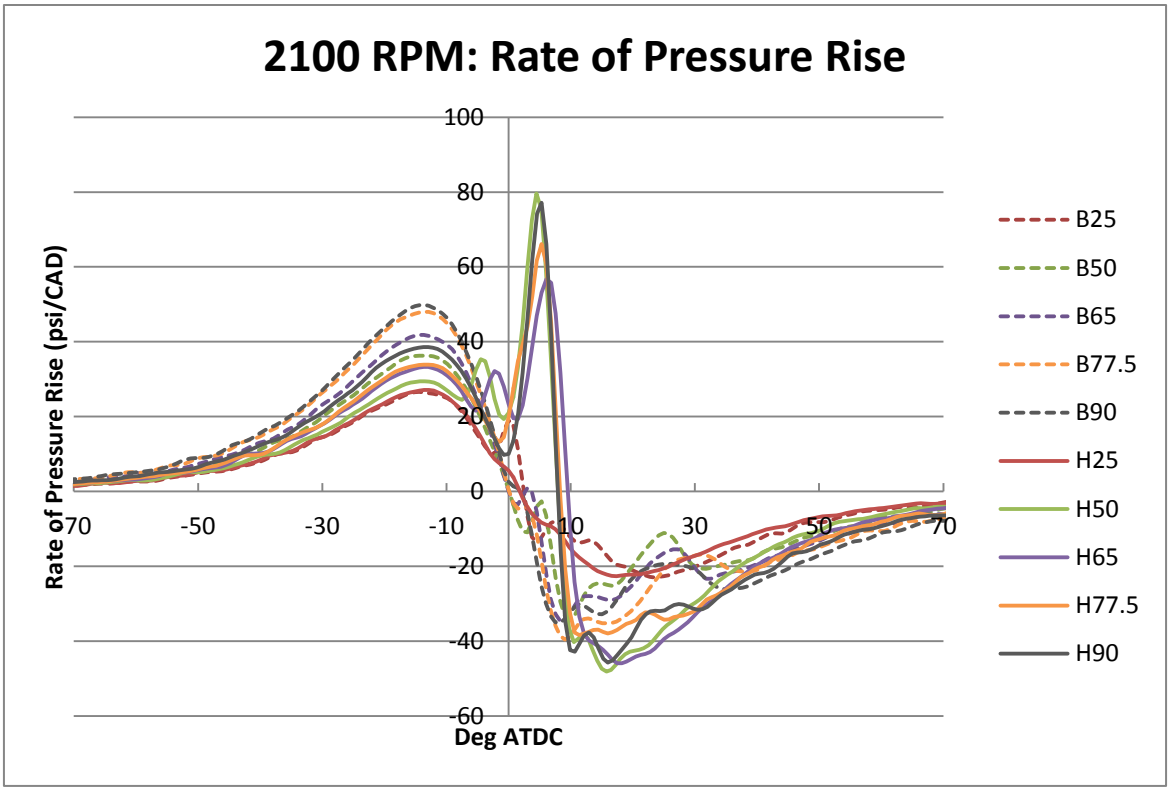

Figure 26. Rate of pressure rise curves for 2100 rpm.

In each of the 1300 rpm, 1500 rpm, and 1800 rpm cases (excluding the 25% load cases) the MRPR under dual-fuel operation was near 90 psi/deg, which was the established knock threshold. The MRPR in the dual-fuel 2100 rpm cases fell short of 80 psi/deg. Due to limitations in the H_2 delivery system, the 2100 rpm case was receiving the maximum possible H_2 delivery. Although the knock indicator did trigger at 2100 rpm, it did so less frequently than in the other cases. This indicates that the same level of knock was not reached. Fewer combustion cycles reached the 90 psi/deg threshold, lowering the average MRPR for the runs.

Injection timing is another parameter that greatly affects combustion. An attempt was made to control the injection timing with a circuit that was intended to augment the injection signal between the ECM and the injectors. This was pursued in the absence of an unlocked ECM where the injection timing values could be modified by changing the ECM maps. Issues with supply of electrical components and a compressed time schedule lead to the decision to abandon the circuit before it was finished. The circuit design is briefly outlined in Appendix C.

The engine was allowed to change injection timing as H_2 was added. The injection strategy used by the ECM at 1300 rpm was a single main injection. Above 1300 rpm the ECM used a pilot and a main injection. It was observed that the pilot injection duration, the main injection duration, and the timing between the pilot and main injections were constant with respect to time.

Figure 27 shows the main injection timing for both diesel-only and dual-fuel operation. The main injection timing for dual-fuel operation was advanced compared to diesel-only, with the two becoming approximately equal at the maximum load at each engine speed. As the load decreased, the amount the main injection timing for dual-fuel operation advanced compared to diesel-only operation increased. This can be seen in Figure 28 which shows the shift in timing between diesel-only and dual-fuel operation. Under diesel-only operation, the main injection timing was somewhat constant at 50% load and above, with 25% load main injection timing being advanced compared to higher loads. A different trend was seen with dual-fuel operation: main injection timing was continually retarded as load increased at each speed.

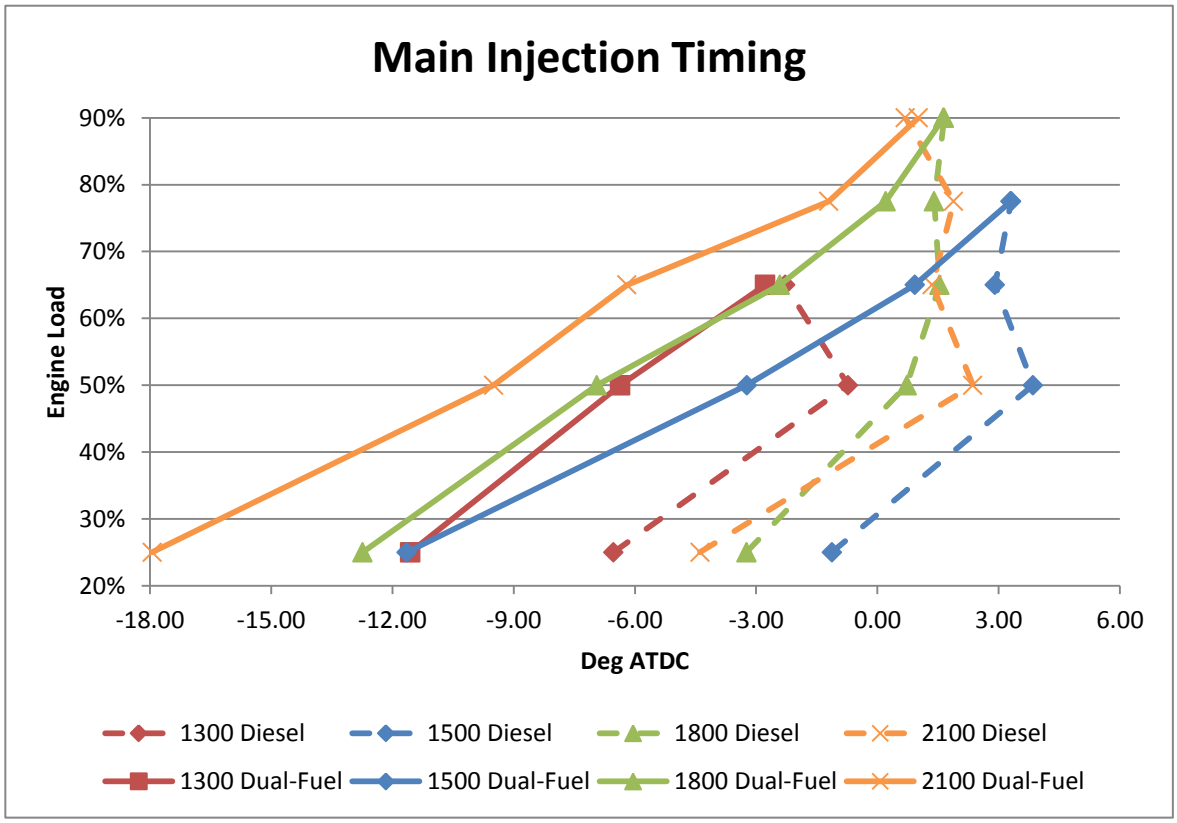

Figure 27. Main injection timing during diesel-only and dual-fuel operation.

The values in Figure 28 were calculated by taking the injection timing during dual-fuel operation and subtracting the injection timing during diesel-only operation at each point. Both main injection timing and pilot injection timing were shifted by the same amount at each point. The graph of the pilot injection values can be seen in Figure 29. As was mentioned above, the injection strategy at 1300 rpm did not use a pilot injection. In dual-fuel operation at 25% load there was no pilot injection.

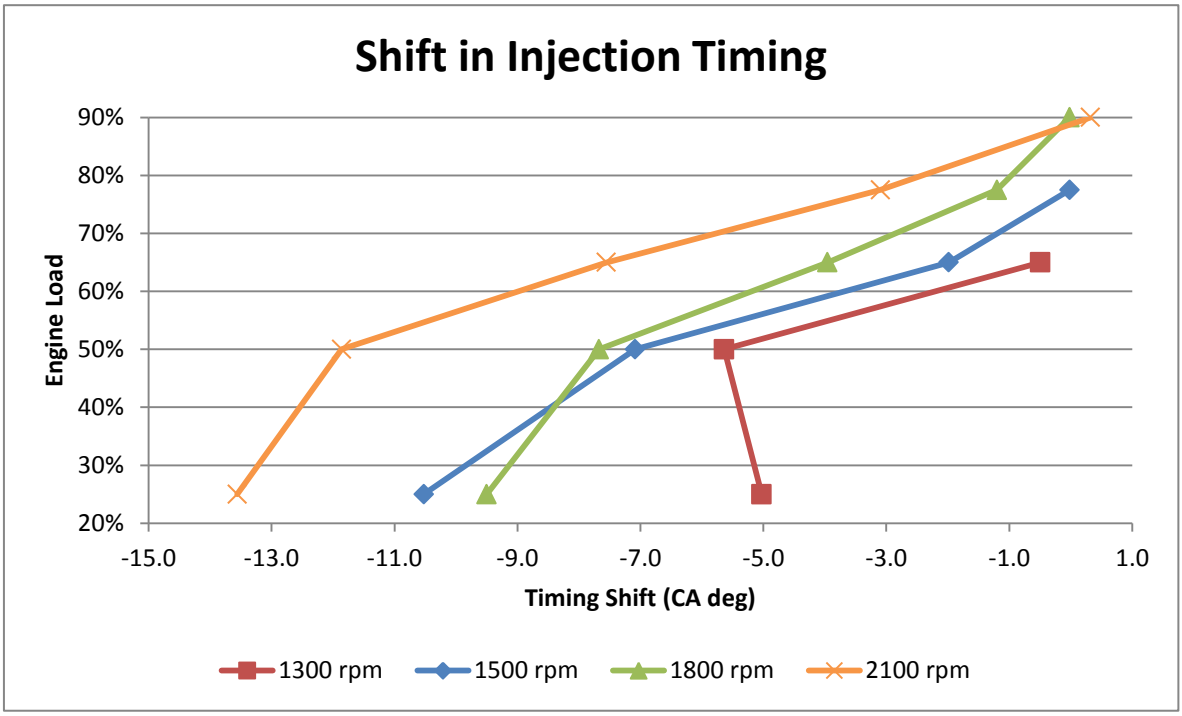

Figure 28. Shift in injection timing between dual-fuel and diesel-only combustion.

Had the ECM not reduced boost pressure during dual-fuel operation, the increase in peak in-cylinder pressure and MRPR would have been even greater. Being able to retard the injection timing would allow for SOC later in the cycle. Maximum cylinder pressure and MRPR would remain lower and would potentially allow a greater amount of H_2 to be added while avoiding diesel knock. This comes with the tradeoff of reduced thermal efficiency.

Without precise knowledge of the ECM logic, it is difficult to be sure of why boost pressure was reduced and injection timing was advanced during dual-fuel operation. The change in control could have been caused by a change in physical sensor readings, virtual sensor readings, or a shift in control maps. The answer is most likely a complex combination of all three. Inlet manifold

pressure readings were likely altered by the addition of H_2 after the turbocharger. Different outputs from the injection timing maps are also likely since the ECM reduced fuel delivery to maintain the desired speed and load during dual-fuel operation.

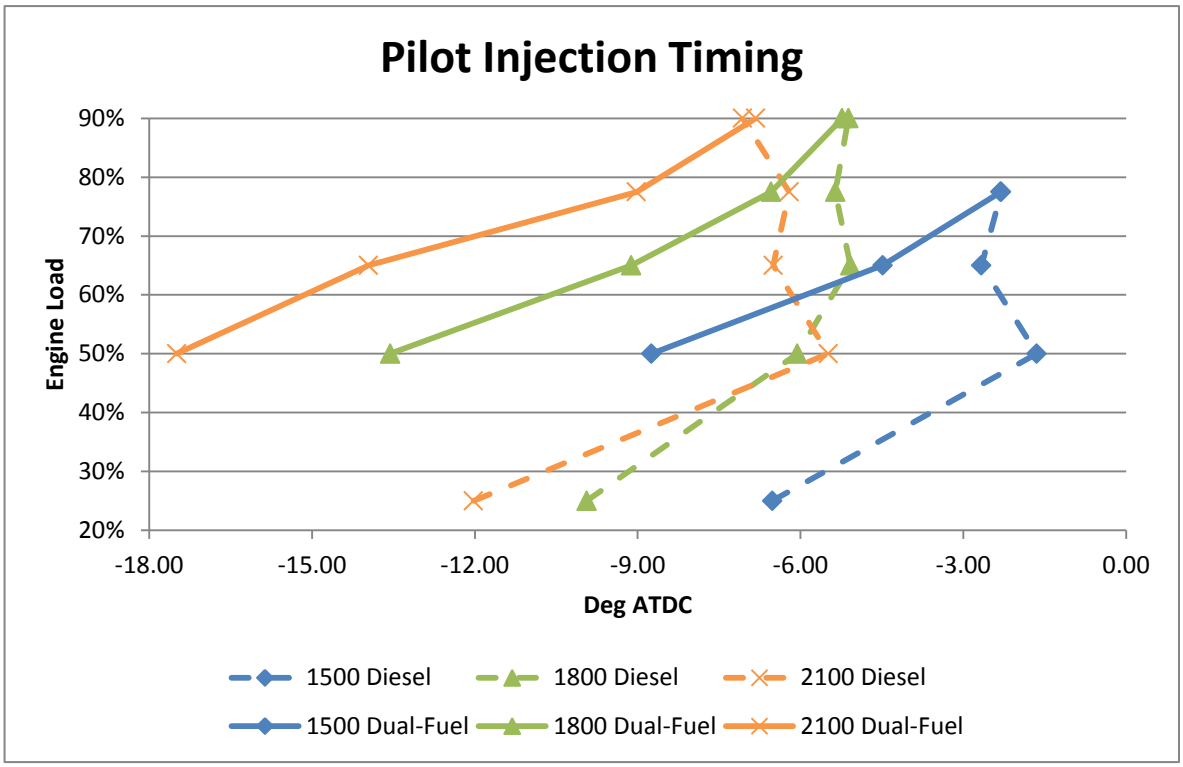

Figure 29. Pilot injection timing during diesel-only and dual-fuel operation.

6.3. Emissions

The emissions from an engine are becoming more important as emissions standards become increasingly stringent. Knowing how dual-fuel diesel-hydrogen operation affects emissions is critical to assessing the feasibility of such an alternative fuel technology. Below, the emissions of NO_x, CO_2, CO, and HC during both diesel-only and dual-fuel operation are presented and discussed.

It is typical for NO_x emissions to increase in an engine using H_2 as a fuel. This is because the higher burn temperature of H_2 causes increased NO_x formation via the thermal formation mechanism. NO_x emissions for the CAT C6.6 ACERT engine can be seen in Figure 30. Except for the 25% load cases, where a different type of combustion occurred, NO_x emissions increased during

dual-fuel operation. For diesel-only combustion, NO_x emissions were relatively constant at each speed and as speed increased NO_x emissions were reduced. For dual-fuel operation (ignoring the 25% load points), NO_x emissions decreased as load increased at each speed. As speed increased, NO_x emissions decreased with 1500 rpm and 1800 rpm producing near identical NO_x emissions. Maximum load at 1500 rpm, 1800 rpm, and 2100 rpm produced NO_x emissions that were close to diesel-only operation, a 27%, -3%, and 28% increase, respectively. NO_x emissions were highest at 50% load, increasing 106%, 150%, 210%, and 224% at 1300 rpm, 1500 rpm, 1800 rpm, and 2100 rpm, respectively.

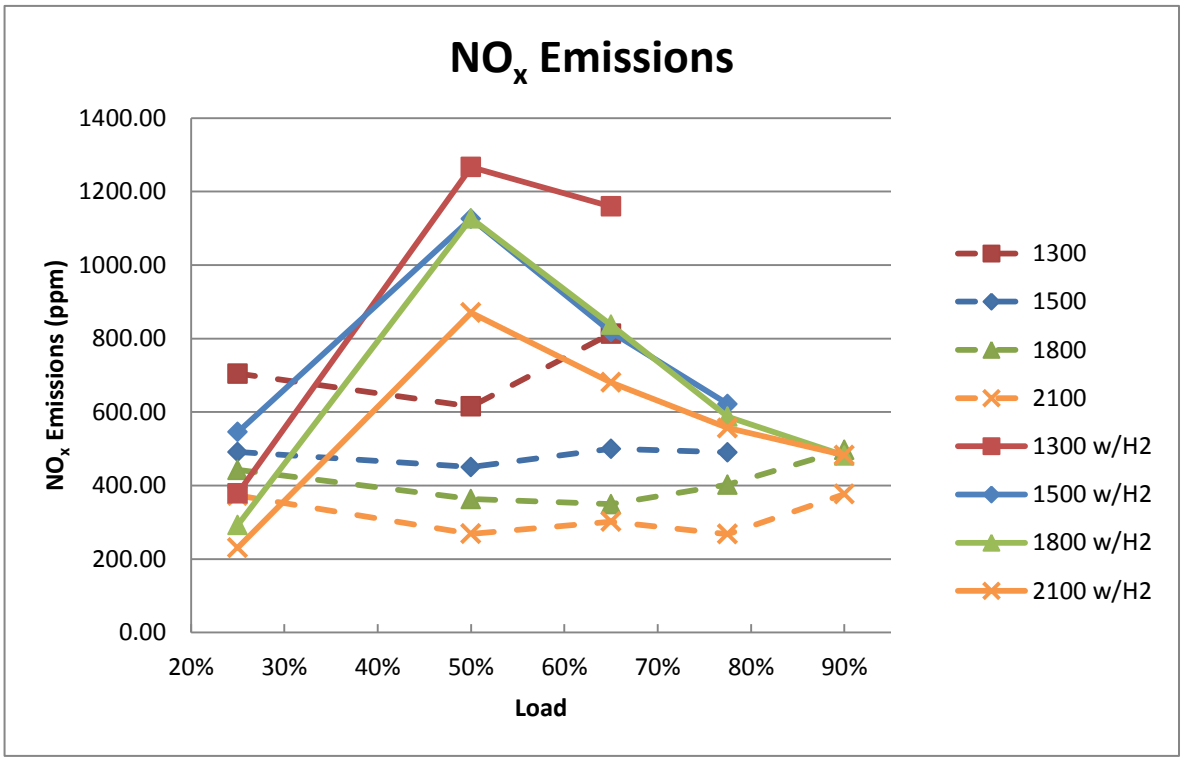

Figure 30. NO_x emissions for diesel-only and dual-fuel operation.

The two emissions currently regulated by the EPA are NO_x and particulate matter (PM). The literature indicates that H_2 addition reduces the amount of particulate matter. This result could not be verified since the lab was not equipped with an emissions sampler that can measure PM. However, NO_x increased, which is consistent with the literature. The increased level of NO_x would need to be reduced be some suitable means as discussed in the literature review. One of the leading strategies used by diesel OEMs is SCR. Since the ratio of NO_2 to NO_x is of interest for the

efficient operation of an SCR system, the NO_2/NO_x ratio is reported in Figure 31. For Cu-zeolite SCR catalysts, currently one of the most popular, an NO_2/NO_x ratio of approximately 0.4-0.6 provides the optimum conditions for the reduction of NO_x emissions. At higher loads, in diesel-only operation, the NO_2/NO_x ratio falls away from 0.5 down towards 0.3. The addition of H_2 brings this ratio up above diesel-only levels to between 0.4 and 0.6. This would favor the use of a SCR system for NO_x reduction in dual-fuel operation.

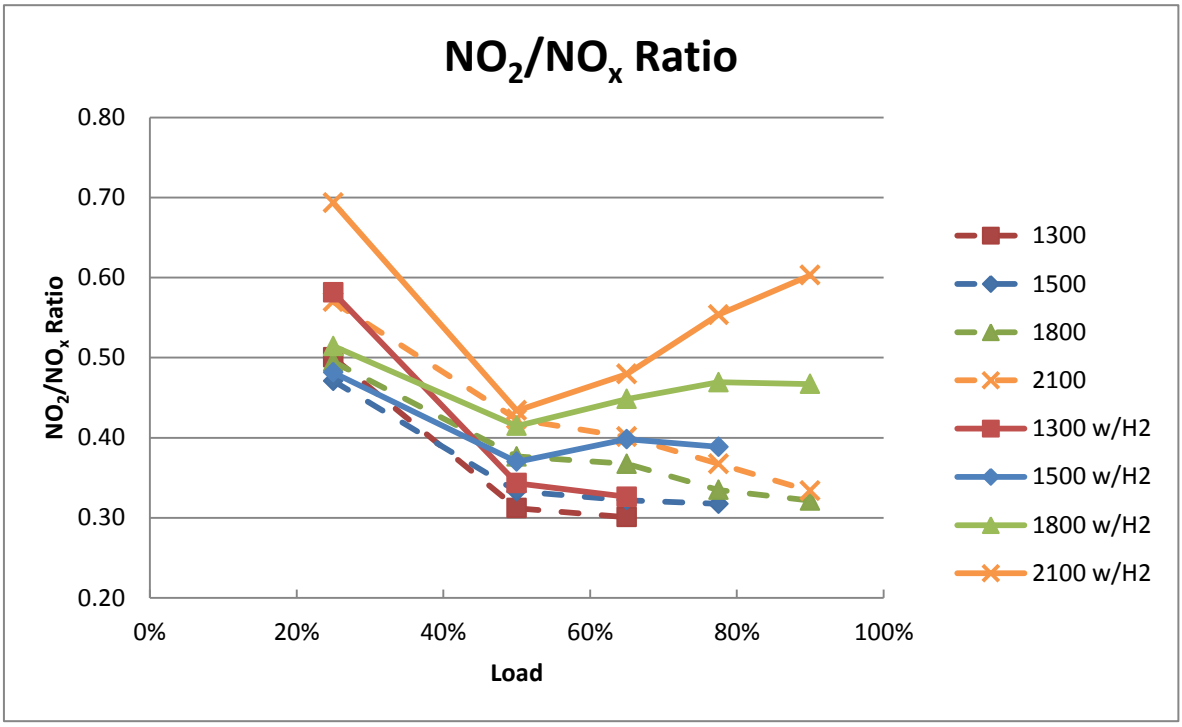

Figure 31. NO_2/NO_x ratio for diesel-only and dual-fuel operation.

After NO_x and PM, CO_2 is the emission of most interest. The main rationale for exploring H_2 as an alternative fuel is to reduce CO_2 emissions. Figure 32 shows the results for CO_2 emissions from the C6.6 engine during both diesel-only and dual-fuel operation. The results clearly show a reduction of CO_2 in dual-fuel operation which was expected since part of the diesel fuel is replaced by H_2. In both modes of operation, CO_2 emissions increased as load increased. This was also expected since it requires more fuel energy to produce a higher load. Discounting the 25% load points, the CO_2 reduction ranges between 10.2% at 1800 rpm-77.5% load and 47.6% at 2100 rpm-50% load. In general, as load increased the percentage reduction of CO_2 decreased. This can be explained by a greater increase in operating efficiency in dual-fuel operation at lower loads.

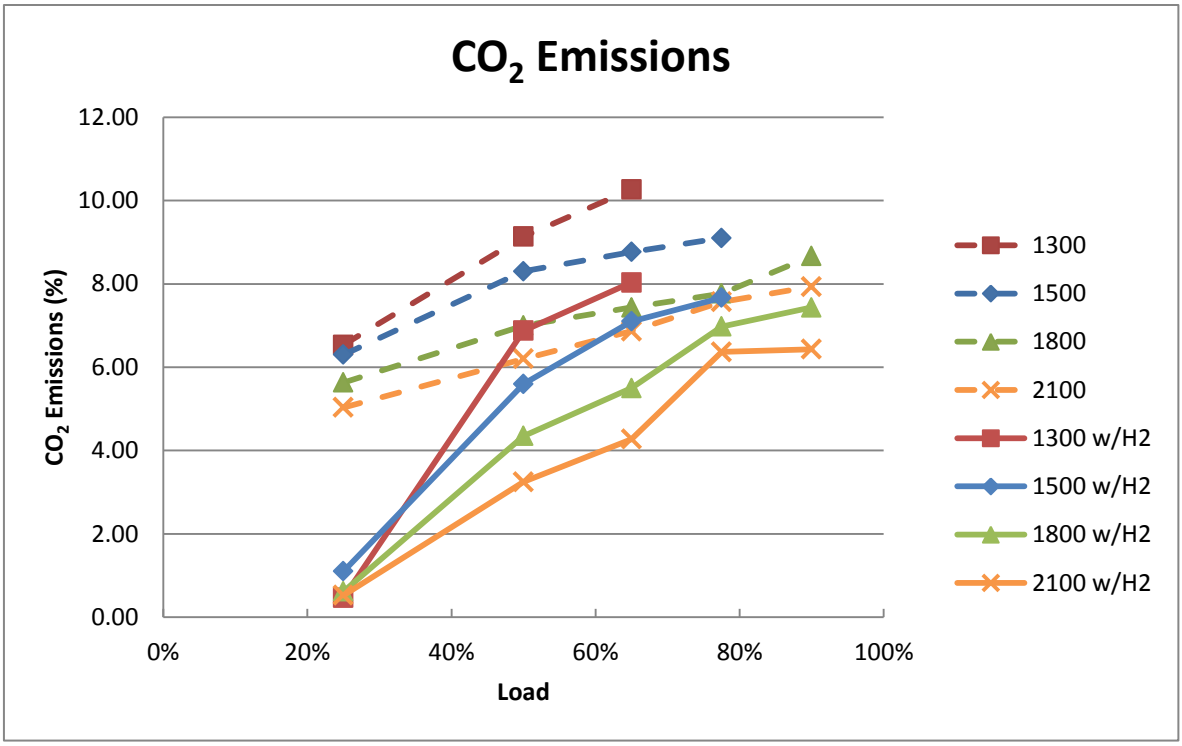

Figure 32. CO_2 emissions for diesel-only and dual-fuel operation.

The results for CO emissions can be seen in Figure 33. The emissions levels of CO were very low compared to the CO reading resolution of 0.01%, ranging between 0.0067% and 0.0733% average. At or below 65% load, dual-fuel operation produced lower CO emissions than diesel-only. Above 65% load, diesel-only operation produced lower CO emissions. The results are in the same range as those obtained by Bottelberghe [33]. The 25% load cases in dual-fuel operation show low levels of CO emissions.

The results for unburnt HC emissions can be seen in Figure 34. HC emissions were also very low compared to the 1 PPM resolution, ranging between 0 and 2.8 PPM average for all cases. With a few exceptions, HC emissions were lower in diesel-only operation than dual-fuel operation. The author questioned the functionality of the HC emissions reading, however, Bottelberghe [33] reports having performed a check with the exhaust gas analyzer on a 2-stroke engine to verify the functionality of the instrument. Since the ACERT technology is advertised as being low emissions, it is reasonable to expect very low HC emissions. In addition, the results are in the same range as those reported by Bottelberghe.

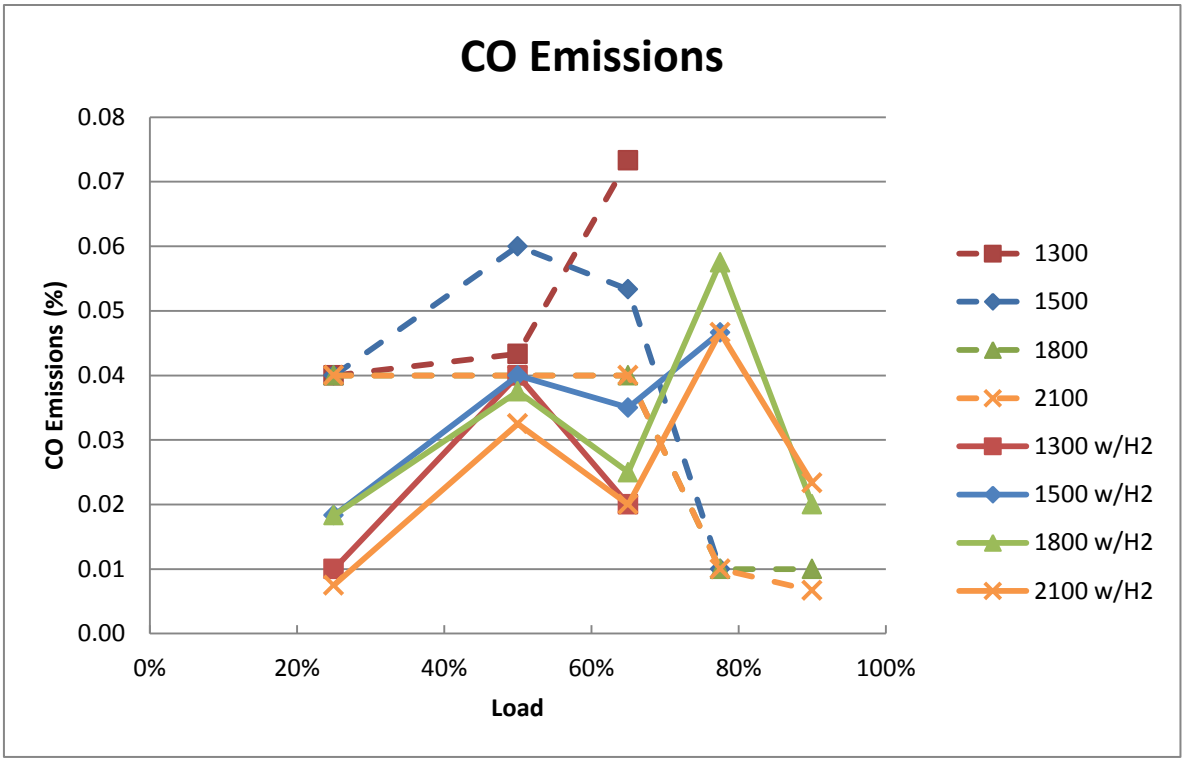

Figure 33. CO emissions for diesel-only and dual-fuel operation.

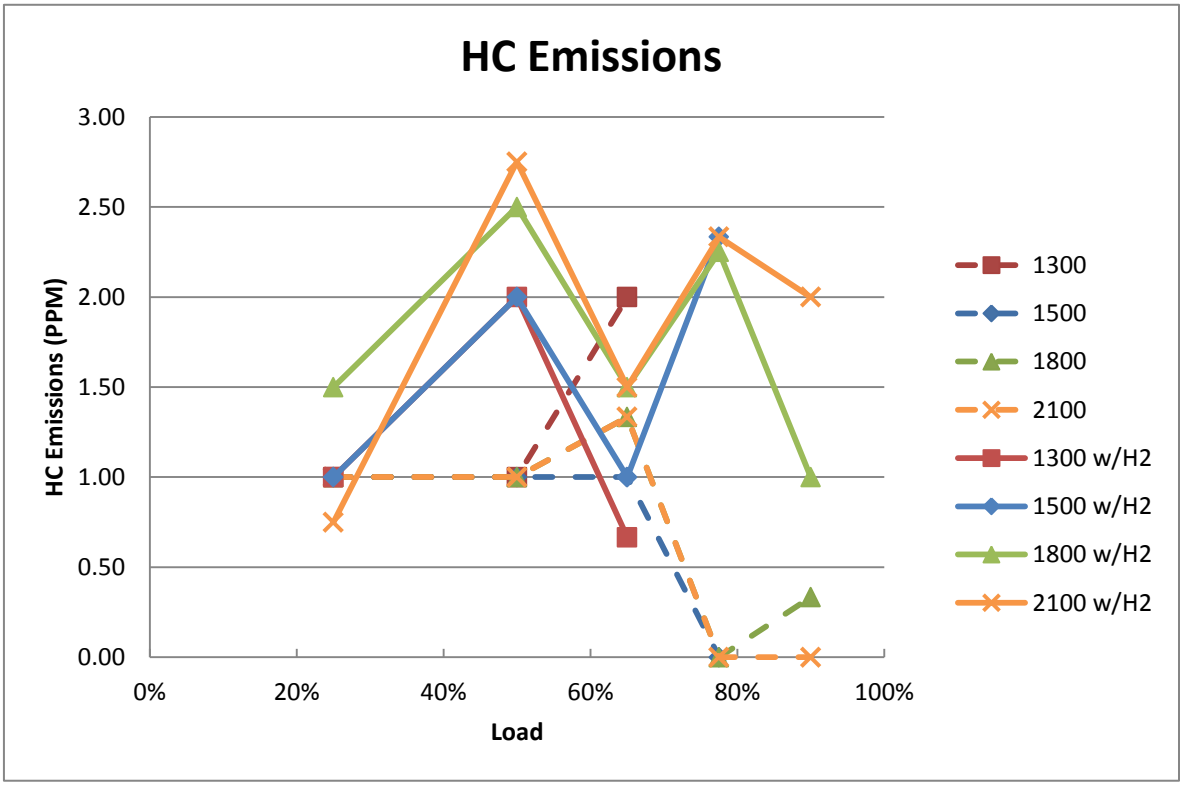

Figure 34. HC emissions for diesel-only and dual-fuel operation.

It was previously discussed that unstable combustion was occurring for the 25% load cases: cycle to cycle variations in the shape of the in-cylinder pressure curves were high. From the emissions results it was observed that CO_2 emissions at the 25% load cases were near zero. This indicates one of two things: either diesel fuel was being injected but not burned, or diesel injection was reduced to near zero. A further look at the emissions reveals that HCs did not increase during dual-fuel combustion at 25% load. If diesel fuel had been injected but not burned, there would have been a spike in HC emissions. Therefore, it seems likely that the supply of diesel fuel was practically zero. In this case, the NO_x emissions would be expected to increase from the high temperatures of H_2-only combustion. The results show that NO_x emissions actually decreased in these cases. One explanation for this is that the engine was operating in homogeneous charge compression ignition (HCCI) mode. HCCI combustion is characterized by a lean, homogeneous mixture of air and fuel in the combustion chamber which is auto-ignited by compression resulting in near constant volume combustion. As discussed by Antunes et al. [49], this mode of combustion with H_2 can produce near-zero NO_x emissions. This mode of combustion is difficult to obtain because of the high autoignition temperature of H_2. It is difficult to control the ignition timing in HCCI operation which would produce unstable combustion.

CHAPTER 7. CONCLUSIONS

In this work a 6-cylinder, heavy-duty diesel engine was run near the knock limit in diesel-hydrogen dual-fuel operation across a wide range of operating conditions. A number of observations were made from the in-cylinder pressure trace and emissions measurements.

- A maximum H_2 substitution of 74% was achieved at 2100 rpm and 50% load. As load increased, the percentage of H_2 that could be supplemented decreased.
- H_2 addition increased the thermal efficiency of the engine at all operating points; up to a 32.4% increase over diesel-only operation.
- Peak in-cylinder pressure increased by up to 40% during dual-fuel operation. As load increased, the percent increase in peak in-cylinder pressure decreased.
- In dual-fuel operation a large peak in the RPR occurred after TDC corresponding to the combustion of H_2. MRPR increased by up to 281%. Except for at 1300 rpm, the increase in MRPR decreased as load increased.
- Injection timing was advanced by up to 13.6° during dual-fuel operation. As the load increased, the injection timing was advanced less until timing between dual-fuel and diesel-only were approximately equal at the maximum load at each speed.
- NO_x emissions increased by up to 224% during dual-fuel operation. The increase in NO_x emissions decreased as load increased. Hydrogen addition increased the NO_2/NO_x ratio, favoring high SCR efficiency.
- CO_2 reduction ranged between 10.2% and 47.6% during dual-fuel operation.
- CO and HC emissions were largely unchanged during dual-fuel operation.
- At 25% the engine was run on nearly 100% H_2. NO_x emissions were below diesel-only levels and CO_2 emissions were nearly 0, however, the combustion was unstable.

These observations show that a large percentage of H_2 can be used to displace diesel fuel in a compression ignition engine. Dual-fuel diesel-hydrogen operation, though not without challenges, may provide a feasible means to reducing $C0_2$ emissions and mitigating global warming.

Future work in the NDSU engine test lab could include completion of the injection delay circuit to investigate the possibility of extending the envelope of the knock limit by delaying injection

timing. Even more helpful to the investigation of the injection timing would be acquiring an unlocked ECU. This would allow not only injection timing to be controlled, but a large number of other parameters such as rail pressure, injection quantity, boost pressure, injection strategy, etc. A study with an SCR system during dual-fuel operation would give insight into the possibility of meeting emissions regulations during dual-fuel operation. Other work could include investigating the mode of combustion observed at 25% load in this study.

REFERENCES

[1] J. Conti and P. Holtberg, "International Energy Outlook 2011," U.S. Energy Information Administration, eia.gov, 2011.

[2] "Key World Energy Statistics," International Energy Agency, Paris, 2010.

[3] B. T. Fichman and R. Repice, "Annual Energy Review 2011," US Energy Information Administration, eia.gov, 2012.

[4] P. McCaffrey, "The Hydrogen Revolution: Is It Feasible?," in *U.S. National Debate Topic 2008-2009: Alternative Energy*, New York, The H.W. Wilson Company, 2008.

[5] L. Webster, "The Future of Diesel in the US: Analysis," Popular Mechanics, 10 September 2009. [Online]. Available: http://www.popularmechanics.com/cars/alternative-fuel/diesel/4330313. [Accessed 28 May 2013].

[6] G. Schmidt, "Water Vapor: Forcing or Feedback?," RealClimate.org, 6 April 2005. [Online]. Available: http://www.realclimate.org/index.php?p=142. [Accessed 9 June 2013].

[7] I. Sample, "Heat: How We Got Here," *The Guardian,* 30 June 2005.

[8] McGee and Michael, "CO2 Now," Pro Oxygen, 2013. [Online]. Available: co2now.org. [Accessed 12 June 2013].

[9] R. Di Silvestro, "The Proof Is in the Science," *National Wildlife,* April/May 2005.

[10] O. o. T. a. A. Quality, "Emission Standards Reference Guide," United Stated Environmental Protection Agency, 14 November 2012. [Online]. Available: http://www.epa.gov/otaq/standards/allstandards.htm. [Accessed 15 June 2013].

[11] D. &. Company, "Understanding Emissions Regulations," John Deere, 2013. [Online]. Available: http://www.deere.com/wps/dcom/en_US/services_and_support/emissions_information/understanding_emission_regulations/regulations.page?. [Accessed 16 June 2013].

[12] O. o. t. P. Secretary, "President Obama Announces Historic 54.5 mpg Fuel Efficiency Standard," The White House, 29 July 2011. [Online]. Available: http://www.whitehouse.gov/the-press-office/2011/07/29/president-obama-announces-historic-545-mpg-fuel-efficiency-standard. [Accessed 16 June 2013].

[13] T. Miyamoto, H. Hasegawa, M. Mikami, N. Kojima, H. Kabashima and Y. Urata, "Effect of Hydrogen Addition to Intake Gas on Combustion and Exhaust Emission Characteristics of a Diesel Engine," *International Journal of Hydrogen Energy,* vol. 36, no. 20, pp. 13138-13149, 2011.

[14] N. Saravanan, G. Nagarajan, K. M. Kalaiselvan and C. Dhanasekaran, "An Experimental Investigation on Hydrogen as a Dual Fuel for Diesel Engine System with Exhaust Gas Recirculation Technique," *Renewable Energy,* vol. 33, no. 3, pp. 422-427, 2008.

[15] N. Saravanan, G. Nagarajan, G. Sanjay, C. Dhanasekaran and K. Kalaiselvan, "Combustion Analysis on a DI Diesel Engine with Hydrogen in Dual Fuel Mode," *Fuel,* vol. 87, no. 17-18, pp. 3591-3599, 2008.

[16] N. Saravanan and G. Nagarajan, "An Insight on Hydrogen Fuel Injection Techniques with SCR System for NOx Reduction in a Hydrogen-Diesel Dual Fuel Engine," *Internaltional Journal of Hydrogen Engergy,* vol. 34, no. 21, pp. 9019-9032, 2009.

[17] P. K. Bose and D. Maji, "An Experimental Investigation on Engine Performance and Emissions of a Single Cylinder Diesel Engine Using Hydrogen as Inducted Fuel and Diesel as Injected Fuel with Exhaust Gas Recirculation," *International Journal of Hydrogen Engergy,* vol. 34, no. 11, pp. 4847-4854, 2009.

[18] E. Tomita, N. P. Z. Kawahara and S. Fujita, "Hydrogen Combustion and Exhaust Emissions Ignited with Diesel Oil in a Dual Fuel Engine," in *International Fall Fuels and Lubricants Meeting and Exposition*, San Antonio, TX, 2001.

[19] S. Lambe and H. Watson, "Optimizing the Design of a Hydrogen Engine with Pilot Diesel Fuel Ignition," *International Journal of Vehicle Design,* vol. 14, no. 4, pp. 370-389, 1993.

[20] G. K. Lilik, H. Zhang, J. M. Herreros, D. C. Haworth and A. L. Boehman, "Hydrogen Assisted Diesel Combustion," *Internation Journal of Hydrogen Energy,* vol. 35, no. 9, pp. 4382-4398, 2010.

[21] M. M. Roy, E. Tomita, N. Kawahara, Y. Harada and A. Sakane, "An Experimental Investigation on Engine Performance and Emissions of a Supercharged H2-Diesel Dual-Fuel Engine," *International Journal of Hydrogen Energy,* vol. 35, no. 2, pp. 844-853, 2010.

[22] M. Y. Selim, "Sensitivity of Dual Fuel Engine Combustion and Knocking Limits to Gaseous Fuel Composition," *Energy Conversion and Management,* vol. 45, no. 3, pp. 411-425, 2004.

[23] College of the Desert, "Hydrogen Fuel Cell Engines and Related Technologies Course Manual," December 2001. [Online]. Available: http://www1.eere.energy.gov/hydrogenandfuelcells/tech_validation/h2_manual.html. [Accessed 29 October 2011].

[24] S. Verhelst and T. Wallner, "Hydrogen-Fueled Internal Combustion Engines," *Progress in Energy and Combustion Science,* vol. 35, pp. 490-527, 2009.

[25] S. Szwaja and K. Grab-Rogalinski, "Hydrogen Combustion in a Compression Ignition Diesel Engine," *Internation Journal of Hydrogen Engergy,* vol. 34, no. 10, pp. 4413-4421, 2009.

[26] J. Gomes Antunes, R. Mikalsen and A. Roskilly, "An Experimental Study of a Direct Injection Compression Ignition Hydrogen Engine," *International Journal of Hydrogen Energy,* vol. 34,

no. 15, pp. 6516-6522, 2009.

[27] A. Boretti, "Advantages of the Direct Injection of Both Diesel and Hydrogen in a Dual Fuel H2ICE," *International Journal of Hydrogen Energy,* vol. 36, no. 15, pp. 9312-9317, 2011.

[28] A. Boretti, "Advances in Hydrogen Compression Ignition Internal Combustion Engines," *International Journal of Hydrogen Energy,* vol. 36, no. 19, pp. 12601-12606, 2011.

[29] M. K. Heiman and B. D. Solomon, "Fueling U.S. Transportation: The Hydrogen Economy and Its Alternatives," *Environment,* October 2007.

[30] J. Ogden and D. Sperling, "The Hope for Hydrogen," *Issues in Science and Techonology,* Spring 2004.

[31] W. W. Pulkrabek, Engineering Fundamentals of the Internal Combustion Engine, New Jersey: Prentice Hall, 1997.

[32] B. D. Hsu, Practical Diesel-Engine Combustion Analysis, Warrendale, PA: Society of Automotive Engineers, 2002.

[33] K. J. Bottelberghe, *Performance Analysis of an Advanced Emission Reduction Technology Engine During Diesel-Hydrogen Dual-Fuel Operation,* North Dakota State University: Thesis, 2011.

[34] D. Lata and A. Misra, "Analysis of Ignition Delay Period of a Dual Fuel Diesel Engine with Hydrogen and LPG as Secondary Fuels," *International Journal of Hydrogen Energy,* vol. 36, no. 5, pp. 3746-3756, 2011.

[35] J. Naber and D. Siebers, "Hydrogen Combustion Under Diesel Engine Conditions," *International Journal of Hydrogen Energy,* vol. 23, no. 5, pp. 363-371, 1998.

[36] D. B. Lata, A. Misra and S. Medhekar, "Investigations on the Combustion Parameters of a Dual Fuel Diesel Engine with Hydrogen and LPG as Secondary Fuels," *International Journal of Hydrogen Engergy,* vol. 36, no. 21, pp. 13808-13819, 2011.

[37] D. Lata and A. Misra, "Theoretical and Experimental Investigations on the Performance of Dual Fuel Diesel Engine with Hydrogen and LPG as Secondary Fuels," *International Journal of Hydrogen Energy,* vol. 35, no. 21, pp. 11918-11931, 2010.

[38] T. Gatts, H. Li, C. Liew, S. Liu, T. Spencer, S. Wayne and N. Clark, "An Experimental Investigation of H2 Emissions of a 2004 Heavy-Duty Diesel Engine Supplemented with H2," *International Journal of Hydrogen Energy,* vol. 35, no. 20, pp. 11349-11356, 2010.

[39] J. Kubesh and D. D. Brehob, "Analysis of Knock in a Dual-Fuel Engine," *SAE Technical Paper,* no. 922367, 1992.

[40] Z. Liu and G. A. Karim, "Knock Characteristics of Dual-Fuel Engine Fuelled with Hydrogen Fuel," *International Association for Hydrogen Energy,* vol. 20, no. 11, pp. 919-924, 1995.

[41] M. M. Roy, E. Tomita, N. Kawahara, Y. Harada and A. Sakane, "Comparison of Performance and Emissions of a Supercharged Dual-Fuel Engine Fueled by Hydrogen and Hydrogen-Containing Gaseous Fuels," *International Journal of Hydrogen Energy,* vol. 36, no. 12, pp. 7339-7352, 2011.

[42] M. Ettefagh, M. Sadeghi, V. Pirouzpanah and H. Arjmandi Tas, "Knock Detection in Spark Ignition Engines by Vibration Analysis of Cylinder Block: A Parametric Modeling Approach," *Mechanical Systems and Signal Processing,* vol. 22, no. 6, pp. 1495-1514, 2008.

[43] K. Burgdorf and I. Denbratt, "Comparison of Cylinder Pressure Based Knock Detection Methods," *SAE Techinical Paper,* no. 972932, 1997.

[44] S. Szwaja, K. R. Bhandary and a. J. D. Naber, "Comparisons of Hydrogen and Gasoline Combustion Knock in a Spark Ignition Engine," *International Journal of Hydrogen Energy,* vol. 32, no. 18, pp. 5076-5087, 2007.

[45] N. Saravanan and G. Nagarajan, "Performance and Emissions Study in Manifold Hydrogen Injection with Diesel as an Ignition Source for Different Start of Injection," *Renewable Energy,* vol. 34, no. 1, pp. 328-334, 2009.

[46] H. Mathur, L. Das and T. N. Patro, "Hydrogen-Fuelled Diesel Engine: Performance Improvement Through Charge Dilution Techniques," *International Journal of Hydrogen Energy,* vol. 18, no. 5, pp. 421-431, 1993.

[47] S. Liu, H. Li, C. Liew, T. Gatts, S. Wayne, B. Shade and N. Clark, "An Experimental Investigation of NO2 Emission Characteristics of a Heavy-Duty H2-Diesel Dual Fuel Engine," *International Journal of Hydrogen Energy,* vol. 36, no. 18, pp. 12015-12024, 2011.

[48] J. Chong, A. Tsolakis, S. Gill, K. Theinnoi and S. Golunski, "Enhancing the NO2/NOx Ratio in Compression Ignition Engines by Hydrogen and Reformate Combustion, for Improved Aftertreatment Performance," *International Journal of Hydrogen Energy,* vol. 35, no. 16, pp. 8723-8732, 2010.

[49] J. Gomez Antunes, R. Mikalsen and A. Roskilly, "An Investigation of Hydrogen-Fuelled HCCI Engine Performance and Operation," *International Journal of Hydrogen Energy,* vol. 33, no. 20, pp. 5823-5828, 2008.

APPENDIX A. SAMPLE SPREADSHEETS

LabVIEW Measurement							SAE J1349 Correction Factor	H2 Rate [SCFM]	Fuel Rate [gal/h]	Pulse dt [ms]	Exhaust Manifold [F]	Air Flow [CFM]	Power Engine	Power H2	Power Diesel	% H2	Therm Eff
Writer_Ve	2		Speed [RPM]	Torque [ft-lb]	Speed [Deg/s]	Deg/sample		24	1.9237	0.6151	692.9	291.0	300776	386592	250082	0.607	0.472
Reader_V	2		2118.5	293.0	12711.0	7.63E-01	1.04786			Filtered Pressure		Raw Pressure		Filtered Pressure			
Separator	Tab							Raw Pressure		Max Rate	Max Rate	Peak		Peak	PP	Pilot Deg	Main Deg
Decimal_S			Cycle	Time	Tvalue	Pvalue	Cell	Begin	End	Press Rise	Timing	Pressure	PP Timing	Pressure	Timing	ATDC	ATDC
Multi_Hea	No		1	0.049802	-0.05739	1211.050417	854	655	1054	57.266	7.627	1527.281	10.678	1500.642	9.915	-14.492	-6.865
X_Column	One		2	0.106385	0.085226	1211.050417	1797	1598	1997	62.386	7.627	1530.795	9.152	1511.662	10.678	-14.492	-6.865
Time_Pre	Absolute		3	0.162967	0.045177	1218.077762	2740	2541	2940	68.191	6.864	1504.442	10.678	1506.962	9.915	-14.492	-6.865
Operator	lee.kersting		4	0.219609	0.125763	1198.752649	3684	3485	3884	55.372	7.627	1478.090	9.915	1468.998	10.678	-14.492	-6.865
Descriptio	Data from the LabVI		5	0.276431	0.013919	1196.995727	4631	4432	4831	61.701	8.390	1481.603	9.915	1476.629	10.678	-14.492	-6.102
Date	7/12/12		6	0.333194	-0.12479	1225.105106	5577	5378	5777	62.544	6.864	1529.038	9.152	1505.336	9.915	-14.492	-6.865
Time	12:12.7		7	0.389836	0.032479	1198.752649	6521	6322	6721	72.336	7.627	1557.147	9.152	1533.772	9.915	-14.492	-6.102
***End_of_	Header***		8	0.446478	-0.1072	1204.023072	7465	7266	7665	68.435	6.864	1513.226	10.678	1511.165	9.915	-14.492	-6.865
						1207.975975			Average	63.529	7.436	1515.203	9.915	1501.896	10.201	-14.492	-6.674
Channels	7								Stdev	5.791	0.539	26.634	0.706	20.553	0.395	0.000	0.353
Samples	83	83	83	83	83	83	83		d(Ave.)/dCAD	60.527	6.865						
Date	7/12/12	7/12/12	7/12/12	7/12/12	7/12/12	7/12/12	7/12/12		**Minimum Pressure**			%O2	%CO	%CO2	ppm HC	ppm NO	ppm NO2
Time	12:12.7	12:12.7	12:12.7	12:12.7	12:12.7	12:12.7	12:12.7		0.462759			12.7	0.03	4.1	2	319	329
X_Dimens	Time	Time	Time	Time	Time	Time	Time										
X0	0.00E+00	0.00E+00	0.00E+00	0.00E+00	0.00E+00	0.00E+00	0.00E+00		Flags	0							
Delta_X	6.00E-05	6.00E-05	6.00E-05	6.00E-05	6.00E-05	6.00E-05	6.00E-05										

Time (s)	Raw Pressure Sensor (V)	TDC Sensor (V)	Injector Pulse (V)	Raw Pressure Reading (psi)	High Frequency Pressure Component (psi)	Filtered Raw Pressure Reading (psi)	Rate or Pressure Rise (psi/deg)	Adjusted Rate of Pressure Rise (psi/deg)
X_Value	Dev0/Ai0	Dev0/Ai1	Dev0/Ai2	Dev0/Ai0 (Formula Result)	Dev0/Ai0 (Filtered)	Dev0/Ai0 (Filtered) 1	Dev0/Ai0 (Formula Result) 1	Rate of Pressure Rise
0	0.60928	-0.00122	1.361416	104.2436	-1.80159	108.994588	-2.19087	-2.17173
6.00E-05	0.604396	-0.00122	1.363858	100.7299	1.421379	107.706462	-1.703803	-1.68892
0.00012	0.601954	-0.00122	1.363858	98.97311	0.732406	106.421166	-1.700059	-1.68521
0.00018	0.601954	-0.00122	1.363858	98.97311	-0.83111	104.808316	-2.133314	-2.11468
0.00024	0.604396	0.000733	1.363858	100.7299	-0.41191	102.847128	-2.594061	-2.5714
0.0003	0.59707	-0.00073	1.363858	95.45944	-0.5894	100.886043	-2.593924	-2.57127
0.00036	0.599512	0.000733	1.361416	97.21628	2.498555	99.29439	-2.105276	-2.08689
0.00042	0.589744	0.001221	1.363858	90.18893	-2.49232	98.104551	-1.573799	-1.56005
0.00048	0.594628	0.001709	1.361416	93.7026	2.100569	97.025004	-1.427915	-1.41544
0.00054	0.594628	0.000733	1.363858	93.7026	-1.89711	95.783039	-1.642745	-1.62839
0.0006	0.58486	0.001221	1.356532	86.67526	-0.33991	94.396299	-1.834239	-1.81822
0.00066	0.582418	0.001221	1.361416	84.91842	2.678632	92.951543	-1.910977	-1.89428
0.00072	0.587302	-0.00024	1.358974	88.4321	-0.82187	91.340687	-2.130676	-2.11206
0.00078	0.58486	-0.00024	1.358974	86.67526	-2.54806	89.545542	-2.374437	-2.3537
0.00084	0.582418	-0.00073	1.361416	84.91842	1.783121	87.87177	-2.213894	-2.19455
0.0009	0.57265	-0.00024	1.361416	77.89108	0.340211	86.569724	-1.722215	-1.70717
0.00096	0.579976	-0.00024	1.361416	83.16159	1.531626	85.463951	-1.462604	-1.44983
0.00102	0.57265	-0.00024	1.361416	77.89108	-4.1194	84.210501	-1.657935	-1.64345
0.00108	0.577534	-0.00073	1.358974	81.40475	3.061803	82.740236	-1.944718	-1.92773
0.00114	0.570208	-0.00024	1.361416	76.13424	-1.36591	81.265105	-1.951154	-1.93411
0.0012	0.570208	-0.00073	1.358974	76.13424	1.473463	79.975278	-1.706053	-1.69115
0.00126	0.562882	-0.00122	1.361416	70.86373	-1.53482	78.81414	-1.535835	-1.52242
0.00132	0.570208	-0.00122	1.361416	76.13424	1.733827	77.553082	-1.668	-1.65343
0.00138	0.570208	-0.00024	1.3663	76.13424	-2.25995	76.152599	-1.852416	-1.83623
0.00144	0.565324	-0.00024	1.363858	72.62057	0.581608	74.930465	-1.616516	-1.6024
0.0015	0.56044	-0.00024	1.3663	69.1069	1.478156	74.156979	-1.023088	-1.01415
0.00156	0.562882	0.000733	1.361416	70.86373	0.024536	73.643135	-0.679661	-0.67372
0.00162	0.567766	0.000244	1.351648	74.37741	-1.59963	73.02407	-0.818837	-0.81168
0.00168	0.562882	0.000244	1.339438	70.86373	-0.78396	72.289447	-0.971685	-0.9632
0.00174	0.565324	0.001221	1.336996	72.62057	2.882454	71.734292	-0.734302	-0.72789
0.0018	0.553114	0.000733	1.34188	63.83639	-2.20416	71.470758	-0.348576	-0.34553
0.00186	0.557998	0.000733	1.346764	67.35006	2.344645	71.178191	-0.386978	-0.3836
0.00192	0.557998	-0.00024	1.351648	67.35006	-2.5454	70.413383	-1.011609	-1.00277
0.00198	0.56044	0.002198	1.351648	69.1069	0.561429	69.158562	-1.65975	-1.64525
0.00204	0.553114	0.001709	1.356532	63.83639	-0.03261	67.865275	-1.71063	-1.69569
0.0021	0.550672	0.001709	1.356532	62.07955	1.645783	66.889025	-1.291285	-1.28001
0.00216	0.555556	0.004151	1.35409	65.59322	-0.5962	66.139516	-0.991374	-0.98271
0.00222	0.553114	0.006593	1.349206	63.83639	-2.22413	65.398969	-0.979521	-0.97096
0.00228	0.550672	0.010012	1.336996	62.07955	1.682722	64.668934	-0.965616	-0.95718
0.00234	0.555556	0.015873	1.297924	65.59322	1.311272	64.063919	-0.800253	-0.79326
0.0024	0.550672	0.020757	1.249084	62.07955	-2.55599	63.657117	-0.538076	-0.53338
0.00246	0.550672	0.023687	1.20757	62.07955	1.477128	63.44878	-0.275567	-0.27316
0.00252	0.550672	0.026618	1.173382	62.07955	0.011063	63.315692	-0.176035	-0.1745
0.00258	0.538462	0.023199	1.153846	53.29537	-1.39564	63.015867	-0.396578	-0.39311
0.00264	0.540904	0.015385	1.14652	55.05221	2.859678	62.20847	-1.067943	-1.05861
0.0027	0.550672	0.003175	1.141636	62.07955	-1.5056	60.685559	-2.014353	-1.99676
0.00276	0.543346	-0.00806	1.124542	56.80904	-3.00021	58.820402	-2.467039	-2.44549
0.00282	0.543346	-0.01783	1.151404	56.80904	4.1295	57.384768	-1.898912	-1.88232

Figure A1. Partial sample of output file from LabVIEW with calculations.

Board Time	Absorber RPM-C	Fuel Flow [gal/h]	EGT #5 Comp In [F]	Torque [ft-lb]	Barometer [psi]	Pressure	Humidity [%]	EGT #1 Exh Man [F]	EGT #2 Exh Elbow [F]	EGT #4 Comp Out [F]	EGT #8 Coolant In [F]	Air Temp. [F]	Supply Volts	Air Flow [CFM]
Average	2118.506	1.92370389	61.30311	279.5938	14.48256	0.348182	55.58485	692.9163	564.79105	198.0695	139.1963	95	13.2988	290.9991
1339.939	2122	1.840107	61.83801	267.6852	14.482853	0.349432	56.17762	682.7986	553.49527	214.4899	139.37647	95	13.3	289.7631
1340.442	2122	1.675381	62.36654	272.9039	14.482366	0.347906	56.17609	689.4518	560.77033	213.8992	145.34575	95	13.3	289.112
1340.946	2119	1.731629	61.77583	273.6875	14.482853	0.349432	56.19593	681.3063	552.71802	212.1271	137.54216	95	13.3	288.6896
1341.449	2127	1.767788	60.90531	269.5859	14.482853	0.347906	56.21424	672.6322	544.32372	210.2617	129.11677	95	13.3	289.4639
1341.953	2127	1.65931	61.49602	267.1183	14.482853	0.34638	56.24018	679.3165	551.35006	209.7953	135.33477	95	13.3	288.8832
1342.457	2122	1.595027	61.90019	272.7705	14.483097	0.347906	56.25849	685.006	557.81678	209.3912	140.74443	95	13.3	287.3869
1342.961	2122	1.687434	61.90019	273.1206	14.48261	0.349432	56.26154	684.7573	557.7546	208.3341	140.68225	95	13.3	287.5101
1343.465	2120	1.775823	61.62038	273.4707	14.482853	0.347906	56.26459	682.8608	555.8892	207.3703	138.19505	95	13.3	288.144
1343.967	2125	1.731629	61.99346	271.5867	14.483097	0.347906	56.25544	685.8765	559.3091	206.7796	140.93097	95	13.3	288.6896
1344.471	2122	1.7477	62.36654	273.8209	14.48261	0.347906	56.24476	691.1929	564.9053	206.2511	145.87428	95	13.3	288.6544
1344.975	2123	1.771806	61.83801	273.2707	14.482853	0.347906	56.2829	684.2909	558.15877	205.194	139.03448	95	13.2	288.3024
1345.477	2122	1.731629	61.80692	271.7701	14.483097	0.347906	56.29664	685.9387	560.05526	204.6344	140.37135	95	13.3	287.9151
1345.981	2120	1.71154	61.83801	268.3688	14.482853	0.347906	56.26612	684.9749	559.3091	203.9504	139.74955	95	13.3	288.0735
1346.485	2123	1.687434	62.05564	271.0031	14.483097	0.347906	56.22034	688.3015	562.60464	203.5462	142.82746	95	13.3	287.739
1346.989	2122	1.651275	61.93128	271.4033	14.483097	0.347906	56.16999	686.6848	561.42322	202.8933	141.61495	95	13.3	286.6648
1347.493	2123	1.675381	61.74474	271.9202	14.483341	0.347906	56.11963	684.2909	559.3091	202.2094	139.09666	95	13.3	286.4886
1347.997	2116	1.683416	62.02455	272.1536	14.483584	0.347906	56.08606	687.1512	562.26265	201.8985	142.20566	95	13.3	286.4005
1348.501	2117	1.727611	62.05564	276.5219	14.48261	0.347906	56.0586	688.2393	563.44407	201.4321	142.98291	95	13.3	286.929
1349.005	2113	1.824036	62.05564	277.6056	14.482366	0.349432	56.04639	689.1099	564.15914	201.1523	143.6358	95	13.3	288.1087
1349.509	2119	1.86823	61.46493	282.5409	14.482853	0.347906	56.02808	682.1146	556.88408	200.1574	136.39183	95	13.3	289.0768
1350.01	2110	1.968673	61.96237	280.9069	14.482853	0.347906	55.97925	689.3586	563.75497	200.1574	142.23675	95	13.3	289.9214
1350.514	2112	2.093222	61.90019	283.6413	14.48261	0.347906	55.90295	691.6281	565.5271	200.0331	143.13836	95	13.3	291.2756
1351.016	2122	2.121346	62.08673	286.9592	14.48261	0.349432	55.84497	695.1102	568.6361	199.9398	145.12812	95	13.3	292.5062
1351.52	2117	1.984744	61.90019	282.3408	14.482853	0.347906	55.81598	695.2968	567.98321	199.5978	143.88452	95	13.3	292.5413
1352.022	2120	1.984744	61.46493	283.4745	14.482122	0.347906	55.79004	691.4727	563.94151	198.9449	139.34538	95	13.3	292.2601
1352.523	2112	1.988762	61.80692	281.2904	14.48261	0.347906	55.78088	696.5715	568.51174	199.1625	143.26272	95	13.3	292.2601
1353.025	2112	2.016885	61.74474	280.7735	14.48261	0.347906	55.77325	697.5663	569.32008	199.0693	143.54253	95	13.3	291.9789
1353.529	2123	2.036974	61.40275	282.4575	14.482853	0.349432	55.76562	693.4625	564.87421	198.3853	138.87903	95	13.3	292.5413
1354.033	2123	1.928496	61.30948	280.6401	14.48261	0.347906	55.74579	695.7631	566.95724	198.292	140.34026	95	13.3	292.5765
1354.537	2122	1.912425	60.96749	280.8402	14.482853	0.347906	55.73816	691.9701	562.91554	197.9189	136.67164	95	13.3	292.1898
1355.037	2122	1.964655	61.68256	281.7072	14.482853	0.347906	55.70611	699.7737	570.87458	198.2298	143.54253	95	13.3	291.8207
1355.54	2114	1.924478	61.06076	279.8398	14.48261	0.347906	55.67865	691.6281	562.63573	197.4526	136.11202	95	13.3	291.1174
1356.042	2122	1.928496	61.43384	281.107	14.48261	0.347906	55.63134	696.4471	567.64122	197.7324	140.5268	95	13.3	291.3284
1356.546	2123	1.948585	61.37166	280.8402	14.48261	0.349432	55.58099	696.8824	567.88994	197.6391	140.77552	95	13.3	291.68
1357.05	2122	1.880284	61.52711	279.2063	14.483097	0.347906	55.53521	698.2192	569.5688	197.7635	142.45438	95	13.3	291.5218
1357.554	2121	1.828054	61.30948	278.0558	14.482853	0.349432	55.51232	693.4625	564.93639	197.1106	138.10178	95	13.3	290.8184
1358.058	2122	1.811983	60.43896	277.0888	14.482366	0.347906	55.49096	684.9749	556.8219	196.1157	130.578	95	13.3	290.1501
1358.561	2122	1.783859	60.87422	277.0221	14.482122	0.349432	55.4818	689.3897	561.42322	196.3334	135.17932	95	13.3	289.9214
1359.065	2119	1.811983	61.12294	278.6227	14.48261	0.347906	55.48943	691.4727	563.75497	196.3955	137.44889	95	13.3	289.7631
1359.567	2113	1.832071	61.09185	279.3063	14.48261	0.347906	55.49096	690.0115	562.26265	196.0846	136.29856	95	13.3	290.0797
1360.071	2114	1.924478	61.27839	279.5731	14.482366	0.347906	55.48943	692.8096	565.43383	196.2401	139.18993	95	13.3	290.6602
1360.575	2113	1.988762	60.87422	279.2729	14.481878	0.347906	55.49706	690.5711	562.97772	195.6805	136.70273	95	13.3	291.4691
1361.079	2123	1.940549	61.34057	281.2404	14.48261	0.347906	55.50469	694.3019	566.67743	195.9603	140.18481	95	13.3	292.0668
1361.581	2116	1.86823	61.02967	280.4734	14.482853	0.349432	55.48486	690.8509	563.25753	195.6183	136.88927	95	13.3	291.3636
1362.085	2115	1.928496	61.15403	278.2559	14.48261	0.347906	55.45281	692.0634	564.2835	195.525	137.69761	95	13.3	291.0822
1362.588	2125	1.984744	61.09185	279.1896	14.48261	0.347906	55.38567	693.2759	565.46492	195.4939	138.63031	95	13.3	291.5921
1363.092	2123	1.932514	61.18512	279.5564	14.48261	0.347906	55.29564	693.0583	565.15402	195.3074	138.25723	95	13.3	291.7855
1363.596	2121	1.86823	61.30948	279.7231	14.482366	0.347906	55.23156	695.3279	567.33032	195.3696	140.5268	95	13.3	291.2053
1364.1	2121	1.856177	60.99858	280.4234	14.482853	0.347906	55.16899	692.9961	565.30947	195.183	138.22614	95	13.3	290.5722
1364.604	2117	1.848142	61.09185	279.0729	14.48261	0.347906	55.11711	692.4365	564.68767	194.9032	138.19505	95	13.3	290.1501
1365.108	2113	1.888319	61.15403	278.3059	14.482366	0.349432	55.10491	692.8407	565.30947	194.9343	138.87903	95	13.3	290.7305
1365.61	2123	1.892337	61.09185	280.7735	14.482366	0.347906	55.10948	691.939	564.47004	194.6856	137.79088	95	13.3	291.4339
1366.114	2120	1.856177	61.37166	279.4063	14.482122	0.347906	55.11559	695.3589	567.92103	194.8099	141.21078	95	13.3	291.1701
1366.616	2122	1.880284	60.96749	280.7402	14.48261	0.347906	55.12627	690.9131	563.78606	194.4058	137.23126	95	13.3	291.1174
1367.12	2113	1.900372	60.53223	280.3067	14.482366	0.347906	55.14	685.5656	558.31422	193.8462	132.31904	95	13.3	291.1174
1367.622	2113	1.960638	60.68768	280.4567	14.48261	0.349432	55.16594	687.3688	560.02417	193.8151	133.62482	95	13.3	291.4339
1368.126	2111	2.036974	60.99858	281.3237	14.48261	0.347906	55.19951	690.5089	562.729	194.0949	136.08093	95	13.3	291.557
1368.63	2116	2.06108	60.59441	281.5738	14.482122	0.347906	55.22087	688.83	560.89469	193.6907	133.81136	95	13.3	292.348
1369.131	2116	1.972691	61.06076	283.0577	14.482366	0.347906	55.2224	694.9237	566.73961	194.1881	138.72358	95	13.3	292.6995
1369.635	2121	1.980726	60.90531	282.1741	14.482853	0.347906	55.21019	694.0221	565.49601	194.0016	137.51107	95	13.3	292.5062
1370.139	2115	2.024921	60.34569	281.924	14.48261	0.349432	55.17968	687.7419	558.93602	193.3798	131.54179	95	13.3	292.1898
1370.641	2122	2.065098	60.87422	283.5579	14.482366	0.347906	55.19341	693.8666	565.18511	193.7529	136.60946	95	13.3	292.0668
1371.145	2123	1.972691	60.90531	282.841	14.482366	0.34638	55.23003	694.8615	566.1489	193.8772	137.85306	95	13.3	292.5413
1371.649	2116	1.95662	61.37166	281.1403	14.481878	0.347906	55.30633	700.209	571.37202	194.3125	142.51656	95	13.3	292.2953
1372.149	2114	2.053045	60.90531	282.9577	14.482122	0.347906	55.38109	695.8564	566.80179	193.7218	138.16396	95	13.3	292.225
1372.652	2122	2.032956	60.9364	284.3082	14.482366	0.347906	55.45281	698.0949	569.04027	193.8772	139.56301	95	13.3	292.6116
1373.156	2113	1.968673	60.96749	283.4412	14.48261	0.347906	55.49096	696.2606	567.01942	193.7218	137.82197	95	13.3	292.2601
1373.66	2111	2.073133	61.15403	283.5746	14.482366	0.347906	55.51843	699.3385	569.78643	193.8151	140.15372	95	13.3	292.348
1374.164	2119	2.105275	60.99858	286.9926	14.482366	0.347906	55.51995	698.499	569.00918	193.5974	139.00339	95	13.3	292.5413
1374.666	2109	2.036974	60.99858	285.0085	14.482366	0.349432	55.50317	699.4317	569.81752	193.7218	139.34538	95	13.3	292.1371
1375.17	2121	2.133399	61.06076	285.8588	14.482366	0.347906	55.45281	699.4006	569.72425	193.5974	139.34538	95	13.3	293.2442
1375.674	2115	2.137416	61.30948	285.0418	14.482122	0.349432	55.39788	703.6911	573.79704	193.9083	142.7031	95	13.3	293.2969
1376.178	2114	2.173576	61.40275	285.7254	14.48261	0.347906	55.3048	705.3388	575.22718	193.9705	143.76016	95	13.3	293.4024

Water Vapor [psi]	Dry Air [psi]
0.8165	14.028709
Temp [F]	Press [psi]
60	0.2563
62	0.2751
64	0.2952
66	0.3165
68	0.3391
70	0.3632
72	0.3887
74	0.4158
76	0.4446
78	0.475
80	0.5073
82	0.5414
84	0.5776
86	0.6158
88	0.6562
90	0.6988
92	0.7439
94	0.7914
96	0.8416
98	0.8945
100	0.9503

Figure A2. Partial sample of DYNOmite output data spreadsheet with calculations.

		Cycle										
Deg	Time	1	2	3	4	5	6	7	8	Average	Stdev	%
-16.7792	-1.32E-03	25.18597	23.42914	23.42914	19.91546	21.6723	21.6723	23.42914	25.18597	22.98993	1.818498	7.90998
-16.0165	-1.26E-03	21.6723	23.42914	23.42914	21.6723	19.91546	26.94283	25.18597	19.91546	22.77032	2.47343	10.86252
-15.2539	-1.20E-03	23.42914	21.6723	23.42914	21.6723	25.18597	23.42914	23.42914	25.18597	23.42913	1.328044	5.668342
-14.4912	-1.14E-03	21.6723	23.42914	23.42914	21.6723	23.42914	21.6723	23.42914	25.18597	22.98993	1.242271	5.403546
-13.7285	-1.08E-03	26.94283	26.94283	26.94283	21.6723	23.42914	28.69967	25.18597	25.18597	25.62519	2.251817	8.787512
-12.9658	-1.02E-03	25.18597	23.42914	23.42914	19.91546	23.42914	23.42914	25.18597	23.42914	23.42913	1.626514	6.942273
-12.2031	-9.60E-04	23.42914	21.6723	23.42914	18.15863	25.18597	26.94283	23.42914	23.42914	23.20953	2.561011	11.03431
-11.4404	-9.00E-04	23.42914	21.6723	18.15863	26.94283	21.6723	23.42914	26.94283	25.18597	23.42914	2.969602	12.67482
-10.6777	-8.40E-04	23.42914	21.6723	25.18597	21.6723	26.94283	26.94283	25.18597	19.91546	23.86835	2.614263	10.95284
-9.915	-7.80E-04	25.18597	21.6723	19.91546	23.42914	25.18597	23.42914	25.18597	23.42914	23.42913	1.878137	8.016246
-9.15231	-7.20E-04	23.42914	23.42914	21.6723	19.91546	25.18597	26.94283	21.6723	19.91546	22.77032	2.47343	10.86252
-8.38962	-6.60E-04	28.69967	23.42914	19.91546	19.91546	23.42914	28.69967	25.18597	28.69967	24.74677	3.726822	15.05983
-7.62693	-6.00E-04	21.6723	23.42914	21.6723	28.69967	28.69967	21.6723	26.94283	25.18597	24.74677	3.078952	12.44183
-6.86423	-5.40E-04	21.6723	25.18597	25.18597	26.94283	16.40179	23.42914	21.6723	23.42914	22.98993	3.218968	14.00165
-6.10154	-4.80E-04	23.42914	19.91546	16.40179	19.91546	28.69967	23.42914	23.42914	25.18597	22.55072	3.756279	16.65702
-5.33885	-4.20E-04	23.42914	30.4565	21.6723	23.42914	16.40179	26.94283	23.42914	23.42914	23.64874	4.032265	17.05065
-4.57616	-3.60E-04	19.91546	23.42914	25.18597	23.42914	25.18597	25.18597	28.69967	25.18597	24.52716	2.47343	10.08445
-3.81346	-3.00E-04	26.94283	26.94283	26.94283	23.42914	21.6723	25.18597	25.18597	26.94283	25.40559	1.978192	7.786446
-3.05077	-2.40E-04	21.6723	16.40179	23.42914	19.91546	25.18597	25.18597	25.18597	23.42914	22.55072	3.114538	13.81126
-2.28808	-1.80E-04	23.42914	26.94283	19.91546	25.18597	21.6723	23.42914	23.42914	23.42914	23.42914	2.099826	8.962456
-1.52539	-1.20E-04	21.6723	23.42914	25.18597	23.42914	21.6723	23.42914	26.94283	25.18597	23.86835	1.818503	7.618892
-0.76269	-6.00E-05	28.69967	25.18597	23.42914	25.18597	23.42914	25.18597	23.42914	26.94283	25.18598	1.878145	7.457108
0	0	25.18597	26.94283	23.42914	26.94283	23.42914	21.6723	28.69967	26.94283	25.40559	2.382636	9.378394
0.762693	6.00E-05	25.18597	19.91546	23.42914	25.18597	25.18597	26.94283	26.94283	26.94283	24.96637	2.382633	9.54337
1.525385	1.20E-04	21.6723	21.6723	25.18597	26.94283	19.91546	25.18597	26.94283	23.42914	23.86835	2.614263	10.95284
2.288078	1.80E-04	28.69967	21.6723	25.18597	26.94283	26.94283	28.69967	30.4565	28.69967	27.16243	2.727756	10.04239
3.050771	2.40E-04	25.18597	26.94283	26.94283	21.6723	25.18597	25.18597	25.18597	32.21334	26.0644	2.969603	11.39333
3.813463	3.00E-04	28.69967	23.42914	21.6723	25.18597	26.94283	25.18597	25.18597	30.4565	25.84479	2.807416	10.8626
4.576156	3.60E-04	25.18597	23.42914	25.18597	21.6723	25.18597	25.18597	28.69967	25.18597	24.96637	1.978189	7.923414
5.338849	4.20E-04	28.69967	28.69967	28.69967	28.69967	26.94283	26.94283	30.4565	26.94283	28.26046	1.242271	4.395793
6.101541	4.80E-04	25.18597	26.94283	25.18597	23.42914	28.69967	30.4565	28.69967	30.4565	27.38203	2.614266	9.547377
6.864234	5.40E-04	25.18597	26.94283	25.18597	25.18597	28.69967	28.69967	25.18597	28.69967	26.72321	1.74109	6.515273
7.626927	6.00E-04	26.94283	26.94283	25.18597	25.18597	26.94283	26.94283	28.69967	30.4565	27.16243	1.741087	6.409908
8.389619	6.60E-04	28.69967	25.18597	25.18597	25.18597	28.69967	32.21334	30.4565	32.21334	28.48005	3.03387	10.65261
9.152312	7.20E-04	28.69967	28.69967	25.18597	25.18597	30.4565	30.4565	30.4565	32.21334	28.91926	2.561016	8.855743
9.915005	7.80E-04	30.4565	28.69967	25.18597	30.4565	28.69967	26.94283	30.4565	32.21334	29.13887	2.251812	7.727864
10.6777	8.40E-04	28.69967	23.42914	30.4565	30.4565	30.4565	28.69967	32.21334	30.4565	29.35848	2.645698	9.0117
11.44039	9.00E-04	28.69967	30.4565	32.21334	30.4565	28.69967	28.69967	26.94283	32.21334	29.79769	1.863406	6.253526
12.20308	9.60E-04	28.69967	25.18597	28.69967	30.4565	28.69967	30.4565	28.69967	32.21334	29.13887	2.046658	7.023807
12.96578	1.02E-03	33.97017	30.4565	32.21334	28.69967	28.69967	32.21334	28.69967	32.21334	30.89571	2.046652	6.624389
13.72847	1.08E-03	26.94283	28.69967	30.4565	23.42914	28.69967	28.69967	30.4565	30.4565	28.48006	2.382632	8.365968
14.49116	1.14E-03	30.4565	28.69967	26.94283	28.69967	30.4565	28.69967	32.21334	32.21334	29.79769	1.863406	6.253526
15.25385	1.20E-03	28.69967	28.69967	30.4565	32.21334	25.18597	30.4565	25.18597	32.21334	29.13887	2.777811	9.533008
16.01655	1.26E-03	32.21334	28.69967	26.94283	30.4565	26.94283	28.69967	35.72701	32.21334	30.2369	3.03386	10.03363
16.77924	1.32E-03	32.21334	28.69967	32.21334	25.18597	28.69967	28.69967	33.97017	28.69967	29.79768	2.807411	9.421575

Figure A3. Partial sample of pressure curve averaging spreadsheet.

.

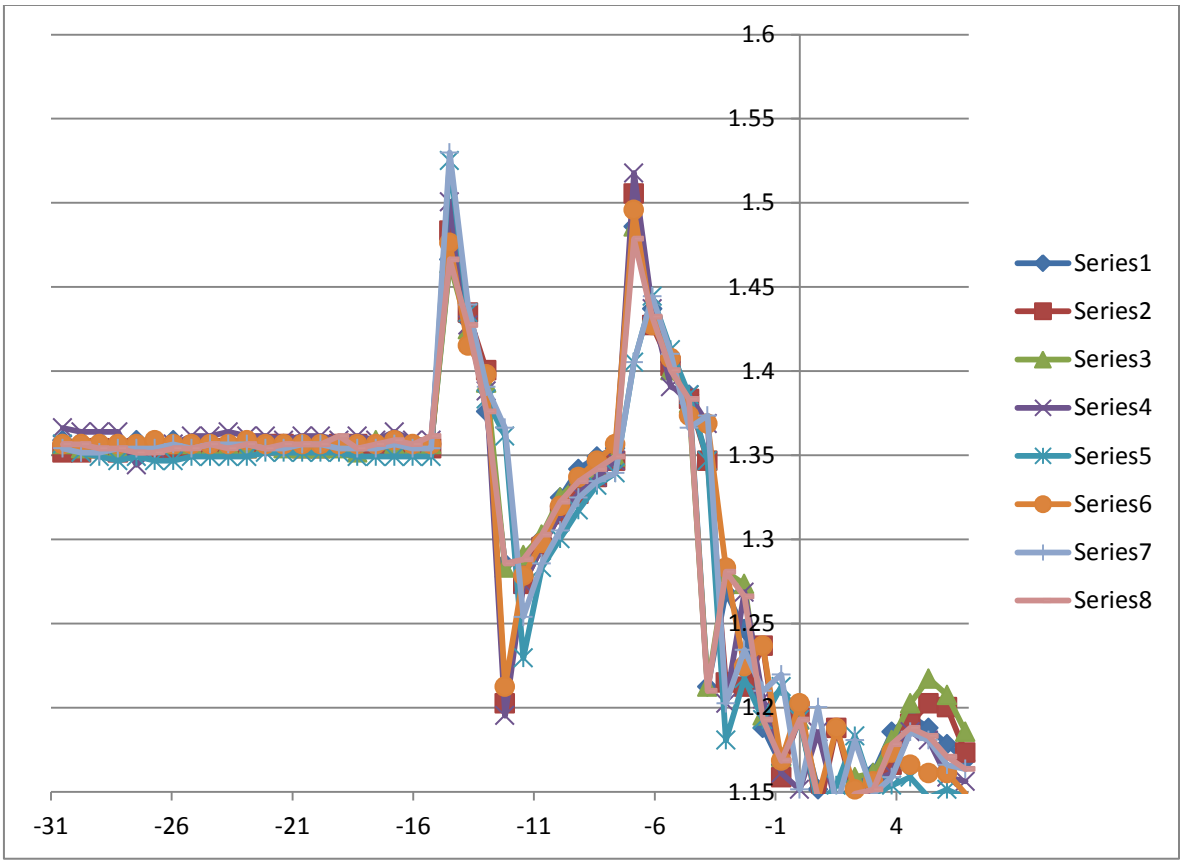

Figure A4. Sample of injection timing graph.

APPENDIX B. ADDITIONAL EMISSIONS RESULTS

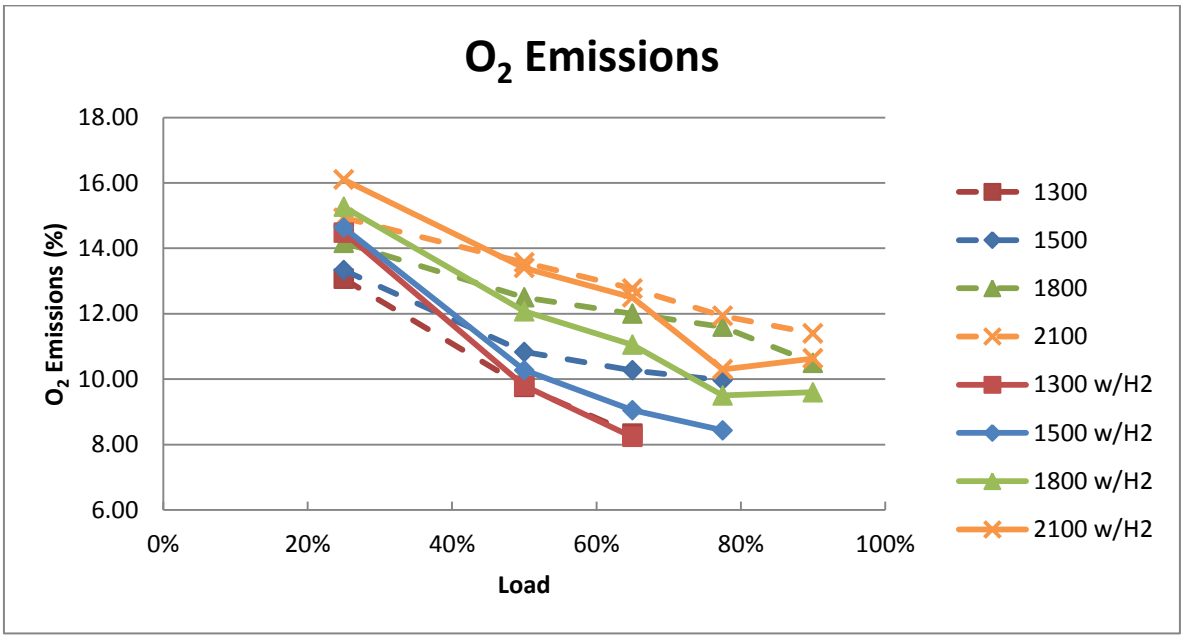

Figure B1. O_2 emissions for diesel-only and dual-fuel operation.

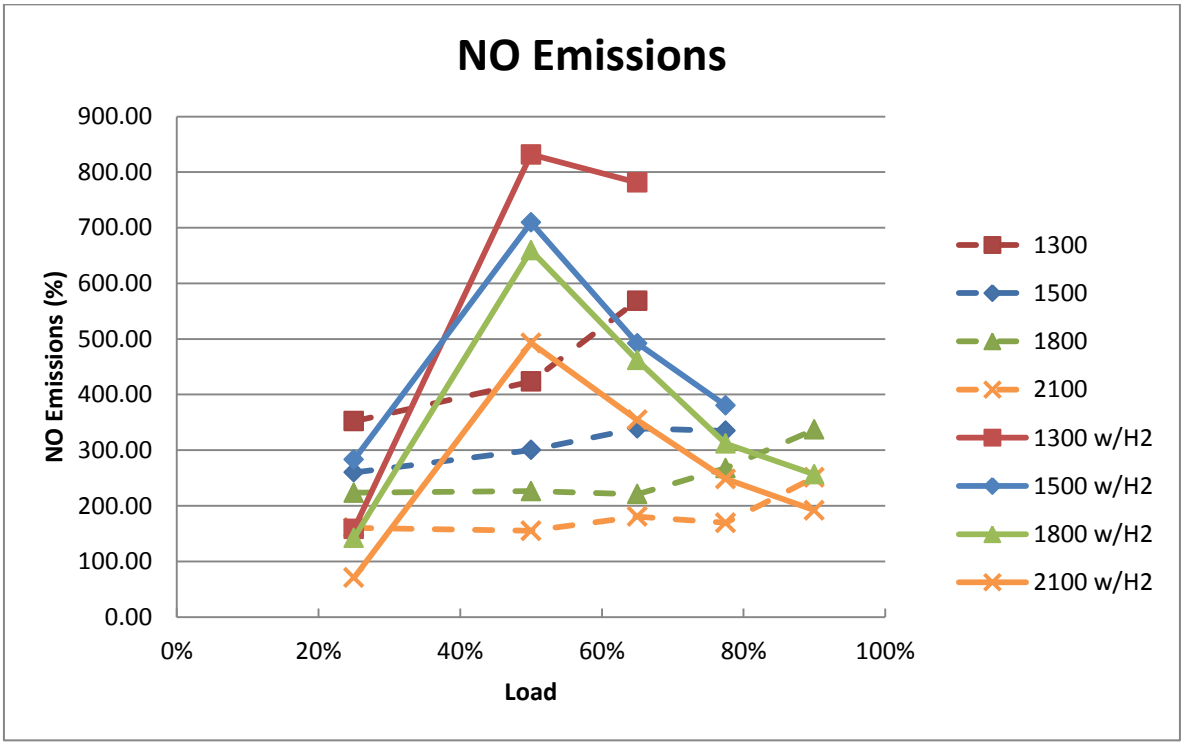

Figure B2. NO emissions for diesel-only and dual-fuel operation.

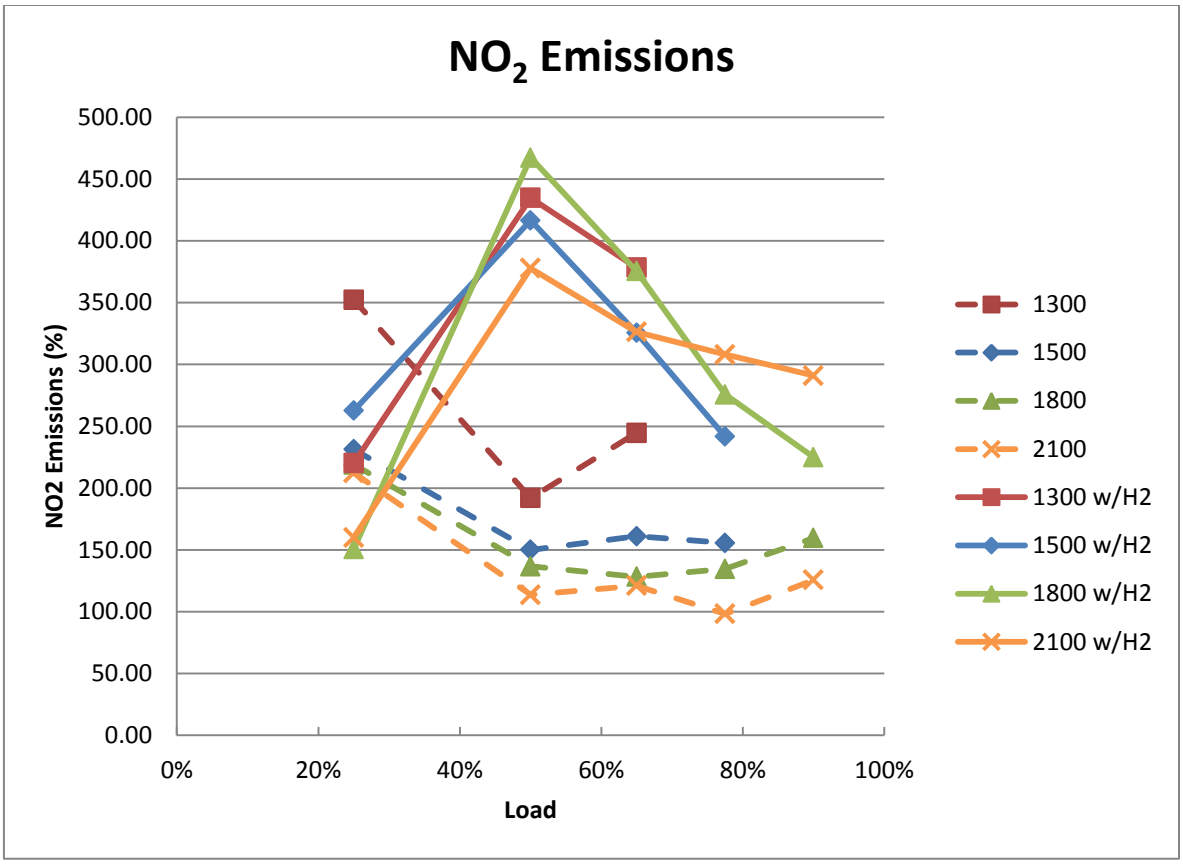

Figure B3. NO_2 emissions for diesel-only and dual-fuel operation.

APPENDIX C. INJECTION DELAY CIRCUIT

One key engine control that can be used to help control start of combustion is ignition timing. Retarding the SOC brings the potential to increase the amount of H_2 added during dual-fuel operation. If combustion started later in the cycle, cylinder pressures and temperatures would be lower, leading to a reduction in the maximum in-cylinder pressure and MRPR for the same heat-release profile.

The CAT ACERT ECM provided for testing was a "locked" unit, meaning it could not be modified. Ideally, with an "unlocked" ECM, the values for injection timing and other operating characteristics could be modified though a computer program, allowing many more variables to be controlled.

One idea to gain partial control over the injection timing was to design an "injection delay circuit," to be used between the ECM and the injector. The injector signals would pass through the circuit and be delayed by some time, allowing the injection timing to be retarded but not advanced. This was acceptable since interest was only in retarding the timing. The circuit was design to delay the injection signal by up to 1 ms and could be controlled by the operator. This would allow control of injection timing relative to the ECM's timing. A schematic of the injector signal and how it could be controlled can be seen in Figure C1.

Both pilot and main injection signals were in the form of a step-function that started at 0 V, held at 90 V for 0.2 ms, and dropped back to 0 V. After the main injection there were also a varying number of quick "pulses" up to 30 V. The circuit was designed to eliminate the pulses after the main injection, which controlled the load of the engine. In order to regain the ability to control load, the circuit was designed to extend the injection pulse duration.

The circuit was designed, modeled, and tested using computer software. A prototype printed circuit board (PCB) and components for the circuit were ordered and assembled by hand. Each of the 6 injector leads would split and run through the board on its own separate delay circuit. Due to component availability and time constraints, the circuit was never finished or physically tested. Much thanks to Dr. Majura Selekwa for his help in designing the circuit. Pictures of the modeled and nearly complete assembled board can be seen in Figure C2.

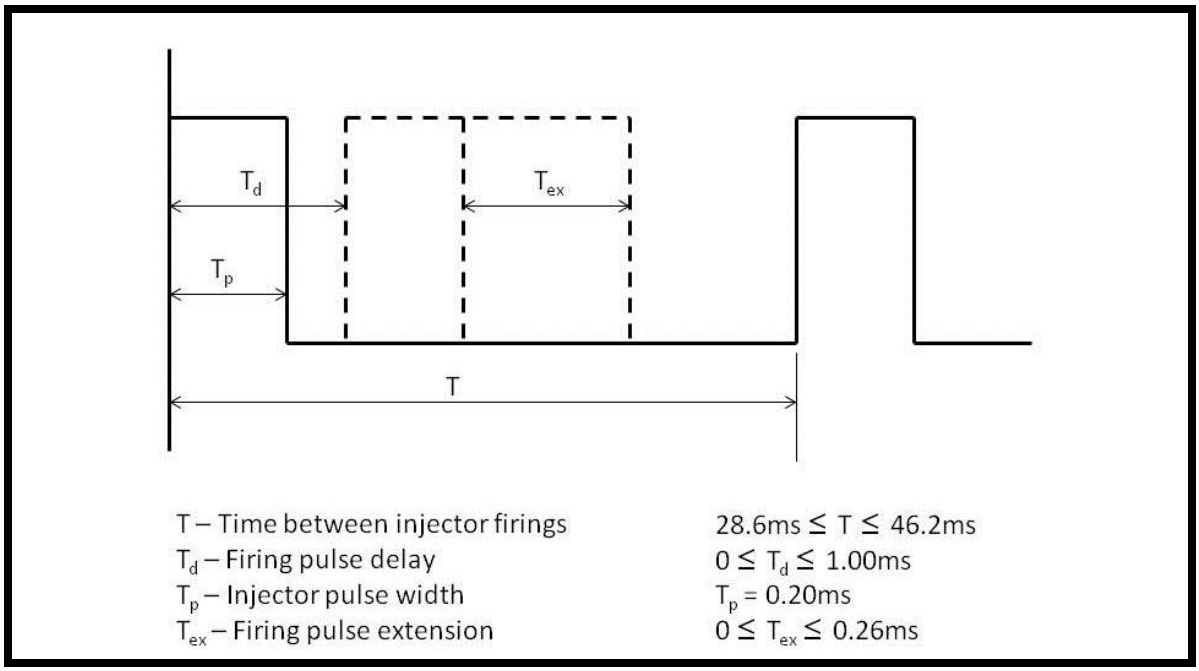

Figure C1. Injector signal with injector delay circuit parameters and values.

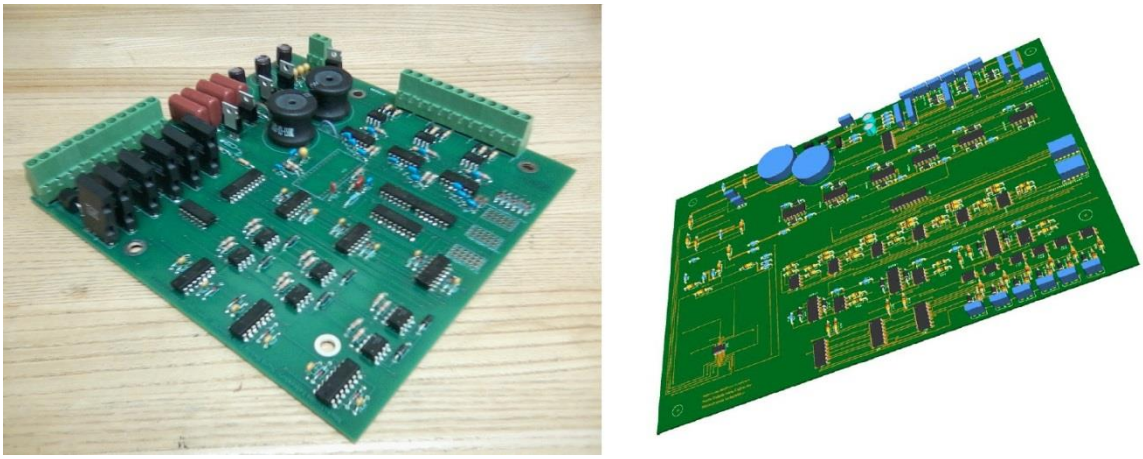

Figure C2. Nearly complete circuit on the left. A model of the injector delay circuit on the right.